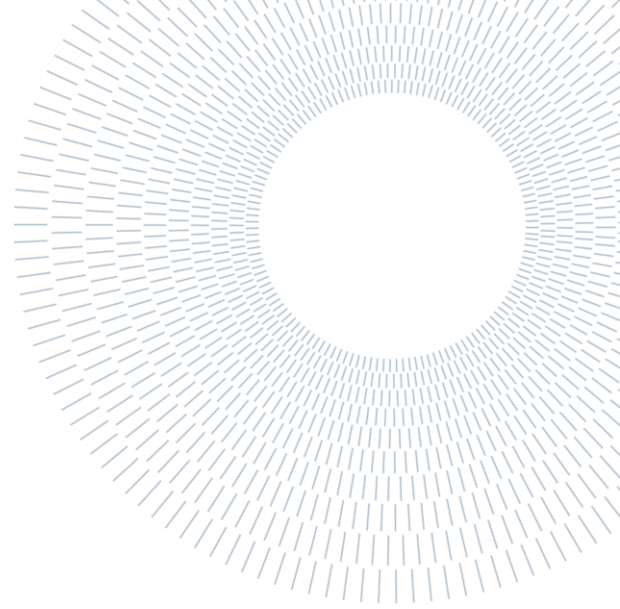




**POLITECNICO
MILANO 1863**

**SCUOLA DI INGEGNERIA INDUSTRIALE
E DELL'INFORMAZIONE**



EXECUTIVE SUMMARY OF THE THESIS

Quantitative measures of autonomic activations during cognitive tasks: a methodological approach

TESI MAGISTRALE IN BIOMEDICAL ENGINEERING – INGEGNERIA BIOMEDICA

AUTHOR: Giulio Steyde

ADVISOR: Prof. Anna Maria Bianchi

CO-ADVISOR: Eng. Alessandra Calcagno

ACADEMIC YEAR: 2020-2021

1. Introduction

1.1 Biosignals and cognitive tasks

The number of research studies that investigate the effect that cognitive functions have on biological signals has been increasing in the last years. The main aim is to uncover the main physiological mechanisms that underly a variety of cognitive processes and possibly exploit this knowledge for research, therapy and commercial applications.

Most studies focus on the monitoring of the Central Nervous System (CNS). However, the equipment necessary to do so is impractical to use out of the clinic or academia. Autonomic signals such as the heart rate variability (HRV), the electrodermal activity (EDA) and the respiratory signals can be easily acquired with inexpensive instrumentation and, indeed, several consumer-grade wearable devices are already available for this purpose. For this reason, the number of studies that adopt autonomic indices as a correlate of cognitive functioning is nowadays increasing. Moreover,

given the deep interrelation between the CNS and the Autonomous Nervous System (ANS), it is reasonable to hypothesise and study a correlation between the measures obtained from these two branches.

1.2 Open Problems

Some open problems that limit practical applications of autonomic signals in the monitoring of cognitive processes have been identified. Very few studies investigate electrodermal responses during cognitive tasks. It is also unclear how the sympathetic nervous system differs in the control of the heart rhythm and skin conductance during cognitive tasks. Moreover, the most commonly applied methods to analyze the HRV make assumptions that are often unsatisfied in real-life conditions, namely about the stationarity of the signal and the frequency range of the respiratory activity. To transfer the findings to practical applications these conditions must be lifted.

1.3 The BASE project

The key idea of the BASE project is to investigate the physiological mechanisms that could lead to the generation of software bugs. This objective is pursued by acquiring and integrating different biological signals on experienced programmers during tasks of code comprehension and code writing. Both central and autonomic signals are investigated. Two research studies in the BASE project were conducted: study one took place at Universidade de Coimbra while the second at Politecnico di Milano [1].

1.4 Objective of the thesis

The objective of this thesis is to address the open problems identified and investigate possible solutions to extract robust and interpretable quantitative indices of mental effort and cognitive load from autonomic signals. The original intention was to continue with the acquisitions of the study 2 of the BASE project and use it to conduct all the analyses. However, the acquisitions were stopped due to the ongoing COVID-19 pandemic before the minimum number of subjects that had been stated in the experimental protocol design was reached. In addition, the EDA signal had to be discarded due to quality concerns and was not used in future analysis. A second simpler protocol called N-Back was added to overcome these limitations and obtain a more extensive analysis with a focus on EDA and its relation with the other autonomic signals of interest.

2. Data Acquisition

2.1 BASE Project. Study 2

2.1.1 Participants

Sixteen subjects participated in this study. The average age was 29, standard deviation 9.6. Twelve were males and 4 females. Among the sixteen subjects who participated in the BASE protocol, three subjects were discarded because the quality of the signals was unsatisfactory. All participants were asked to answer a technical questionnaire meant to assess their coding skills in C programming language. Only subjects with a score equal to or higher than 4 out of 10 were eligible.

2.1.2 Equipment and setup

The following autonomic signals were acquired using the ProComp Infinity polygraph: Electrocardiogram (ECG), EDA, and Respiration activity. The sampling rates were 2048Hz, 256Hz and 256Hz, respectively. In addition, Electroencephalographic (EEG) and Functional Near-Infrared Spectroscopy (fNIRS) signals were also acquired.

2.1.3 Experimental Tasks and Procedure

The experiment is divided into 2 runs, each composed of three tasks presented in random order:

Text Reading- read a short text in natural language (English). This task lasted for 60 seconds.

Code reading – read a short snippet of simple code in C language. This task lasted for 5 minutes.

Code programming – develop a function in C language in Eclipse environment. Subjects were allowed to stop this task after 5 minutes. The maximum time was 20 minutes.

During code programming two tasks of different difficulty were presented in random order (one for each run). The difficult task is called RLE and the easy task is called SPLIT. Also the text and code snippets presented were different in each run.

Before each task and after the completion of the last a relaxation phase of 30 seconds was conducted. During this phase, called “fixation”, subjects were asked to watch a black cross on a grey screen and relax. After each run, an Experiment Evaluation form was presented. The form, which took about 1 minute to be filled, asked to give a score from 0 to 5 to the following experiences: mental effort, task fulfilment, pressure with time and discomfort.

The code programming task was evaluated by an expert who assigned a performance score and manually labelled starting from the screen recordings into:

Read problem: the time spent by the participant to read the assignment, before starting to write the solution.

Writing: the time spent actually writing code. There may be multiple Writing sessions for each Code programming task.

2.2 N-Back protocol

2.2.1 Participants

Thirty-one healthy subjects were enrolled in the study. Four subjects were excluded due to the low

quality of acquired data. Among the remaining 27 subjects the mean age was 25.2 ± 2 years. The males were 14 and the females 13.

2.2.2 Equipment and setup

The ECG, EDA, and respiratory signals were acquired using the ProComp Infinity polygraph, maintaining the same sampling frequencies used for the BASE protocol. Subjects observed a screen connected to the PC running the protocol.

2.2.3 Experimental Tasks and Procedure

The experimental protocol is composed of 6 phases. Each lasted 5 minutes, except for N-Back which lasted 7 minutes. Subjects had to stay seated unless instructed otherwise. In brief, the tasks were:

Relaxation: look at a relaxing image. This phase is used to acquire a baseline.

Sit: look at a grey screen. In this task no sympathetic activation is expected.

Stand: stand up. This is a sympathetic stressor without cognitive effort.

Controlled Respiration: breath at a constant rate of 12 breaths per minute. This is a parasympathetic stressor. It will be called Resp for brevity.

N-back: press "Enter" if the letter on the screen is the same as the one shown N times before. Four sequences of $20+N$ consecutive letters were shown. N is an integer determining the difficulty, which was varied between 0 and 3 and is fixed during a sequence. Two sessions were performed. This task was selected to elicit cognitive effort.

3. Data Analysis

All analyses were conducted in MATLAB environment. The procedure was the same for both protocols. The features were computed in time windows corresponding to the different experimental tasks.

Regarding the BASE protocol, for the code programming task only the Read Problem phase and 5 minutes extracted from the longest Writing session were selected for each subject. Read Problem was only considered in RLE since most subjects spent little time reading the instructions of SPLIT and windows of sufficient length could not be obtained.

3.1 HRV and Respiratory Signals

3.1.1 Pre-processing

The ECG signal was downsampled to 256Hz. The R peaks were identified using the Pan-Tompkins algorithm and manually corrected. The tachogram was then extracted using the identified peaks. The respiratory signal was low-passed and downsampled to 256Hz and then furtherly low-passed with a FIR filter with a cut-off frequency of 10Hz. The respirogram was extracted from the respiratory signal taking one sample for each peak identified in the ECG. The respirogram was then filtered with a high pass FIR filter with passband frequency set at 0.02Hz and rescaled with a logarithmic transformation.

3.1.2 Bivariate time-variant modelling

The tachogram and respirogram were modelled using a bivariate autoregressive model [2] sketched in Figure 1.

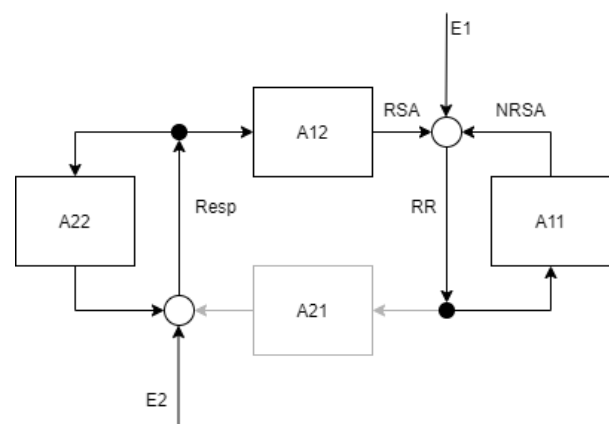


Figure 1. Block diagram of the bivariate autoregressive model

The tachogram (RR time series) is modelled as the sum of a component dependent on its past values, weighted according to the parameters of block A11, the past values of the respirogram, weighted with A12, and a white noise (E1). The component dependent on the respirogram is the RSA, while the component dependent only on itself is the Non-Respiratory Sinus Arrhythmia (NRSA).

The respirogram (Resp) is modelled as a signal only influenced by its past values, weighted according to A22, and a white noise E2. The block A21 represents the effect of the RR series on the respirogram and is marked in grey because it was omitted from the model, forcing to 0 its parameters

since the influence of the tachogram on the respirogram is assumed to be neglectable.

The parameters were estimated at each sample using a time-variant adaptation of a recursive least square filter (RLS) with forgetting factor, which is a hyperparameter that determines how past values are weighted in the prediction of the next. The use of the forgetting factor relaxes the condition of stationarity [3]. Its value was set to 0.985. The order of the model set to 9. A condition that prevents the updating of the parameters when the a-priori prediction error exceeds an adaptive threshold was implemented to reduce the dependence of the model on the outliers. The partial spectrograms of RSA and NRSA, the total spectrograms of RR and Resp and the spectrogram of the coherence were computed from the parameters using the residuals method [4]. An example of total spectrogram of the HRV is presented in Figure 2.

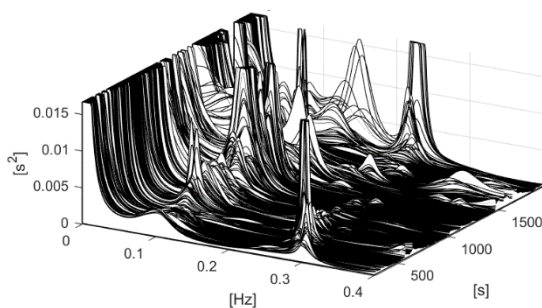


Figure 2. 3-D Spectrogram of the tachogram

The instantaneous respiratory frequency was estimated from the respiratory signal and used to adapt the bands used for feature extraction.

3.1.3 Features extraction

Time-frequency features were computed integrating the spectrograms in the desired frequency range and then computing the mean in the time window of interest.

From the spectrogram of the tachogram were extracted: P Tot, HF and LF NU obtained integrating respectively in $f > 0.04$, $f \in (0.15, 0.4\text{Hz}]$ and $f \in (0.04, 0.15\text{Hz}]$. LF NU was normalized dividing by P Tot. In addition, LF/HF was computed by dividing LF non normalized by HF. From the spectrogram of the tachogram multiplied by the magnitude squared coherence was obtained P Coer integrating in $f > 0.04$. P Coer NU is P Coer divided by P Tot. LF NRSA was obtained integrating in $(0.04, 0.15\text{Hz}]$ the partial spectrogram NRSA and dividing by P Tot. HF RSA was

obtained integrating the partial spectrogram RSA in a frequency range wide 0.25Hz centred at the respiratory frequency. From the HRV signal were also computed RMSSD, SDNN, pNN50 and mean HR [5]. From the respiratory signal was computed the mean Respiratory Frequency.

3.2 EDA Signal

The signal was low-passed and down-sampled to 16Hz. Additionally, it was low passed at 5Hz using a FIR filter.

3.2.1 Decomposition Analysis

The signal was decomposed in the phasic and tonic components using Continuous Decomposition Analysis [6]. From the Phasic component were computed the peak frequency, the mean impulse amplitude and the Integrated Skin Conductance Response (ISCR). From the Tonic component was computed the mean.

3.2.2 Time-Frequency Analysis

A RLS time-variant autoregressive algorithm was applied to the Phasic component of EDA to obtain its spectrogram. The forgetting factor was varied using the Fortescue method. The order was set to 7 after inspection of the prediction error. TVSymp was obtained integrating the spectrogram in the band from 0.045 to 0.25Hz. StdTVSymp is the standard deviation of TVSymp.

3.3 Statistical Analysis

3.3.1 Differences across Tasks

The features extracted were tested for significance using the Friedman test comparing the values obtained in the different experimental tasks. Results are considered significant if $p < 0.05$. Paired comparisons were performed applying the Bonferroni correction.

3.3.2 Correlations

Correlations were evaluated using the Spearman coefficient rho and considered significant when $p < 0.05$. The features were correlated with each other and, for the BASE protocol, with the outcomes of the Evaluation Form, the Performance score and the EEG features, namely the power in the Theta and Alpha bands which had already been computed in [1]. For the N-Back protocol

were also correlated with the score obtained in the N-Back test.

4. Results

4.1 BASE protocol

4.1.1 Differences across tasks

The heart rate increased and P Tot decreased significantly in both difficulty levels during Writing.

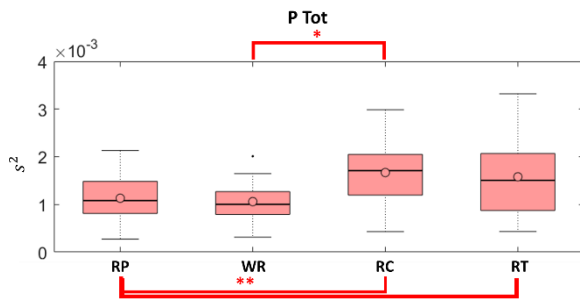


Figure 3. *P Tot* in RLE. Boxplots refer to: Read Problem, Code Writing, Read Code and Read Text.

This finding is in agreement with other studies (e.g., [7]). In RLE, but not SPLIT, during code writing also P Coer, HF and SDNN decreased, while the respiratory rate increased.

4.1.2 Correlations

P Coer calculated in Code Reading (which was selected as the low effort task) positively correlated with the performance. HR at rest negatively correlated with the score. During the writing task SDNN positively correlated with Score and Performance while LF NRSA and P Tot positively correlated with the Fulfillment. During the writing phase RMSSD positively correlated with the Power in the Theta and Alpha bands of the EEG while SDNN only correlated in the Theta band. HR and LF NRSA were found to correlate negatively with the power in the alpha band.

4.2 N-Back protocol

4.2.1 Cross-correlation between EDA and RR

A time-delay of about 2.5s of EDA with respect to the inverse of the RR series was identified from the normalized cross-correlation. The analysis in frequency domain did not identify significant correlation at any frequency.

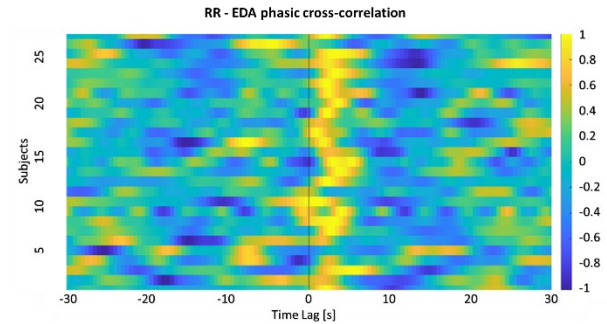


Figure 4. Normalized cross-correlation between EDA phasic component and RR series among subjects

4.2.2 Differences between N-Back and the other tasks

HRV and Respiration

During the N-Back task, P Tot was significantly lower compared to both the Sit and Resp phases, while no difference was detected with the Stand. HF was lower only compared to Resp while HF RSA was also significantly lower compared to Sit. Similarly, LF NU did not differ from Sit to N-back while LF NU NRSA did.

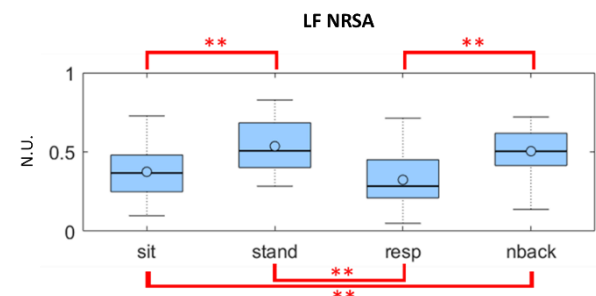


Figure 5. LF NRSA. N-Back protocol

P Coer was lower during N-Back compared to Resp while P Coer NU was also lower compared to Sit. The only significance found in the time-domain analysis of HRV is that RMSSD and SampEn increased during N-Back compared to Stand. The respiratory rate was significantly higher during N-Back compared to both Sit and Stand.

EDA

All the indices extracted increased very significantly ($p < 0.01$) during the cognitive task compared to Sit. Except for Peak Amplitude, the increase was significant also when compared to Resp. Furthermore, Peak Frequency, ISCR, The Tonic Mean and TVSymp also discriminated between Stand and N-Back which are both considered sympathetic stressors.

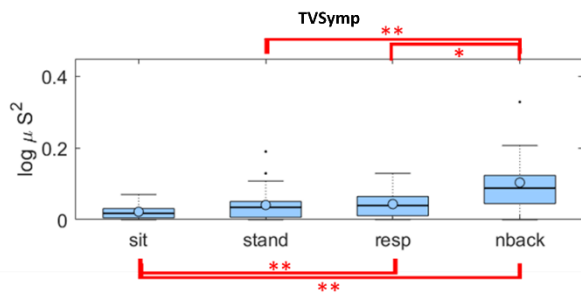


Figure 6. TVSymp. N-Back protocol

4.2.3 Correlations

All the EDA features significantly correlate with each other, some features with high coefficients (e.g. ISCR and Tonic Mean, $\rho=0.8$). Several significant, but much lower, correlations were also found between EDA and HRV features. HF RSA is negatively correlated with the Peak Frequency, ISCR, TVSymp and stdTVSymp. Similar correlations but with positive coefficients were found with LF NRSA. Furthermore, P Coer is negatively correlated with TVSymp, stdTVSymp and ISCR while RMSSD is negatively correlated with Peak Frequency and ISCR. HR is positively correlated with the Peak Frequency.

5. Conclusions

In both protocols, significant variations in autonomic indices were observed. In the study of the HRV and respiratory signals, the results obtained confirm that during cognitive tasks the total power of the HRV is reduced. Two mechanisms are linked to this effect: the increased heart rate and the decreased effect of the RSA. The N-back protocol also captured a reduction in the parasympathetic and an increase in the sympathetic tone during the cognitive task compared to low effort tasks.

The descriptors obtained from the EDA signal proved to be very sensitive to the cognitive task and less sensitive to the stressors commonly used in the analysis of the HRV to elicit a sympathetic and parasympathetic activation: sit to stand and controlled respiration. Indeed, EDA features did not vary significantly between the forced respiration and the standing tasks while the HRV features did. On the contrary, the Stand and the N-back tasks induced similar effects in the HRV features which makes it more difficult to discriminate between them while the descriptors

extracted from the EDA signal behave differently under the two conditions.

These results, confirmed by the low correlation coefficients identified among the features extracted from the two signals, suggest that the information provided by the two is not redundant but rather should be used in combination to discriminate conditions in which the sympathetic activation is induced by the cognitive load from the ones in which is induced by orthostatic stressors.

6. References

- [1] A. Calcagno *et al.*, "EEG monitoring during software development," in *20th IEEE Mediterranean Electrotechnical Conference, MELECON 2020 - Proceedings*, 2020, pp. 325–329.
- [2] A. Bianchi, B. Bontempi, S. Cerutti, P. Gianoglio, G. Comi, and M. G. N. Sora, "Spectral analysis of heart rate variability signal and respiration in diabetic subjects," *Med. Biol. Eng. Comput.*, vol. 28, no. 3, pp. 205–211, 1989.
- [3] A. M. Bianchi, L. Mainardi, E. Petrucci, M. G. Signorini, M. Mainardi, and S. Cerutti, "Time-Variant Power Spectrum Analysis for the Detection of Transient Episodes in HRV Signal," *IEEE Trans. Biomed. Eng.*, pp. 136–144, 1993.
- [4] G. Baselli, "Spectral and Cross-Spectral Analysis of Heart Rate and Arterial Blood Pressure Variability Signals," 1986.
- [5] F. Shaffer and J. P. Ginsberg, "An Overview of Heart Rate Variability Metrics and Norms," *Front. Public Heal.*, vol. 5, no. September, pp. 1–17, 2017.
- [6] M. Benedek and C. Kaernbach, "A continuous measure of phasic electrodermal activity," *J. Neurosci. Methods*, vol. 190, no. 1, pp. 80–91, 2010.
- [7] J. F. Thayer and R. D. Lane, "Claude Bernard and the heart – brain connection: Further elaboration of a model of neurovisceral integration," *Neurosci. Biobehav. Rev.*, vol. 33, pp. 81–88, 2009.



POLITECNICO
MILANO 1863

SCUOLA DI INGEGNERIA INDUSTRIALE
E DELL'INFORMAZIONE

Quantitative measures of autonomic activations during cognitive tasks: a methodological approach

TESI DI LAUREA MAGISTRALE IN
BIOMEDICAL ENGINEERING-INGEGNERIA BIOMEDICA

Author:	Giulio Steyde
Student ID:	10561045
Advisor:	Prof. Anna Maria Bianchi
Co-advisor:	Eng. Alessandra Calcagno
Academic Year:	2020-21

Abstract

The widespread diffusion of smartphones and wearable devices has enlarged the scope of applications of biomedical signal processing. Despite the advantages of autonomic signals in terms of practicality and cost of acquisition, in order to explore the brain mechanisms underlying cognitive processes and extract quantitative correlates for cognitive load most studies focus on signals and images deriving from the central nervous system. Nevertheless, brain imaging methodologies generally fail to represent real-world conditions and cannot be transferred out of academia or clinic.

This thesis aims to find quantitative indices of cognitive load from autonomic signals with a focus on methodologies that could allow their use in non-controlled conditions.

HRV, EDA and respiratory signals were acquired with two different protocols: the first focuses on programming and is part of a multidisciplinary project, called BASE, conducted with the Universidade de Coimbra. The second includes a series of standard autonomic stressors and elicits cognitive load with the N-Back test.

Along with classical time-domain batch methods, mono- and bi-variate time-variant models were applied to track frequency variations in time and compute new indices. This approach is well-known in the study of the HRV but relatively new in the study of EDA. The relations between the HRV and the EDA signals, which are still under-researched, were also analysed.

Lastly, several indices able to significantly ($p < 0.05$) discriminate cognitive load from other conditions (sit, stand and controlled respiration) were identified. The multimodal approach allowed investigating the commonalities and differences in the information provided by HRV and EDA signals. Specifically, the results suggest that they react differently to different stressors and thus provide complementary information which allows discriminating cognitive load from a wider set of autonomic activations.

Key-words: autonomic system, signal processing, cognitive load, EDA, HRV.

Sommario

La capillare diffusione di smartphones e dispositivi wearable ha esteso gli ambiti di applicazione dell'analisi di segnali. Nonostante i vantaggi dei segnali autonomici, sia per quanto riguarda la praticità che il costo di acquisizione, la maggior parte degli studi scientifici volti a indagare i meccanismi fisiologici che si accompagnano ai processi cognitivi ed estrarre indici quantitativi di sforzo mentale si concentrano su segnali e immagini del sistema nervoso centrale. Tuttavia, gli studi che fanno uso di tecniche di brain imaging difficilmente possono ricreare le condizioni della vita reale e la strumentazione non può essere usata fuori dal laboratorio o ospedale.

L'obiettivo di questa tesi è identificare indici quantitativi di sforzo cognitivo con un focus su metodologie che possano essere utilizzate anche in situazioni non-controllate. L'HRV, l'EDA e il segnale respiratorio sono stati acquisiti all'interno di due protocolli: il primo si concentra su task di programmazione e rientra nel progetto BASE, condotto assieme all'università di Coimbra. Il secondo si compone di una serie di stimoli autonomici e uno stimolo cognitivo (N-back).

Oltre che ai classici metodi batch, sono stati applicati degli algoritmi mono- e bi-variati per seguire gli andamenti nel tempo ed estrarre nuovi indici. Questo approccio, già validato nello studio di HRV, è invece relativamente nuovo nello studio di EDA. Sono state inoltre analizzate le relazioni tra il segnale di HRV e EDA, che sono ancora poco studiate in letteratura. Infine, vari indici che variano significativamente ($p < 0.05$) tra il task cognitivo e gli altri task sono stati identificati. L'approccio multimodale ha permesso di ricercare gli aspetti in comune e le differenze tra l'informazione fornita dai due segnali. In particolare i risultati suggeriscono che varino in maniera diversa in risposta ai vari stimoli e che quindi forniscano informazione complementare che permette di distinguere lo sforzo cognitivo da un numero più ampio di stimoli autonomici.

Parole chiave: Sistema autonomo, analisi di segnali, sforzo cognitivo, EDA, HRV.

Contents

Abstract	i
Sommario	iii
Contents	v
1. Introduction	1
1.1 Biosignals and cognitive processes	1
1.2 The Autonomous Nervous System	3
1.2.1 The regulation of the heart.....	4
1.2.2 The electrodermal activity.....	6
1.3 Extraction and analysis of the signals of interest	8
1.3.1 Heart Rate Variability	8
1.3.2 Respiratory signal.....	11
1.3.3 Multivariate Analysis: HRV and Respiratory signal	13
1.3.4 Electrodermal Activity.....	14
1.4 Applications in cognitive tasks.....	19
1.4.1 The HRV and respiratory signals.....	19
1.4.2 The Electrodermal Activity	20
1.5 Open problems.....	22
1.6 Analysis of biosignals in software engineering: the BASE project.....	25
1.6.1 Study 2 of the BASE project	26
1.7 Objective of the thesis	28
2. Data Acquisition	29
2.1 BASE Protocol	29
2.1.1 Experimental setup	29
2.1.2 Experimental Protocol	31

2.1.3	Manual Annotation.....	33
2.1.4	Dataset Validation.....	33
2.2	N-Back protocol.....	34
2.2.1	Experimental Setup.....	34
2.2.2	Experimental Protocol.....	35
2.2.3	Dataset Validation.....	36
3.	Materials and Methods: Data Analysis.....	37
3.1	Pre-processing.....	37
3.1.1	Electrocardiogram - Tachogram.....	37
3.1.2	Respiratory signal - Respirogram.....	38
3.1.3	Galvanic Skin Response.....	39
3.2	Bivariate analysis: HRV and respiration.....	40
3.2.1	Model description.....	40
3.2.2	Time-Variant autoregressive algorithm.....	43
3.2.3	Spectral estimation.....	46
3.2.4	Instantaneous respiratory frequency.....	48
3.2.5	Feature extraction.....	48
3.3	EDA Analysis.....	51
3.3.1	Phasic and Tonic Decomposition.....	51
3.3.2	Time-frequency analysis.....	52
3.3.3	Features extraction.....	55
3.4	Analysis of interactions: HRV-EDA.....	57
3.5	Statistical analysis.....	60
3.5.1	Differences across tasks.....	60
3.5.2	Correlations.....	61
4.	Results and Discussion.....	64
4.1	TVAR Model validation.....	64
4.1.1	Model order.....	64
4.1.2	Control on the error.....	66
4.1.3	Initialization.....	68
4.2	Spectrograms and features extraction.....	69

4.2.1	Spectrograms.....	69
4.2.2	Time-Frequency domain features	74
4.3	EDA decomposition analysis	78
4.4	EDA Time-frequency analysis	80
4.4.1	Time-Frequency domain features	83
4.5	EDA - HRV Cross-Correlation.....	85
4.6	Statistical Analysis: Differences Across Tasks.....	87
4.6.1	BASE protocol.....	87
4.6.2	N-Back Protocol.....	94
4.7	Statistical Analysis: Correlations.....	103
4.7.1	BASE.....	103
4.7.2	N-Back protocol.....	107
5.	Conclusion and future development	111
	Bibliography.....	114
A.	Appendix	123
	List of Figures.....	129
	List of Tables	133

1. Introduction

1.1 Biosignals and cognitive processes

The number of research studies that investigate the effect that cognitive functions have on biological signals has been increasing in the last years. The main aim is to uncover the main physiological mechanisms that underly a variety of cognitive processes and possibly exploit this knowledge for research, therapy and commercial applications.

Most of these studies focus on the monitoring of the activity of the Central Nervous System (CNS) during cognitive tasks by means of brain imaging techniques such as Electroencephalography (EEG), Functional Magnetic Resonance Imaging (fMRI) or Functional Near-Infrared Spectroscopy (fNIRS). However, the equipment of brain imaging technologies such as MRI and NIRS is bulky and expensive and is not suitable for applications outside laboratories and hospitals. Moreover, even cheaper and lighter brain imaging techniques such as the EEG could affect the validity of research outcomes as they fail to represent real-world conditions during the experiment. Indeed, they need a long set-up time and can be uncomfortable to wear and, for these reasons, the application of such instruments outside the experimental setup is limited. Nowadays, wearable and less expensive devices for EEG recording are also available on the market, but still have some limitations related to comfortability and the quality of the signal compared to more traditional devices [1].

A way to overcome these limitations is to analyse biosignals related to the activity of the Autonomic Nervous System (ANS). Autonomic signals such as the Electrocardiogram (ECG), the heart rate variability (HRV) and the Electro Dermal Activity (EDA) can be acquired much more easily with less expensive instrumentation. Multiple commercial-grade wearable devices equipped with photoplethysmographic (PPG) and galvanic skin response (GSR) sensors are already available at a modest price and open up the possibility of online processing of biological signals in real-world conditions.

Despite autonomic signals cannot give a direct measurement of brain mechanisms, emotion and cognition seem to have an impact also on the ANS [2],[3],[4]. For this reason, the number of studies that adopt autonomic indices as a correlate of cognitive functioning is nowadays increasing. Moreover, given the deep interrelations between the CNS and ANS, which will be discussed in the next chapter, it is reasonable to hypothesize and study a correlation between the measures obtained from these two branches.

1.2 The Autonomous Nervous System

The ANS controls visceral reflexes, is largely involuntary and its activity almost never reaches the level of consciousness. It is influenced by the CNS through the central autonomic network (CAN) with the objective to react to stimuli from the environment and maintain the homeostasis.

The autonomous nervous system can be divided into enteric, sympathetic (SNS) and parasympathetic (PNS), as sketched in Figure 1.1. The enteric nervous system controls gastrointestinal functions. It is almost completely independent from the CNS [2] and therefore not an object of the present work.

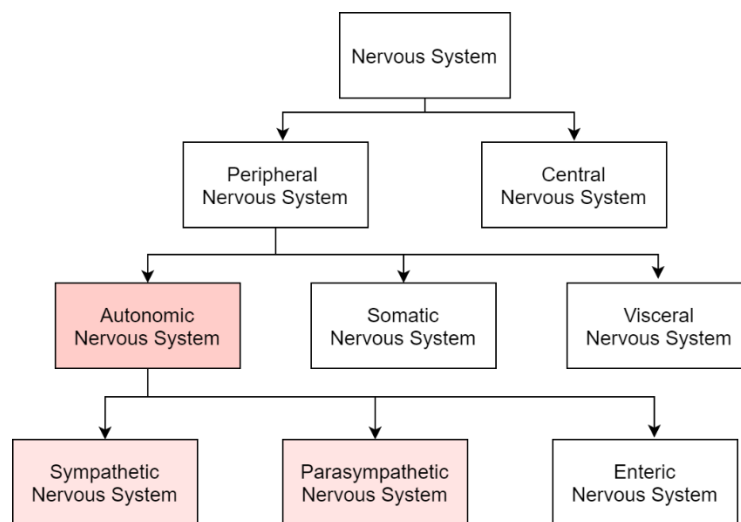


Figure 1.1: Main subdivisions of the nervous system

The sympathetic and parasympathetic branches have much more connections with the CNS and, as described for the first time by Walter B.Cannon in “The Wisdom of the Body” [5], have diametrically different functions. The sympathetic nervous system primes the body for action, triggering the so-called “fight or flight” response. The parasympathetic nervous system, on the other hand, is predominant when the body is at rest and activates the so-called “rest and digest” activities. Both sections are tonically active and work together with each other and the somatic nervous system. The balance between the two varies in response to external or internal stimuli and is mediated by the CNS [2].

A general anatomical organization of the sympathetic and parasympathetic branches of the ANS is reported in Figure 1.2.

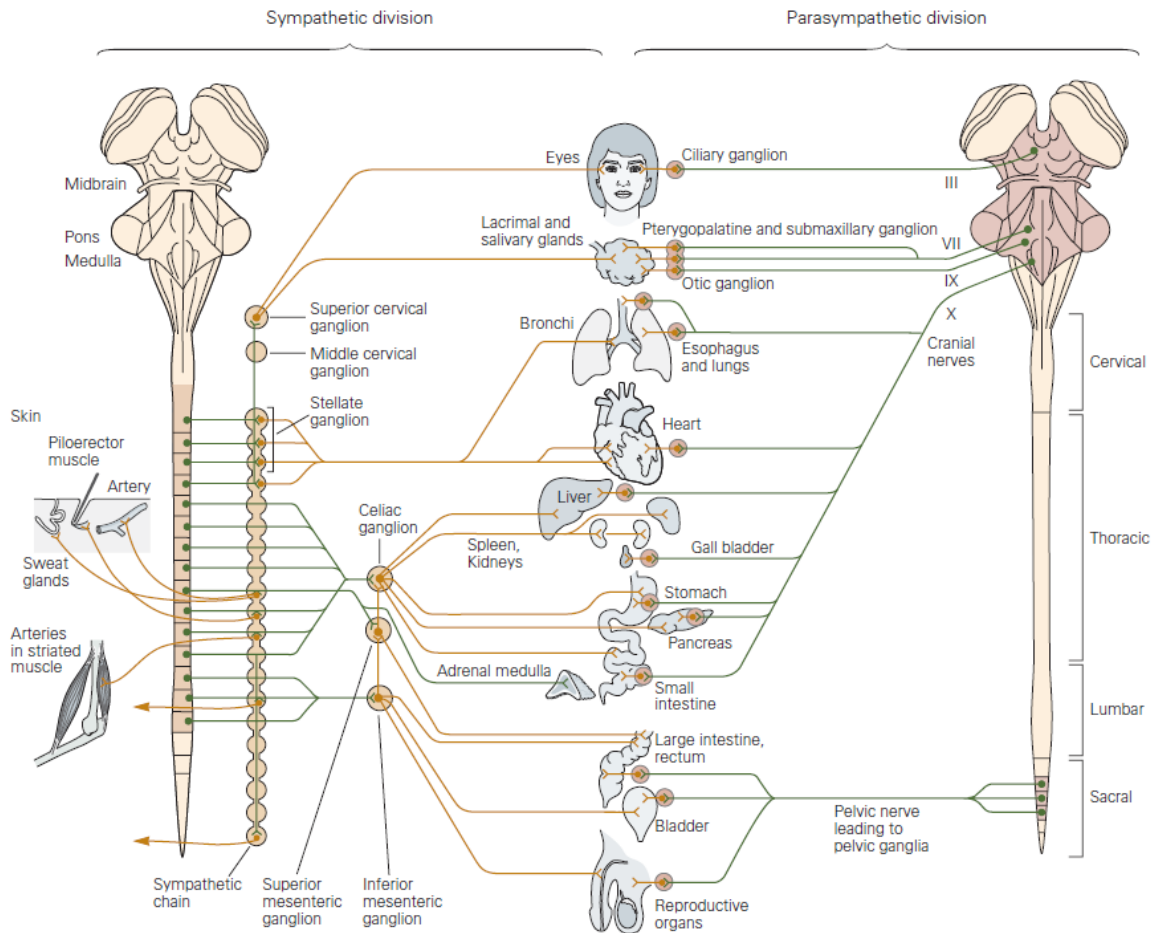


Figure 1.2: The Autonomic nervous system. Adapted from [2].

As depicted in Figure 1.2, many organs are to some degree controlled by the ANS and consequently can be monitored to analyse its activity. Among them, the heart and the skin are arguably the most studied in the biomedical signal processing field for the analysis of the autonomic regulation. This is performed through the analysis of the HRV and the EDA signals. The respiratory activity is also of interest, especially for the study of its interaction with the HRV.

1.2.1 The regulation of the heart

The heart, thanks to the action of the pacemaker cells that are mostly concentrated in the sinoatrial node (SA), has the intrinsic ability to contract rhythmically. In addition to that, the sympathetic and parasympathetic systems act at the SA to finely regulate

the rhythm. As a result, the time distance between successive heartbeats is never constant.

The parasympathetic nervous system has the effect of lowering the heart rate and its action predominates at rest. Indeed, in physiological conditions the heart is under tonic inhibitory control from the vagus nerve [6]. The sino-atrial node has an intrinsic frequency that ranges from 90bpm to 107bpm, decreasing with age. The effect of the tonic parasympathetic activity is to lower the intrinsic frequency of about 20-30bpm [7].

The sympathetic system, instead, has the effect of increasing the heart rate and blood pressure. The increase in blood pressure is obtained by contracting the arteries, on which the SNS has a tonic activity. Indeed at rest the arteries have around half of their maximum diameter [2].

The mechanisms by which the two branches of the ANS affect the heart are different and act with different speeds, creating distinguishable rhythms in the spectrogram of the heart rate variability signal, as will be discussed in chapter 1.3.1.2.

This regulation is strongly dependent on the blood pressure, through the action of the alpha baroreceptors [8], and the respiration, which acts mechanically and at the autonomic level with a mechanism called respiratory sinus arrhythmia (RSA) [9]. The heart rate adapts to maintain the blood pressure in the desired range and synchronizes with respiration to optimize the oxygen intake. These interactions can be studied using multivariate models, as will be discussed in chapter 1.3.3.

However, the control of the heart is not limited to the variation of blood pressure and respiratory activity. Indeed, as was systematically investigated for the first time by Claude Bernard (1813 – 1878), there are direct and indirect connections between the brain and the heart. In particular, many pathways link the frontal cortex to the Central Autonomic Network. As such, the HRV is a reliable index of the CNS-ANS integration [3]. A general overview of these connections is presented in Figure 1.3. These pathways play a central role in heart rate regulation as a response to emotional and cognitive stimuli [3].

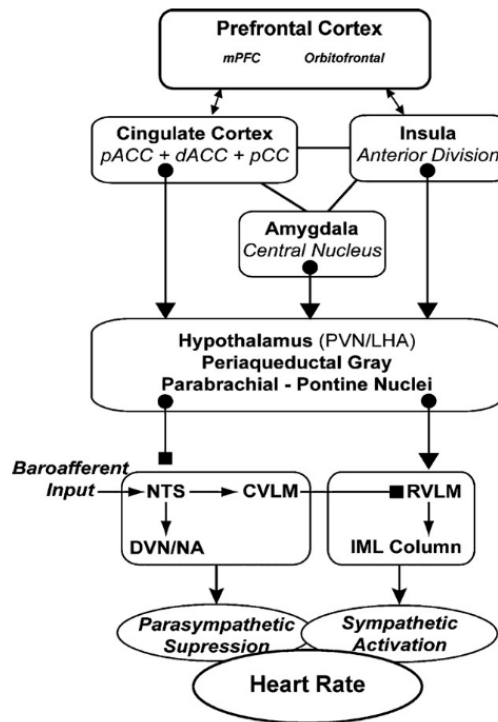


Figure 1.3: Central control of the HRV. Adapted from [3].

1.2.2 The electrodermal activity

EDA measures the changes in the skin conductivity generated by the secretion of sweat from the glands and the filling of the ducts [10]. The sweat rises in a varying number of ducts (shown Figure 1.4) and in different amounts, proportionally to the sympathetic activation. There are two types of sweat glands in the human skin: the apocrine and the eccrine. The apocrine are found in the armpits and the genital area. The eccrine are present in most of the body surface and are primarily involved in thermoregulation. These glands, particularly those located on the palms of the hands and the soles of the feet, are also responsive to a wide range of stimuli and have been more intensely studied.

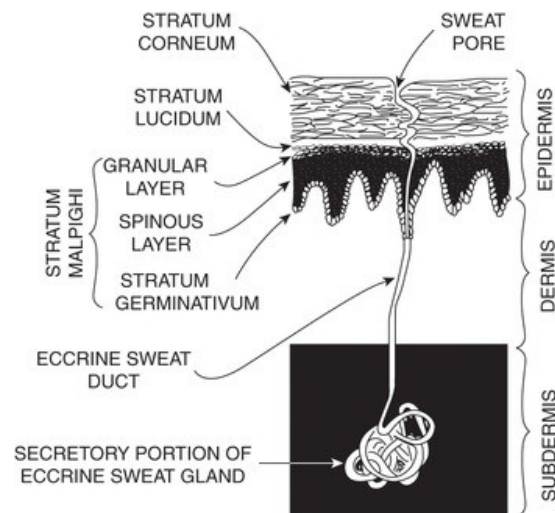


Figure 1.4: The eccrine sweat gland anatomy. From[4].

The skin is exclusively innervated by the sympathetic nervous system. The review by H. Critchley provides a neurophysiological explanation of the mechanisms that produce EDA [11]. The author analyses the different brain regions that have been proven to be related to electro dermal responses. These areas, which are sensitive to different stimuli, generate electro dermal responses using different pathways. Nevertheless, identifying the specific neural pathways involved requires the use of brain imaging techniques and is not possible using standard EDA recordings.

EDA is one of the most used response systems in psychophysiology [4], probably because of its ease of measurement and sensitivity to psychological states. A skin conductance response (SCR) can be measured as a reaction to a single discrete stimulus, which makes it a highly discriminable response. The latency between stimulus presentation and SCR onset is about 1-3 s [4].

Both stimuli that are unexpected and determine a transition from automatic to controlled processing and stimuli that are experienced as relevant and determine an allocation of resources are known to elicit SCRs. Two main typologies of studies can be identified: studies that investigate EDA as a reaction to the presentation of discrete stimuli, such as sound bursts or images, and studies that look for non-specific responses obtained during the presentation of chronic stimuli, such as performing a task.

1.3 Extraction and analysis of the signals of interest

This chapter briefly presents the signals of interest in this thesis, namely the heart rate variability, the electro dermal activity and the respiratory signal, and some of their most common quantitative indices.

1.3.1 Heart Rate Variability

The HRV signal, also called RR series or tachogram, is the time series of the distances between consecutive heartbeats, measured on a time window of the desired length. The interval between two QRS complexes is also called normal-to-normal or NN interval [12].

The HRV can be extracted from the ECG using, for instance, the Pan Tompkins algorithm [13]. A single channel recording is sufficient for this purpose, so it can be obtained with as little as three electrodes, typically placed so as to capture the first lead of the Einthoven triangle [14].

Alternatively, PCG sensors or even high-quality videos of the face can be used [15],[16].

Figure 1.5 shows a typical ECG on which the peaks have been identified and used to create a RR series.

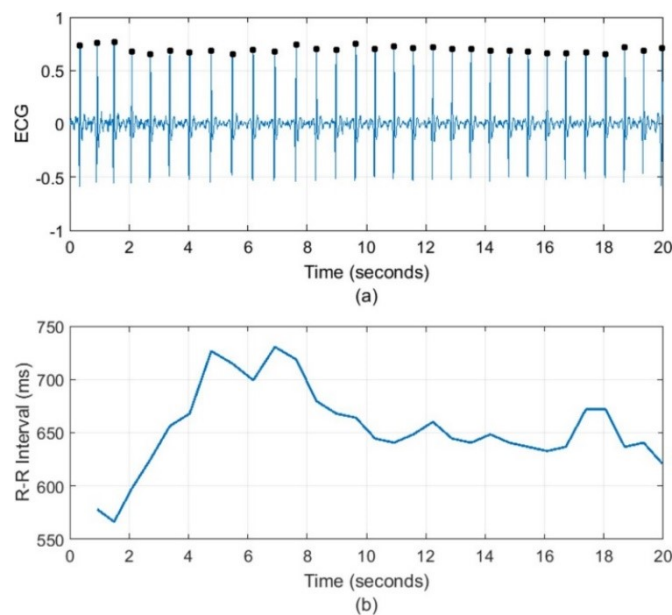


Figure 1.5: ECG signal and corresponding RR series. Adapted from [17].

The HRV signal can be considered as an impulse train in which the heights represent the time distances between heartbeats [18]. Such representation, called interval spectrum, is one of the possible solutions proposed to allow the frequency analysis of the HRV signal [19].

Features can be extracted in the time domain, in the frequency domain or with a non-linear approach. The time windows can be classified as ultra-short-term (between 2 and 5 minutes), short-term (around 5 minutes) and 24-hours measurements [20].

1.3.1.1 Time domain and non-linear analysis

The time domain indices are statistical measures of the HRV signal computed on a time window. The length of the window can vary widely, having care that the measurements obtained on different time windows are not directly comparable and estimate different physiological processes. The window should also be long enough to allow for a robust estimation [20].

The most widespread time domain indices used in literature are:

- **SDNN**: the standard deviation of the NN interval. A time window of 5 minutes for short term recordings and 24h for long-term recordings is recommended for the computation of SDNN [20], even if different window lengths have been proposed in the literature. It should be noted that SDNN is mathematically equal to the total power of the signal, which can be also calculated from the spectral analysis thanks to the Parseval theorem.
- **RMSSD**: the square root of the mean squared difference of successive NN intervals. It is a measure of high frequency variations in heart rate so short term measurements of around 5 minutes are preferred. It is an index of vagally mediated control of the hearth that highly correlates with the power in the high frequency band calculated through spectral analysis
- **pNN50**: the proportion of NN intervals greater than 50ms on the selected time window. It is strongly correlated to RMSSD, which should be preferred thanks to its superior statistical properties [12].

It has been experimentally shown that the HRV presents non-linear characteristics [21]. In particular, it is self-similar, i.e. present the same characteristics at different scales, within a certain range. This property, which is typical of many physiological systems, is called fractality and can be quantified through non-linear analysis [22]. Among the methods that have been proposed in the literature to quantify non-linear dynamics from the HRV most must be conducted on long series (i.e., at least 24 hours) to produce meaningful results. The entropy, which in information theory is

defined as the amount of information produced [23], also requires long series to be estimated. However, a measure of complexity closely related to the entropy called sample entropy (SampEn) can be estimated on short segments.

SampEn is actually a set of statistics defined as “the negative natural logarithm of the conditional probability that two sequences similar for m points remain similar at the next point” the probability is estimated without counting self-matches [24]. The more self-similar a series is, the lowest is the value of SampEn.

1.3.1.2 Frequency domain analysis

In the frequency domain features are extracted from the Power Spectral Density (PSD) of the signal. In short-term recordings, three main spectral components can usually be identified in the spectrum. One in the very low frequencies (VLF) i.e. $<0.04\text{Hz}$, one in the low frequencies (LF) i.e. between 0.04 and 0.15Hz and one in high frequency (HF) i.e. between 0.15 and 0.4Hz . An example of power spectrum is depicted in Figure 1.6.

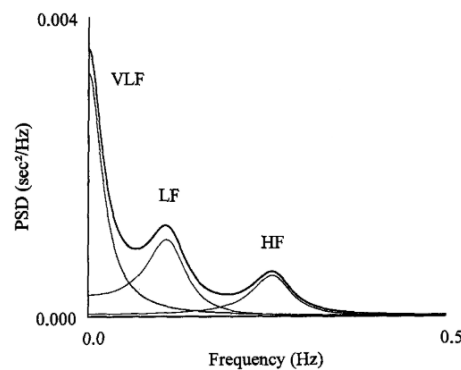


Figure 1.6: Typical HRV spectrum. Adapted from [25]

The most used features are the power in the three frequency bands in absolute and normalized units, the ratio between the power in LF and HF (LF/HF) and the total power of the spectrum.

The distribution of power in these frequency bands reflects variations at the level of the ANS. The interpretation of the VLF is the most dubious, especially for very short recordings (<5 minutes) in which its correct estimation is impossible, so this component is often discarded [12].

The LF is mostly associated with the activation of the SNS but it should be noted that also the PNS system can be involved in this frequency band [26].

The HF component is almost exclusively associated with the vagal activity and synchronization with the respiration, so it is considered a pure indicator of

parasympathetic activation.

The LF/HF ratio is commonly used as an indicator of the sympathovagal balance. Despite the widespread diffusion of this index, some authors warn against its use [27],[28], mainly because the interaction of the ANS on the HRV is actually more complex and non-linear, especially in the LF band [28] which makes this index strongly biased [29].

Different methods for its estimation have been developed. The choice of the best one depends on the specific application and strongly affects the results. Approaches for frequency analysis of the HRV can be divided into parametric and non-parametric.

Non-parametric methods rely on the Fast Fourier Transform of the signal, with appropriate expedients to reduce the variance of the estimation, such as the Welch method and the Bartlett method.

Parametric methods rely on the assumption that the signal can be represented as generated by a mathematical model which takes in input a white noise. The family of the model and its order must be decided a priori and strongly influence the quality of the estimation. The parameters of the model are calculated from the signal and used to compute the power spectrum. In the case of HRV, the most used family of models is the auto regressive (AR), and the order needs to be optimized according to the characteristics of the signal and the algorithm used. Typical values range from 6 to 22 [30].

The extraction of HRV parameters on time windows rely on the assumption of signal stationarity and, therefore, do not consider transient events that could carry meaningful information. In addition, they cannot be used for online processing. To keep track of fast changes time-frequency analysis of the HRV signal is more appropriate. The most common approaches are: non-parametric methods based on linear filtering such as the Short-Time Fourier Transform or the Wavelet Transform, non-parametric quadratic representation, such as the Wigner-Ville distribution and parametric methods with time-varying coefficients [31], [32], [33].

Time-variant algorithms offer a fundamental advantage over classical batch methods for their ability to adapt to always changing physiological conditions and can be used in online applications.

1.3.2 Respiratory signal

The respiratory signal can be acquired in many different ways [34]. Among them several are comfortable and non-invasive, for example chest straps that measure movements, strain sensors [35], sensorized T-shirts equipped with piezoresistive

electrodes and systems based on measurements of respiratory sounds [36]. The respiratory signal can also be extracted from the ECG [37]. In [Figure 1.7](#) is reported an example of a respiratory signal recorded with a sensitive girth sensor.

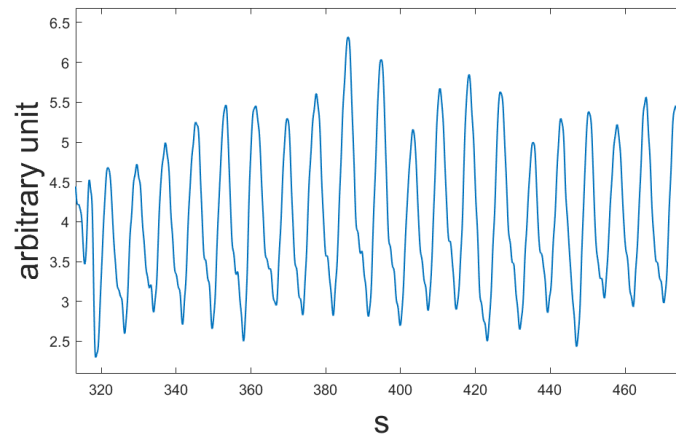


[Figure 1.7](#): Respiratory signal recorded with a girth sensor

Some of the most commonly used features that can be extracted from the respiratory signal measured with wearable devices are the respiratory rate, the inspiratory and expiratory time, the variance of the respiratory signal [38],[39].

Spirometric devices, that can be used to obtain information about gas exchange and metabolic activity, are not discussed in this thesis.

1.3.2.1 *The respirogram*

The respiratory signal is also analysed with the HRV signal to assess their dependencies. To do so, from the respiratory signal it is possible to create a new signal synchronous with the tachogram taking one value of the respiratory signal for each QRS peak of the ECG. This signal is called respirogram and, under normal conditions, contains practically the same information of the whole respiratory signal even if it is irregularly sampled [40]. An example of a tachogram and respirogram series is presented in [Figure 1.8](#).

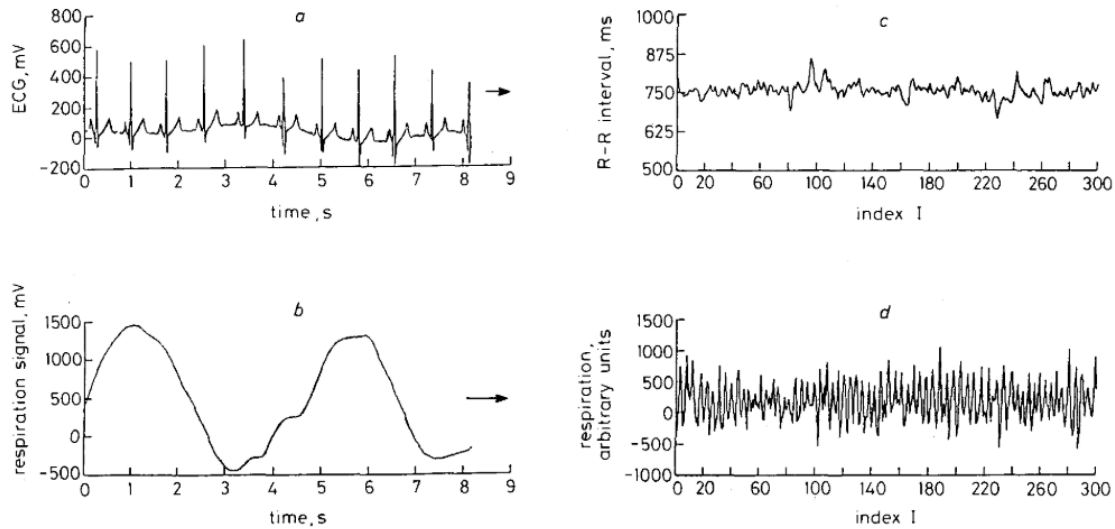


Figure 1.8: ECG and respirogram and respective tachogram and respirogram [40].

1.3.3 Multivariate Analysis: HRV and Respiratory signal

The heart rate, arterial blood pressure and respiration are not independent, due to multiple mutual interactions. These signals, or time series, can be analysed simultaneously to assess and quantify their relations, through for example cross-correlation analysis or, in the frequency domain, computing the cross-spectrum.

However, the simple correlation has some limitations. For example, it cannot be used to assess causality, since it does not provide directionality for the effect, neither it excludes that two series have a common effect. Results are also difficult or impossible to interpret when feedbacks occur.

A deeper understanding of the HRV mechanisms can be obtained using models that consider the complex interactions among the systems that act on the regulation of the heart.

These interactions can be quantified by means of Autoregressive Multivariate (MVAR) analysis [8],[41],[42]. The use of models allows to separate feedforward and feedback actions, identify oscillation sources, evaluate correlations along specific directions, decompose signals and spectra. Physiological knowledge can be used to guide the choice of the model structure using a grey-box approach. On the other hand, the use of interpretative models allows quantifying and better interpret physiological interactions. The parameters can be estimated using least-squares algorithms [31, chapter 5]. These models can be used also for non-stationary signals

with adaptive extensions [41].

The causal interactions (e.g., of the respiratory signal on the HRV) can be assessed from MVAR models relying on the definition of Granger causality. Indeed, C. Granger provided a useful definition of causality based on the assumption that if a stochastic time series X is causing another stochastic time series Y the knowledge of past values of X will help in predicting Y [43]. The definition allows to create partial spectra and define the causality coherence. It should be noted that this is not a definition of “real” causality and to avoid confusion the term “Granger-causality” is more appropriate. Nevertheless, it is an useful definition that found many applications in the biomedical field.

However, these methods can fail in the case of low-quality signals or in situations that do not satisfy the modelling assumptions, for example because of big inter-subjects variations.

1.3.4 Electrodermal Activity

The most common way to measure EDA is to apply two electrodes close to each other on the skin with a small resistor in series with the skin and hold constant the voltage between the two. Since the resistance of the skin is several orders of magnitude higher than the resistance used by the sensor the latter can be considered negligible. Therefore, the conductance on the skin, which is the inverse of the resistance, is straightforwardly extracted from the measured current using Ohm’s law $I = E/R_p$, where E is constant. This technique is called “exosomatic recording” [44].

Two main components can be identified in the recorded signal and are represented in [Figure 1.9](#): Skin Conductance Level (SCL) and Skin Conductance Response (SCR).

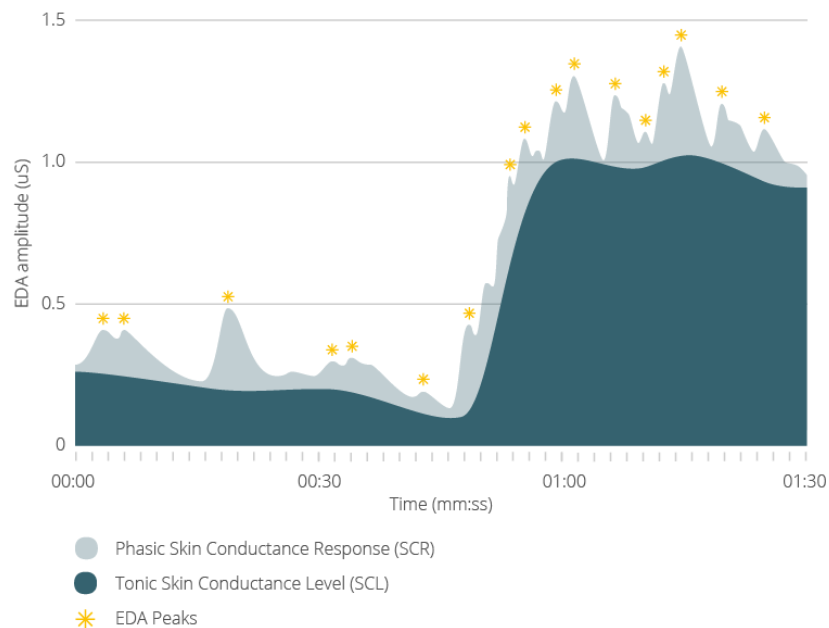


Figure 1.9: Decomposed EDA signal, adapted from [45].

SCL is the tonic component, characterised by slow variations. SCR is the phasic component and its variations are much faster and have lower amplitudes compared to SCL. These variations can be triggered by an external stimulus or happen spontaneously; in this case they are also called “nonspecific SCR” (NS-SCR). The SCR component is the most used to assess psychological states [4].

1.3.4.1 Time Domain analysis

The EDA signal is typically analysed in the time domain, in which many measurements can be conducted. Features can be calculated on the decomposed tonic and phasic signals or directly on the total EDA signal.

From the total signal, some statistics such as mean value, variance (or standard deviation), skewness and kurtosis can be computed [46].

The most common features related to the phasic component are:

- the *amplitude*, defined as the increase in conductance after the stimulus onset;
- the *latency*, defined as the time interval between stimulus onset and SCR initiation;
- the *rise time*, i.e. the interval between initiation and peak;

- the *half recovery time*, that is the interval between the peak and the 50% recovery in amplitude;
- The frequency of SCR events. This feature is computed for NS-SCR.

A graphical representation of the features mentioned that can be computed on a single SCR is presented in Figure 1.10.

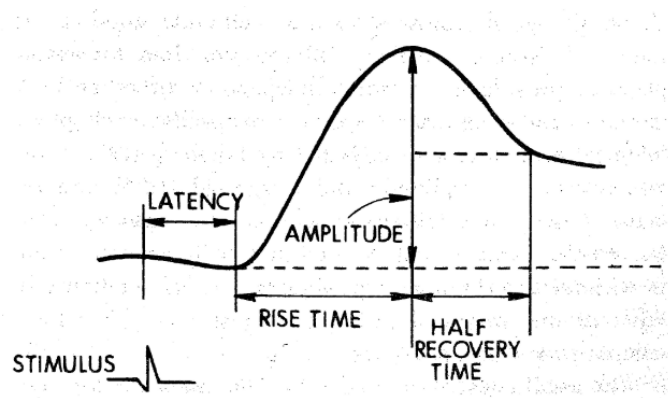


Figure 1.10: Adapted from [4].

Benedek et al. also proposed as feature the area under the phasic driver, called Integrated Skin Conductance Response (ISCR) [47].

Separating the tonic and phasic components and identifying the single SCR peaks is vital for a correct analysis of the EDA signal in the time domain. Visual inspection or simple automatic comparison of individual peaks against a baseline is often impractical. For this reason, several more advanced model-based methods have been proposed for the tonic/phasic decomposition of EDA.

Bach et al. proposed a linear convolution model which assumes that SCRs are generated by a system that is linear and time-invariant [48].

Benedek et al. developed a non-negative deconvolution method called “Discrete Decomposition Analysis”, which is available in Ledalab, a MATLAB toolbox [49]. The algorithm assumes that SCRs have a shape that varies among different subjects but is approximately constant within the same subject and can be represented with a biexponential function which parameters τ_1 and τ_2 have to be estimated. Thus, SCRs can be seen as the response of a system to a driver function composed of positive impulses, which has to be estimated. The remainder is interpolated using a cubic spline to estimate the tonic activity. This is performed starting with a predefined set of parameters which is then optimized re-running the algorithm with many different parameters set. The advantage of this methodology is that peaks can be detected on

the driver, thus solving the problem of overlapping SCRs that cannot be separated by simply imposing a threshold. The same group also proposed a more robust variation of the algorithm, called “Continuous Decomposition Analysis” (also available in Ledalab) that relaxes the condition of non-negativity which will be discussed in chapter 3.3.1.

A different algorithm called *cvxEDA* which perform a non-negative decomposition of the EDA signal by means of convex optimization was also proposed [50]. The algorithm computes a phasic driver similarly to the beforementioned methods but describes the EDA signal as a linear combination not only of phasic and tonic components but also of noise.

1.3.4.2 *Frequency Domain analysis*

Posada-Quintero et al. have recently proposed to study electrodermal activity in the frequency domain analysing the Power Spectral Density of the signal [51]. The activity of the sympathetic nervous system can be discerned as a spectral peak localized in the low frequency band (0.045 – 0.25Hz). The proposed index, called *EDASymp*, was found to be responsive to sympathetic activation induced under orthostatic, physical and cognitive stress. Rocco et al. applied the index to the exploration of the physiological response to an online gambling task [52] and obtained from *EDASymp* comparable discriminative power compared to classical HRV features.

Posada-Quintero et al. introduced also a new more sensitive index, similar to *EDASymp*, called *TVSymp* [53]. This index has the advantage of being time-variant, allowing for better tracking of the sympathetic tone.

The analysis of the EDA signal in the frequency domain was proposed to overcome one of the main limitations of the analysis of HRV in the frequency domain, i.e. the impossibility to perfectly isolate the sympathetic component in the LF band [51].

Ghiasi et al exploited further the EDA time-frequency analysis creating a new index of sympathovagal balance [29]. The index is meant to overcome the limitations of LF/HF produced by the parasympathetic influence in the low frequency band by substituting *EDASymp* to the LF component. Since the skin is exclusively innervated by the SNS, *EDASymp* is expected to be a more reliable index of sympathetic activation. The analysis was carried out in time-frequency using a standard Short Time Fourier Transform for the EDA series and point-process modelling for the HRV series. In the preliminary study, the index yielded satisfactory results.

The first index of EDA in the frequency domain proposed in the literature, *EDASymp*, was calculated applying the Welch method on the phasic component

obtained high passing the recorded EDA signal. The index does not allow to study frequency variations in time. The time-frequency representation needed to compute TVSymp was obtained via variable frequency complex demodulation, a time-frequency method characterized by very high resolution.

A method for visualizing the EDA signal inspired by the spectrogram called EDA-gram based on the sparse decomposition of EDA was also proposed [54]. The new visualization should allow for a more interpretable feature extraction.

Regardless of the method used, both in time and in the frequency domain, for a proper interpretation of the data it should be noted that EDA responses vary widely between subjects and suffer from habituation.

1.4 Applications in cognitive tasks

Some of the indices reported in the previous chapter have already found some applications in the analysis of cognitive functions. Several methods and approaches have been followed yielding heterogeneous results. This chapter contains a brief literature review of some of the methods used and the findings obtained.

1.4.1 The HRV and respiratory signals

Multiple authors reported that subjects with higher levels of HRV at rest usually perform better in cognitive tasks and that during the task can be observed a reduction of HRV and an increase in heart rate (HR). Thayer et al conducted several studies on the topic [3]. The stimuli used to elicit cognitive effort were the Stroop test [55] and the N-back test [56], both in normal and stressful conditions. Similar results were obtained by Hansen et al. [57] that proposed two tasks, one measuring the working memory (2-Back Test) and the other measuring continuous performance (a more complex test involving memory, reaction time and mental arithmetic) [58]. Forte et al. published a systematic review in which the relationship between resting HRV and cognitive function was investigated. Only studies including cognitive measures, measures of the HRV, healthy subjects and that contain measurements at rest were included. Among the 1417 potential articles identified only 20 survived the eligibility criteria and involved a total of 19431 people. All the selected studies found a positive correlation between resting HRV and cognitive performance, except for one study that did not find any correlation. Among the HRV measures reported the most frequent is HF, which is an indicator of vagal tone [59]. The studies from Thayer et al. and Hansen et al. used RMSSD as a measure of HRV, which is an index that highly correlates with HF. A stronger parasympathetic tonic control of the heart seems therefore to be associated with a better functioning of self regulatory mechanisms that allow for a better and quicker response to the environmental needs.

However, not all the results reported are consistent with the hypothesis that higher resting HRV is associated with better performance. Alba et al. investigated the association between the variations of EEG functional connectivity and HRV in resting state and looked for correlation with the results of a cognitive task performed [60]. The results obtained disagree with the previously mentioned studies: subjects with higher levels of HRV (calculated as LF, HF, RMSSD and SDNN) at rest made more mistakes during the cognitive task. The authors hypothesised that the association between resting HRV and cognitive performance may depend on the type and difficulty of the cognitive task.

Backs et al.[61] found a significant difference ($p < 0.05$) in the LF band of the heart rate variability, used as a measure of sympathetic tone, between two different difficulty levels of a working memory task. There also appears to be a widespread consensus that measures of vagally controlled HRV negatively correlate with the level of cognitive workload and stress, as reported among others by [62],[57] and [63].

These findings suggest that differences in HRV among different subjects may be used as a useful predictor of cognitive flexibility.

Alba et al. in the same study mentioned before also found, using partial correlations and multiple linear regression, that the correlation is only significant when mediated by neuronal oscillations (i.e., the correlation between HRV and errors is significant while partial correlation is not), a finding in agreement with the neurovisceral model proposed by Thayer et al.

All the studies mentioned in this chapter apply batch methods for the computation of the HRV. These methods have the limitation that they do not allow to study variations of HRV inside the time window selected, which must last at least a few minutes. Moreover, none of the studies used multivariate analysis to assess interactions among signals.

Grassmann et al. report that mentally demanding tasks generally increase the respiratory rate but do not affect the respiratory amplitude [64]. The result is that cognitive load appears to increase gas exchange, consistently with the higher metabolic demand induced by the cognitive activity.

1.4.2 The Electrodermal Activity

According to [4], performing cognitive tasks determines an increase in SCR: the sympathetic activation is explained as an allocation of resources to the task both because of the reaction to stress and the activation of attentional mechanisms. Indeed, patients with ADHD have reduced skin conductance responses to errors, which has been hypothesised could be caused by reduced processing of error significance [65].

Munro et al. [66] reported a significant increase in NS-SCR and SCL during an attentional task (0-Back test) compared to rest. Hinson et al. found a positive correlation between the level of SCR before the decision and the performance in a gambling task [67]. The relative level of Skin Conductance Responses also appeared to be higher for the good option. The authors made the hypothesis that higher levels of skin conductance are associated with perceived saliency, which produces an increment in arousal.

Some studies that include EDA frequency features and cognitive tasks have been conducted lately by H. Posada-Quintero et al. The authors published three articles that analyse EDA activity during cognitive tasks in 24-hours sleep deprivation [68],[69],[70]. Non-specific and time-frequency indexes of skin conductance were found to be correlated with cognitive performance. The correlation was significant only for the phasic component.

However, the number of studies that investigated electro dermal activity during cognitive tasks is limited compared to the heart rate variability.

1.5 Open problems

Numerous studies have proved that bio-signals related to the ANS can be used to assess psychological states. The results presented bode well that applications that use bio-signals for monitoring mental effort and stress in mentally demanding work conditions could become a reality in the foreseeable future.

However, some issues remain to be solved.

- 1- There is still a considerable dispersion of the knowledge in the field and some inconsistent results. Moreover, the literature lacks studies that investigate EDA responses during cognitive activities and few studies concerning the analysis of EDA in the frequency domain were conducted in general. No studies presenting an online analysis of EDA in the frequency domain were found in the literature review conducted.

The interrelations between the HRV and the EDA signal also remain mostly to be investigated. Practically applicable systems should obtain satisfactory performance in discriminative power. It is expected that combining the information provided by HRV and EDA could enhance the performance of the system. Knowledge of the analogies and differences in the information provided by different sub-systems of the ANS could be exploited to interpret the results and design better models for data processing and feature extraction. On the other hand, our knowledge of the psycho-physical processes involved in cognitive processes is still partial. Interpretative models can be used for a better understanding of these processes and explain the contradictions that arose in the literature.

- 2- Very different protocols, methods and signals have been employed. Some of the methods presented are fit for research studies in controlled conditions but cannot be applied in real-life conditions for a variety of reasons. The most important identified are:
 - a. The standard frequency domain analysis of HRV can produce unreliable results, for example when the fixed frequency bands do not correctly fit the real dynamics of the autonomic control, which often happens when the a-priori hypotheses are not respected. The classical subdivision of frequency bands for the assessment of sympathetic and parasympathetic control of the heart rate recommended by [12] is based on the assumption that the respiratory frequency, which is known to

influence the HRV through the mechanism of the RSA, lies in the HF band (0.015 – 0.4Hz). However, this is not always the case, even in physiological conditions. In some cases, the respiratory rate can fall in a lower range of frequencies, invading in this way the LF band, or can be higher than 0.4 Hz, typically during high-intensity exercise. These effects can significantly affect the results, e.g., including RSA, which is a phenomenon produced by the activity of the PNS, in the LF power computation, which is generally considered an index related to the activity of the SNS.

- b. Most studies in the frequency domain assume the stationarity of the signal, which is a hypothesis that odds with the practical need to track variations in time. Indeed, there is a need for robust, highly discriminative methods that can track the fast changes of the autonomic regulation. This is true for both the HRV and the EDA signals. Another desirable property of practical applications is the ability to give results in real-time. Yet most of the methods presented can only be applied offline and some of them, especially in the frequency domain, can only give results related to relatively long time-windows.

Some methods to solve problem 2 have already been proposed.

Problem 2.a can be addressed including the respiratory signal in the analysis. Goren et al. [71] proposed an algorithm for the automatic detection of time-varying spectral boundaries. Bailón et al. [72] proposed to adapt the high frequency band, centring it at the respiratory frequency. However, when the respiratory frequency is too low the LF and HF band may overlap. Hernando et al. [73] showed that adapting the bands according to the respiratory frequency increases the discriminative power of the HRV frequency features but had to exclude from the analysis the time windows in which the bands overlapped for more than 50%, leaving open the problem of finding methods robust enough to be applied in every physiological condition. Varon et al. [74] proposed an approach based on orthogonal subspace projections to separate linear influences of the respiration on the heart rate. The separation is not frequency-dependent and does not suffer from the problem of bands overlapping. Another possible technique to remove the respiratory component from the HRV is by means of appropriate parametric modelling that includes the respirogram, as described in [40]. The authors also proposed the new indices “Coherent power” and “Incoherent Power” that measure the coherence between the respirogram and the tachogram.

These measures of sympathovagal activity have the advantage that they are not dependent on the selection of frequency bands.

To address problem 2.b time-frequency methods can be applied. In particular, parametric time-variant models have the advantage that they can be applied in online applications.

However, no studies that make use of these strategies in cognitive applications were found in the literature.

1.6 Analysis of biosignals in software engineering: the BASE project

Coding is a complex task that involves heterogenous expertise including language processing, logical thinking and mathematical computations. Developers must read and interpret the code on different abstraction levels [75]. It is therefore a suitable task to be used in studies that investigate cognitive functions.

The doctoral thesis of Sebastian C. Müller [38] provides an investigation of the possible applications of biometric sensors to increase developers' productivity using machine learning. A wide number of different biological signals were extracted and used to develop classification models. Biometric measurements were used to assess the perceived difficulty and to identify code quality concerns, basing on the assumption that more difficult code is more likely to contain bugs. To extend the validity of the findings the studies were conducted both in lab conditions and on the field (i.e., working place).

Gonçales et al. published in 2019 a systematic mapping study focused on measuring the cognitive load of software developers to overcome the dispersion of the knowledge related to this problem [75]. The majority (18 out of 33) of the studies analysed used the EEG, most of the others used a combination of signals. Among the autonomic signals, the most frequently used were the ECG, Blood Volume Pulse (BVP) and EDA. Many of these studies aimed at developing machine learning techniques based on a set of metrics to identify the level of mental workload. The authors warn that the precision and the accuracy of the models identified in the articles that were analysed for the review is still too low for realistic scenarios.

The BASE project is meant to perform a more comprehensive analysis based on biosignals and neuroscientific knowledge. The rationale is not only to develop models for classification but also to better understand the physiological mechanisms that underly the production of bugs. Two reasons are behind the project:

- Software writing is an intensive human-made process that is consequently subject to errors that are difficult to find and have unpredictable consequences. The Software Fail Watch from Tricentis estimated that the global cost of software failures was about 1.7 trillion US dollars in 2017 alone [76].
- Recent studies show that software developers tend to commit a limited set of bug types, which account for most of the errors [77],[78]. The hypothesis that bugs have a causal link with a limited number of contexts that increase the

probability to make mistakes justifies the use of this information to improve software quality [79].

The key idea of the BASE project is to investigate the physiological mechanisms that could lead to the generation of bugs monitoring programmers during tasks of code comprehension and code writing. This objective is pursued by integrating different biological signals and relating the physiological state of the programmer with the line of code with the final goal to use the findings to improve software quality using a biofeedback augmented approach.

Both central and autonomic signals are investigated. Particular attention is devoted to signals that can be recorded with wearable devices and their connection with the brain mechanisms that generated them. The main reason why the analysis of these signals is especially important is that they can be easily acquired in working conditions.

Two research studies in the BASE project were conducted: study one took place at Universidade the Coimbra [79],[78] while the second at Politecnico di Milano [80].

Some findings have already been published in the context of the BASE project. Significant variations have been observed in the power spectral density of the EEG during software development [80]. Significant variations were also found in the pupil diameter during code inspection [79]. HRV features were used to build classification models capable to distinguish code snippets of different complexity with high accuracy [78]. The same group at the University of Coimbra investigated the role of the insula in bug detection using fMRI [81] demonstrating it plays a central role in the “Eureka” moment of bug discovery.

1.6.1 Study 2 of the BASE project

The original objective of the present thesis was to continue with the acquisitions of the study 2 of the BASE project to enlarge the dataset and use it to conduct all the analyses. The protocol included the acquisition of central (i.e. EEG and fNIRS) and autonomic signals (ECG, EDA, respiratory signal). An extensive description of the protocol is reported in chapter 2.1.

However, the acquisitions were stopped due to the ongoing COVID-19 pandemic before the minimum number of subjects that had been stated in the experimental protocol design was reached. In addition, the protocol required the participants to type on a keyboard using both hands. This requirement seriously affected the quality of the recorded EDA signal, which had to be discarded and was not used in future analysis.

A second simpler protocol called N-Back was added to overcome these limitations and obtain a more extensive analysis with a focus on the Electro Dermal Activity and its relation with the other autonomic signals of interest (HRV and respiratory signal). Indeed, understanding if HRV and EDA give similar or complementary information on the activity of the ANS is one of the goals of this work. The protocol contains a cognitive task (N-Back test) and other autonomic stressors, as will be discussed in chapter 2.2. The protocol was designed in such a way that the participants never had to move the hand on which the GSR electrodes were applied. Visual inspection confirmed that the quality of the signal collected for the second protocol is satisfactory. The description of this protocol is reported in chapter 2.2.

1.7 Objective of the thesis

The present work is focused on the analysis of the Autonomic Nervous System signals (i.e., ECG, respiratory signal and skin conductance) during cognitive tasks to investigate the feasibility of using autonomic indices for the assessment of cognitive load and comparing different methods for their analysis.

Two main goals were identified to guide the analysis:

- 1. Identify the most appropriate existing models for the extraction of quantitative indexes of mental effort and cognitive load and explore new techniques.**

For this purpose, a bivariate time-variant autoregressive model was selected for the analysis of the HRV and the respiratory signals acquired with the two protocols. Particular attention was spent on the choice of the most suitable hyperparameters and variations on the original model. Concerning the EDA signal, a time domain analysis was conducted using Continuous Decomposition Analysis. For the analysis in the time-frequency domain, instead, a time-variant approach was adopted and compared with the standard methods used in the literature.

- 2. Investigate the EDA signal during cognitive tasks and evaluate its relations with the HRV and respiratory signals.**

This objective was pursued in two ways:

Firstly, the HRV signal was cross-correlated with the EDA phasic component. The analysis in time domain allowed to identify the time lag between the two signals while the analysis of the cross-spectrum was used to identify if the two signals covary at specific frequencies.

Secondly, the features obtained from the HRV and respiratory signals were correlated with the ones extracted from EDA to evaluate if they provide similar information about the sympathetic activation.

2. Data Acquisition

2.1 BASE Protocol

Data were collected at the Centre for Ultrafast Science and Biomedical Optics (CUSBO), Politecnico di Milano, during the study 2 of the BASE project. The acquisitions started in September 2019.

The minimum number of volunteers was expected to be 30. However, the ongoing COVID-19 pandemic abruptly halted the acquisitions. Ultimately, only sixteen healthy subjects were enrolled in the study and screened to check that they respected the eligibility criteria.

According to the inclusion criteria, subjects had to be at least 18 years old and score at least 4 points out of 10 in a technical questionnaire meant to assess their coding skills in C programming language. Subjects with cardiac implanted devices, metallic prosthesis or known mental conditions were not eligible.

2.1.1 Experimental setup

Several biomedical signals and images were simultaneously recorded from the subjects and are listed in [Table 2-1](#).

Signal / Image	Sampling frequency	Equipment
Electrocardiogram (ECG)	2048 Hz	ProComp Infiniti SKU: T9306M SKU: T3425
Electrodermal activity (EDA)	256 Hz	ProComp Infiniti SKU: SA9309M
Respiration activity	256 Hz	ProComp Infiniti SKU: SA9311M
Screen recording		SensoMotoric Instruments, SMI
Pupilogram and eye movements	60 Hz	
Electroencephalogram (EEG)	256 Hz	64-chan EEG cap + SD LTM EXPRESS, Micromed S.p.A.
Functional Near Infrared Spectroscopy (fNIRS)	1 Hz	Machine designed and developed at the Department of Physics, Politecnico di Milano
Video Recording	30 fps	Logitech webcam

Table 2-1 Instrumentation used in BASE

Data related to the ANS, namely ECG, Respiratory signal and EDA were collected using the ProComp Infiniti [82], an 8-channel polygraph that allows for their synchronous acquisition.

Data of the respiratory signal and EDA were resampled to 2048Hz using previous neighbour interpolation to allow synchronization with the ECG signal. The data were then transferred to a PC in .txt format. The protocol was implemented in MATLAB. The synchronization of signals is fundamental for multivariate analysis. The start of the experiment was signalled using a trigger generated by the computer connected to the NIRS. The trigger is sent to the PC that runs the MATLAB script containing the protocol, the EEG acquisition system and to the ProComp, which saves it on a dedicated channel. The exact duration of the single tasks was saved by the protocol script on a dedicated timestamp file.

The screen used by the volunteers was recorded for the entire duration of the experiment.

2.1.2 Experimental Protocol

Data were acquired in a calm and relaxed environment. Before the beginning of the experiment, the participants were informed of the study objectives and protocol, in particular specifying that all data are treated anonymously and no judgment on the performance is made. It was also stressed that the procedure is non-invasive, safe and painless. Subjects were asked to sign the informed consent, which had been previously accepted by the ethical committee at Politecnico di Milano. The tasks were then explained and the subjects were taught how to use the controls and the equipment.

The first step of the protocol is the acquisition of a baseline for EEG and fNIRS. The subjects were asked to type randomly on the keyboard with their eyes closed for 2 minutes while EEG and fNIRS were collected.

The experiment is composed of two runs that were conducted in sequence. Before the beginning of each run the eye calibration took place. A schematic representation of the experimental protocol is reported in [Figure 2.1](#). Three different tasks were conducted in each run, in random order:

Text reading – read a short text in natural language (English). This task lasted for 60 seconds. Two different texts were presented (one for each run, randomly assigned).

Code reading – read a short snippet of simple code in C language. This task lasted for 5 minutes. Two different snippets were proposed (one for each run, randomly assigned).

Code programming – develop a function in C language in Eclipse environment. Subjects were allowed to stop this task after 5 minutes. The maximum time was 20 minutes. Two tasks of different difficulty were presented in random order (one for each run). The difficult task is called RLE and the easy task is called SPLIT.

Before each task and after the completion of the last task a relaxation phase that lasted for 30 seconds was conducted. During this phase, called “fixation”, subjects were asked to watch a black cross on a grey screen and relax.

After each run an Experiment Evaluation (EE) form was presented. The form, which took about 1 minute to be filled, asked to give a score from 0 to 5 to the following experiences: Mental effort, Task fulfilment, Pressure with time and Discomfort.

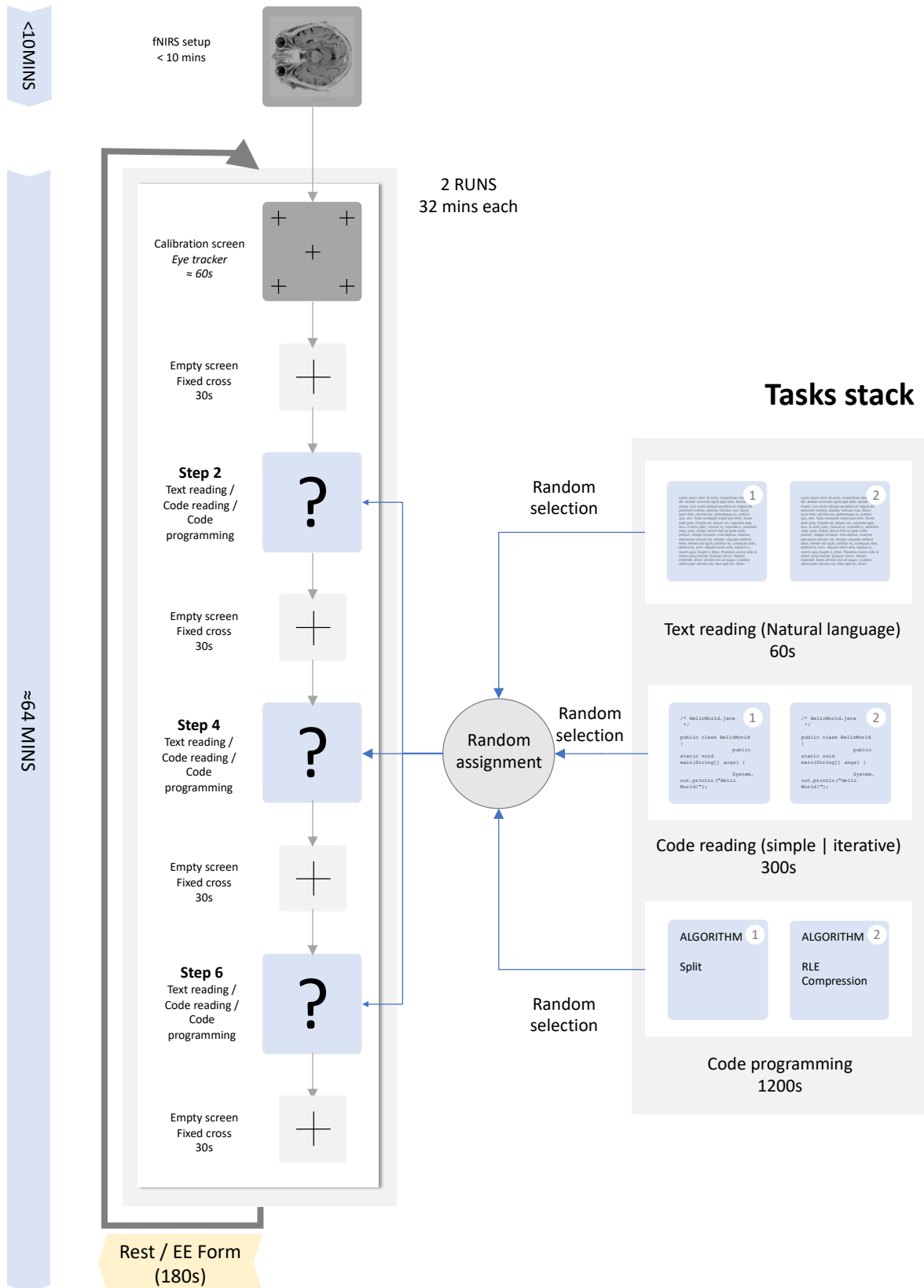


Figure 2.1: Schematic representation of the BASE protocol.

2.1.3 Manual Annotation

The code programming task was manually labelled starting from the screen recordings into:

- **Read problem:** the time spent by the participant to read the assignment, before starting to write the solution.
- **Writing:** the time spent actually writing code. There may be multiple Writing sessions for each Code programmin task.
- **Thinking:** the time during which the subject was not writing and neither reading the assignment. It is assumed to be time spent thinking about the solution. There may be multiple “thinking” sessions for each “code writing” task.

2.1.4 Dataset Validation

Sixteen subjects participated in this study. The average age was 29, standard deviation 9.6. Twelve were males and 4 females. Among the sixteen subjects who participated in the BASE protocol, three subjects were discarded because the quality of the ECG signal was too low to identify the peaks, even after manual correction. The final dataset is therefore composed of thirteen subjects, each one of them performed two runs.

2.2 N-Back protocol

The data related to this second protocol were collected at the B3 lab, Politecnico di Milano [83], specifically for the present thesis. The tasks were selected in order to have a sufficiently long baseline and already validated sympathetic and parasympathetic stressors to compare to the cognitive one.

Thirty-one young, healthy subjects were enrolled in the study. The proficiency test in C was not performed since coding skills are not necessary for this protocol.

2.2.1 Experimental Setup

The signals acquired were: EDA, ECG, BVP and respiratory signal. For their acquisition was used the same instrumentation used for the BASE study, i.e., ProComp Infiniti. The specifications are reported in [Table 2-2](#).

Signal / Image	Sampling frequency	Equipment
Electrocardiogram (ECG)	2048 Hz	ProComp Infiniti SKU T9306M SKU T3425
Electrodermal activity (EDA)	256 Hz	ProComp Infiniti SKU SA9309M
Respiration activity	256 Hz	ProComp Infiniti SKU SA9311M
Blood Volume pressure (BVP)	256Hz	ProComp Infiniti

Table 2-2 Instrumentation used in N-Back

Before the application of the sensors the skin and the electrodes were cleaned using an alcoholic solution to improve the conductivity of the skin. The GSR sensors were applied on the non-dominant hand, which is the left one for all participants.

The protocol was implemented in MATLAB and shown on a desktop connected to a personal computer. A second desktop, oriented to be visible only to the experimenter, was used to visualize the signals and monitor the experiment.

2.2.2 Experimental Protocol

Before the start of the experiment subjects were asked to read and sign an informed consent. After that, volunteers were instructed about the protocol. The participants were also asked to remain as still as possible, in particular not to move the left hand to avoid artefacts in the acquisition of the skin conductance.

The protocol is composed of 6 tasks:

1. **Relaxation:** The participants were presented with a relaxing image of a sunset and asked to remain as still as possible. The stimulus lasted for 5 minutes. This phase is meant to relax the participants and serve as the baseline for further analysis.
2. **Sit:** The participants were asked to remain seated and look at a black screen for 5 minutes. This phase was introduced to obtain a low-stress condition with no cognitive effort.
3. **Stand:** The participants were asked to stand up and remain in a standing position for 5 minutes. The sit-to-stand was introduced as a “gold standard” reference for assessing sympathetic activation without any cognitive load. At the end of the 5 minutes, a message instructed the participants to sit down again. For this task the volunteers were asked to keep the hand relaxed on the thigh.
4. **Controlled respiration:** The participants were instructed to breathe at a fixed frequency of 0.2Hz. Moving instructions (“breath-in”, “breath-out”) were presented on the screen in an intuitive fashion.
5. **Demo:** A short snippet of a N-Back test was presented in order for the participants to get accustomed to the cognitive task. The signals acquired during this part of the protocol were discarded from future analysis.
6. **N-Back:** The N-Back test is a cognitive task commonly used in literature that stimulates working memory and attention. During the designed protocol a sequence of letters was shown on the screen in random order, each letter appeared for two seconds. The participant were asked to “press the Enter key if the letter is equal to the letter shown N letters before or Backspace if it is different”. N is an integer that can vary and determines the difficulty. Since the number of letters proposed is always bigger than N the subjects were asked to answer many times and had to remember always-changing sequences of letters. Two consecutive sessions were proposed. For each session, four levels of difficulty (N=0,1,2,3) were presented in random order. Each level included 20 stimuli (not including the letters at the beginning when the number of letters proposed is still lower than N and the subject did not have to answer yet). Thus in total each volunteer had to guess 160 times

during the experiment. Four performance indices were saved for further analysis: number of correct answers, number of omission errors (i.e. no answer), number of commission errors (i.e. wrong answer) and response time.

A schematic representation of the protocol is depicted in [Figure 2.2](#).



Figure 2.2: Schematic representation of the N-Back protocol

2.2.3 Dataset Validation

Thirty-one subjects participated in the N-Back protocol. Four subjects were excluded due to errors during the acquisition. Among the remaining 27 subjects the mean age was 25.2 years std 2. The males were 14 and the females 13. Because of an error during the experimental setup, four do not have the file containing the final score. Those subjects were obviously excluded from the correlation analysis with the score but were kept for all other analyses.

3. Materials and Methods: Data Analysis

3.1 Pre-processing

The pre-processing methods are the same for both protocols. All data collected were analysed in MATLAB environment. Data were imported from the .txt file saved by the ProComp polygraph and divided into the three signals of interest: ECG, Respiratory signal and EDA. The events (i.e. starting times and durations of the various tasks) were extracted from the timestamp file saved by the MATLAB script implementing the protocol.

3.1.1 Electrocardiogram - Tachogram

The ECG signal was downsampled to 256Hz. A FIR filter was used for the downsampling procedure to avoid Aliasing. The signal was then imported in the Graphical User Interface (GUI) developed at the PHEEL laboratory, Politecnico di Milano [84].

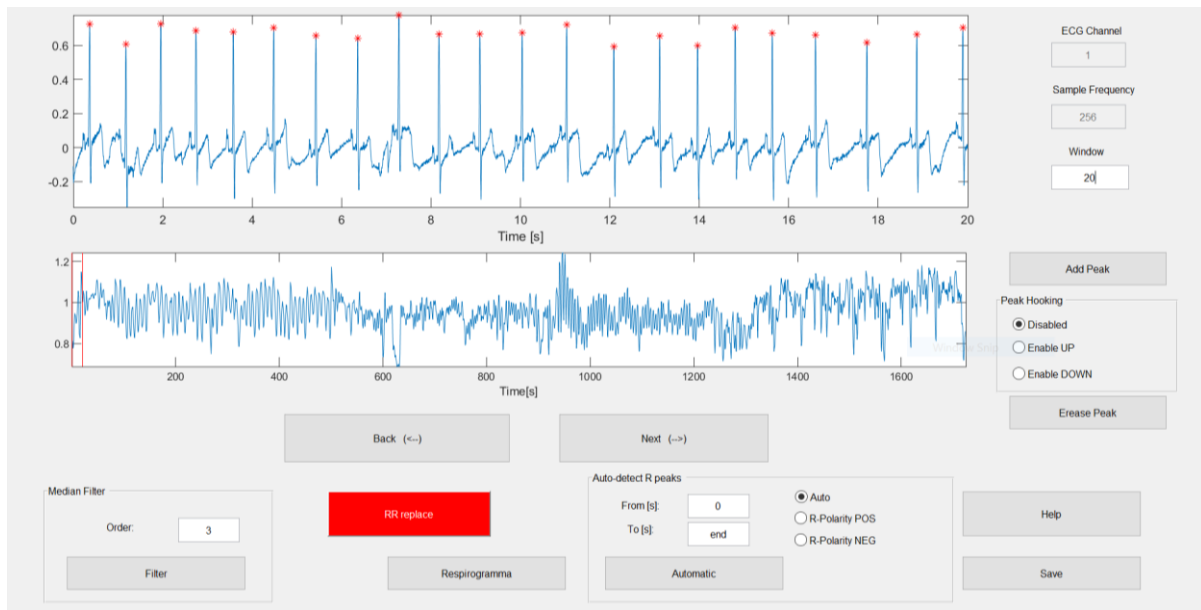


Figure 3.1: GUI Interface for manual correction of the peaks.

The GUI implements the PanTompkins algorithm [13] and provides a practical user interface (depicted in Figure 3.1) for the inspection and manual correction of the identified peaks. The tachogram was extracted after this de-noising procedure using the identified peaks.

3.1.2 Respiratory signal - Respirogram

Similarly to the ECG signal, the respiratory signal was low passed and down-sampled to 256Hz. A more selective low-pass FIR filter was then applied. The digital filter has a cut-off frequency of 10Hz and uses the Kaiserwin window [85]. The respirogram was extracted from the respiratory signal taking one sample for each peak identified in the ECG, thus obtaining a signal which is synchronous with the tachogram, and, as previously discussed, retains basically the same information of the whole respiratory signal.

During the Stand phase of the N-Back protocol the respiratory signal takes visibly different values compared to the other tasks due to the effect of the movement of the band used for the acquisition (Figure 3.2 a). The signal in that time segment was shifted subtracting to it the difference of its mean value and that of the Sit phase. The respirogram was then filtered with a high pass FIR filter with passband frequency set at 0.02Hz to remove slow drift and rescaled with a logarithmic transformation. Figure 3.2 b shows the filtered signal.

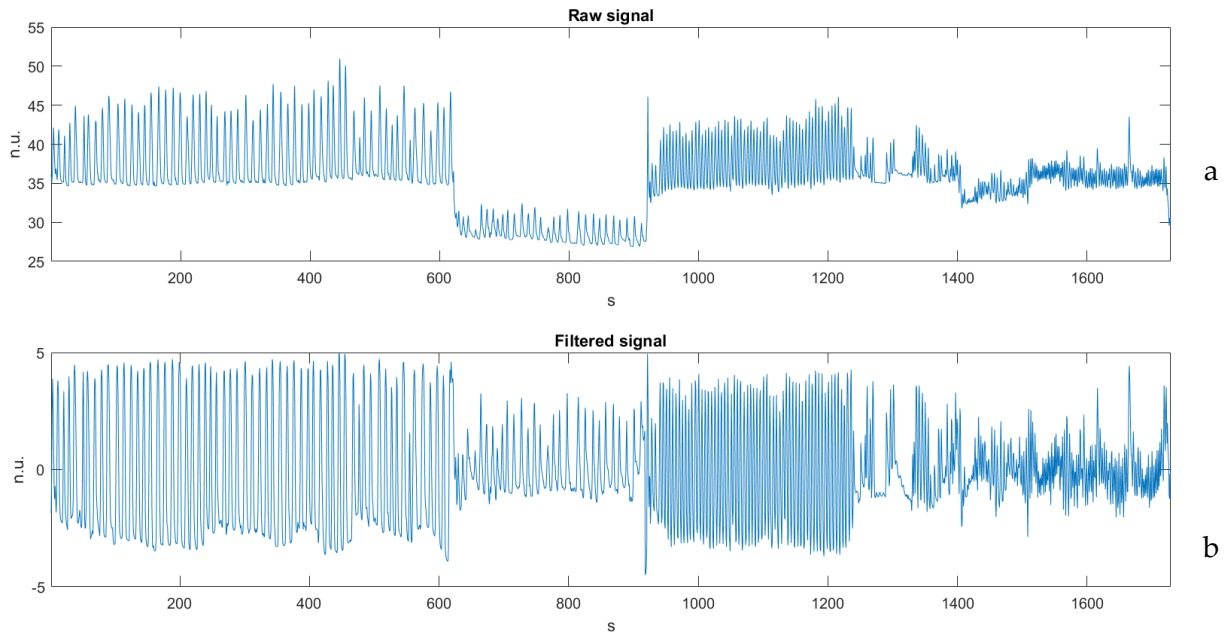


Figure 3.2: Raw and filtered rspiogram.

3.1.3 Galvanic Skin Response

The signal was low passed and downsampled to 16Hz. Additionally, since the useful band of the EDA signal is concentrated at low frequencies it was also low passed at 5Hz using a FIR filter of order 50 designed with the Parks-McClellan algorithm to remove possible high-frequency noise [86].

3.2 Bivariate analysis: HRV and respiration

The method presented in this chapter was selected to satisfy the requirements stated in the objectives of the thesis: obtain an interpretable, time-variant representation of the HRV signal and its interaction with the respiratory signal.

The bivariate model allows to study the causal interactions among the signals, in particular the effect of respiration on the HRV.

The time-variant approach allows to study variations during the different tasks presented during the analysed protocols.

3.2.1 Model description

Following the approach presented in [8] the interactions between the respiratory signal and the RR series were modelled as depicted in Figure 3.3.

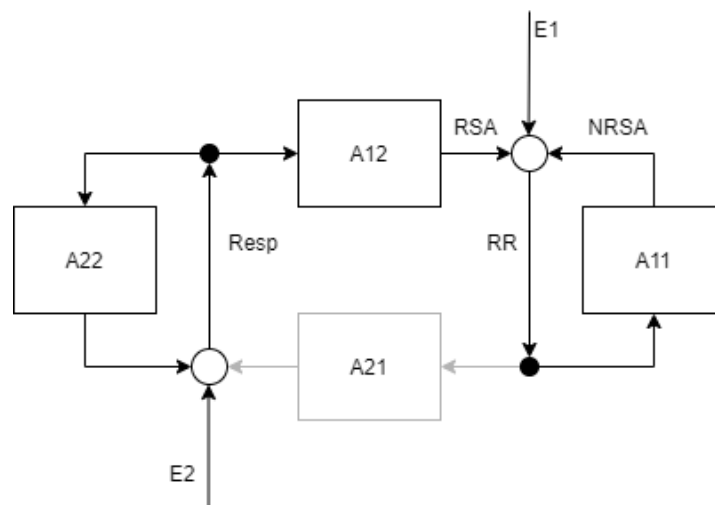


Figure 3.3: Block-scheme of the bivariate model.

The two signals of interest (the RR series and the respirogram) are modelled by means of Multivariate Autoregressive Analysis. The RR series is the sum of a component dependent on its past values, weighted according to the parameters of block A11, the past values of the respirogram, weighted with A12, and a white noise (E1). The component dependent on the respirogram is the RSA, while the component dependent only on itself is the Non-Respiratory Sinus Arrhythmia (NRSA).

As can be observed from the block scheme, the respirogram is modelled as a signal only influenced by its past values, weighted according to A_{22} , and a white noise E_2 . The block A_{21} represents the effect of the RR series on the respirogram and is marked in grey because it was omitted from the model, forcing to 0 its parameters. This choice, which makes the respiratory signal an exogenous input, was made because the influence of the tachogram on the respirogram is assumed to be neglectable. Indeed, physiologically interactions in that direction are not expected and assumed to be only noise [31, p. 278]

The block diagram is equivalent to the system of equation presented in “Eq1”:

$$\begin{bmatrix} RR(t) \\ RESP(t) \end{bmatrix} = \sum_{k=1}^p A_{ij}^{(k)} \begin{bmatrix} RR(t-k) \\ RESP(t-k) \end{bmatrix} + \begin{bmatrix} E_1^1(t) \\ E_2^2(t) \end{bmatrix} \quad Eq 1$$

Where p is the order of the model and A_{21} is imposed null. “Eq1” can be transformed in the frequency domain using “Eq2”

$$A_{ij}(f) = \sum_{k=1}^p a_{ij}^{(k)} e^{-j2\pi f k} \quad Eq2$$

Where a_{ij} are the elements of the matrix A presented in “Eq1”, resulting in “Eq3”:

$$\begin{bmatrix} RR(f) \\ RESP(f) \end{bmatrix} = \begin{bmatrix} A_{11}(f) & A_{12}(f) \\ 0 & A_{22}(f) \end{bmatrix} \begin{bmatrix} RR(f) \\ RESP(f) \end{bmatrix} + \begin{bmatrix} E_1^1(f) \\ E_2^2(f) \end{bmatrix} \quad Eq3$$

With some algebraic manipulation, the system can be rewritten to highlight the reciprocal influences as “Eq4”:

$$\begin{cases} RR(f) = \frac{A_{12}(f)}{1 - A_{11}(f)} RESP(f) + \frac{1}{1 - A_{11}(f)} E_1^1(f) \\ RESP(f) = \frac{1}{1 - A_{22}(f)} E_2^2(f) \end{cases} \quad Eq 4$$

The equations can be represented using the following block schema (Figure 3.4):

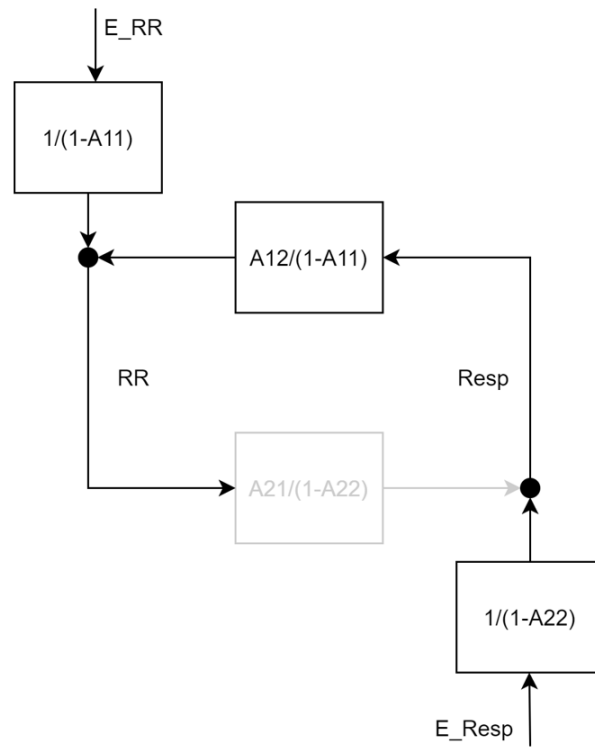


Figure 3.4: Bivariate closed-loop model.

The two signals can also be considered as produced by the modulation of two white noises. Once again, the following equations (“Eq5”) are obtained from the previous ones only with algebraic manipulation.

$$\begin{bmatrix} RR(f) \\ Resp(f) \end{bmatrix} = \begin{bmatrix} H_{11}(f) & H_{12}(f) \\ 0 & H_{22}(f) \end{bmatrix} \begin{bmatrix} E_{RR} \\ E_{RESP} \end{bmatrix} \quad Eq\ 5$$

Where the matrix H is $H = (I - A)^{-1}$ and I is the identity matrix. Since $A_{21}(f)$ is null the element $H_{21}(f)$ is also null and was omitted from “Eq5”.

The correspondent schema is presented in Figure 3.5:

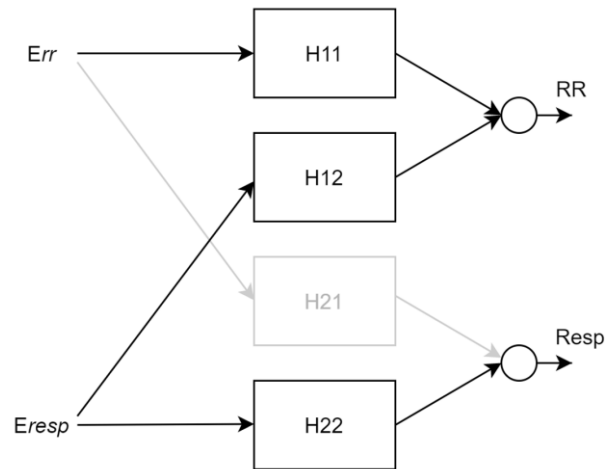


Figure 3.5: Noise generated model.

This representation is especially useful for spectral analysis, as will be explained in chapter 3.2.3.

3.2.2 Time-Variant autoregressive algorithm

A time-variant autoregressive algorithm [32] was chosen to extract the parameters of matrix \mathbf{A} . The algorithm is an adaptation of a recursive least square filter (RLS) with forgetting factor. Specifically, the forgetting factor is a hyperparameter that determines how past values are weighted in the prediction of the next. Admissible values are positive and lower or equal to 1. The model depends on N samples, weighted exponentially (more recent values are weighted more than distant values, following a negative exponential). N can be computed from the formula $N = \frac{1}{1-\lambda}$ where λ indicates the forgetting factor. Setting the forgetting factor to 1 reduces the algorithm to a standard RLS in which the parameters depend on all the available past values. The use of the forgetting factor relaxes the condition of stationarity.

The parameters are updated at every new sample, namely one value from the tachogram and one from the respirogram. The already obtained information is partially retained and only the innovation is added, weighted according to the forgetting factor.

The algorithm minimizes the figure of merit J , which is reported in “Eq6”:

$$J = \frac{1}{t} \sum_{i=1}^t \lambda^{t-i} \varepsilon(i)^2 \quad \text{Eq 6}$$

where λ is the forgetting factor, ε is the prediction error and t is the total number of samples according to the system of equations reported in “Eq7”:

$$\left\{ \begin{array}{l} \mathbf{a}(t) = \mathbf{a}(t-1) + \mathbf{K}(t)\varepsilon(t) \\ \mathbf{K}(t) = \frac{\mathbf{P}(t-1)\boldsymbol{\varphi}(t)}{\lambda + \boldsymbol{\varphi}(t)^T \mathbf{P}(t-1)\boldsymbol{\varphi}(t)} \\ \varepsilon(t) = y(t) - \boldsymbol{\varphi}(t)^T \mathbf{a}(t-1) \\ \mathbf{P}(t) = \frac{1}{\lambda} \left[\mathbf{P}(t-1) - \frac{\mathbf{P}(t-1)\boldsymbol{\varphi}(t)\boldsymbol{\varphi}(t)^T \mathbf{P}(t-1)}{\lambda + \boldsymbol{\varphi}(t)^T \mathbf{P}(t-1)\boldsymbol{\varphi}(t)} \right] \end{array} \right. \quad \text{Eq 7}$$

$\boldsymbol{\varphi}(t)$ is the vector containing the samples, $\mathbf{K}(t)$ is the gain matrix and $\mathbf{P}(t)$ is the covariance matrix.

The elements of $\mathbf{a}(t)$ related to the effect of the RR series on the respiratory signal, which correspond to the block “A21” presented in, were forced to zero.

It should be noted that in the case of stationary signals the algorithm converges to a minimum and stops updating its parameters, while in the case of non-stationary signals after the initialization period the algorithm tracks the continuously varying minimum, provided that the variations of the signal are not too fast with respect to the selected forgetting factor.

3.2.2.1 Initialization

The convergence of the algorithm must be verified before using the computed parameters for further analysis. In order to assure the convergence, a dummy signal was concatenated at the beginning of the signal of interest.

For the BASE protocol, this signal was obtained concatenating 10 times the 30 seconds of the first fixation for each run of each subject. For the N-Back protocol, the 5 minutes of baseline were used.

The values of the gain matrix \mathbf{K} and the prediction error were inspected to confirm

the convergence. The values of the gain matrix should reach a plateau while the prediction error should reduce and become approximately white.

3.2.2.2 *Model order*

The prediction error should be as close as possible to white, to assure that the model is able to capture most of the dynamics of the signal. The quality of the fit depends on the choice of the order and the forgetting factor. The order should be high enough to capture all the relevant dynamics of the signals but should not be too high, to avoid overfitting and excessive sensitivity to the noise.

The HRV is known to contain at least three peaks of interest, positioned at Very Low Frequency, Low Frequency and High Frequency. The minimum number of poles (which is the same as the order of the model) is thus 7, considering that at each peak corresponds a pole which has a complex conjugate in the z-plane and one pole is set at 0Hz and does not have an imaginary component.

Standard methods for optimal spectral estimation, such as the Akaike Information Criterion, cannot be directly applied to the case of time-variant algorithms. Furthermore, the bivariate algorithm selected requires to use the same order for the respirogram and the RR series, even if it is expected that the respirogram has a lower optimum order.

The choice of the correct order was made considering the RR series, which is the signal of primary interest. The prediction error of the RR series, which should be ideally a white noise, was inspected. For each value of the order ranging from 2 to 20 the normalized autocorrelation function (ACF) evaluated for 100 lags was computed. The number of values in the ACF that exceeded the 99% confidence interval computed for a standard normal distribution were summed to verify the whiteness. The spectra obtained as explained in chapter 3.2.3 were also inspected to verify that the algorithm worked as expected.

3.2.2.3 *Forgetting factor*

The performance of the algorithm is strongly dependent on the choice of the forgetting factor. Reasonable values of the forgetting factor are usually close to 1, for example $\lambda = 0.99$ which results in a model which depends on 100 samples.

A higher forgetting factor allows for a more robust estimation of the model parameters but results in a reduced ability of the algorithm to track fast changes in the dynamic of the signal. The choice of the forgetting factor was made considering the trade-off between these two factors.

3.2.2.4 Condition on the error

Samples of both the tachogram and the respirogram can take values that differ significantly from the expected dynamic. This can happen because of measurement noise or very irregular beats or respiratory movements that may not provide relevant information on the functioning of the ANS but can change the behaviour of the algorithm and result in an unreasonable estimation of the model parameters.

To enhance the robustness of the algorithm a condition on the error was implemented. The condition prevents the updating of the parameters when the a priori prediction error – computed using the parameters calculated at the previous step - overcomes a certain threshold, which varies at each iteration according to the formula “Eq8”:

$$\begin{cases} |E_{RR}| < (F_{RR}\sqrt{vvv_{RR}^{old}} + E_{RR}^{old}) \\ |E_{RESP}| < (F_{RESP}\sqrt{vvv_{RESP}^{old}} + E_{RESP}^{old}) \end{cases} \quad Eq 8$$

where E and vvv are the a-priori prediction error and variance and F_{RR} and F_{RESP} are tuneable parameters (the lowest the value, the more restrictive the criterion).

To prevent the algorithm from stopping to update its parameters for a period that is too long, it was imposed that the control cannot be applied more than 4 consecutive times.

3.2.3 Spectral estimation

Since the algorithm provides new coefficients for each input sample the spectra can be computed for each heartbeat. The frequencies are considered in intervals that range from 0 to the Nyquist frequency, computed as half of the inverse of the mean time distance between heartbeats during the entire protocol (or run, for the BASE protocol).

To compute the total spectra of the two signals and their cross-spectrum the method described in [42] was used. For each sample, the matrix \mathbf{A} containing the coefficients is transformed to the frequency domain as presented in the formula “Eq 2”.

The matrix \mathbf{H} was then obtained from \mathbf{A} according to $\mathbf{H} = (\mathbf{I} - \mathbf{A})^{-1}$

From \mathbf{H} the spectral matrix $\Phi(f)$ was computed using “Eq9”:

$$\Phi(f) = H \text{Var} H^T \quad \text{Eq 9}$$

The diagonal elements of $\Phi(f)$ can be written as in “Eq10”

$$\begin{cases} \Phi(1,1) = |H_{11}|^2 \text{Var}(1,1) + |H_{12}|^2 \text{Var}(2,2) & \text{Eq 10.1} \\ \Phi(2,2) = |H_{22}|^2 \text{Var}(2,2) & \text{Eq 10.2} \end{cases}$$

Where Var is the matrix containing the variance of the prediction errors.

$\Phi(1,1)$ and $\Phi(2,2)$ are respectively the total spectra of the tachogram and the respirogram.

$\Phi(1,2)$ is identical to $\Phi(2,1)$ and is the cross-spectrum. The magnitude squared coherence is computed as reported in “Eq11”:

$$C = \frac{\Phi(1,2)}{\sqrt{\Phi(1,1)\Phi(2,2)}} \quad \text{Eq 11}$$

It should be noted that since A_{12} is null C is the causal coherence (in the Granger sense).

The partial spectra are computed as explained in [42] using the residue method and correspond to the transfer blocks presented in Figure 3.5 according to “Eq10”, in which the two spectra are described as the sum of the partial spectra. Since the loop was opened forcing A_{21} to 0, it derives that also H_{21} is null and “Eq 10.2” has only one term. The partial spectrum that identifies the effect of the tachogram on itself will be called PSD11 for brevity while the effect of the respirogram on the tachogram PSD12.

The entire procedure for spectral estimation was repeated for each sample. As a result, from all the spectra presented were computed the spectrograms.

3.2.4 Instantaneous respiratory frequency

The instantaneous respiratory frequency was extracted to adapt the HF band centring it at the respiratory frequency.

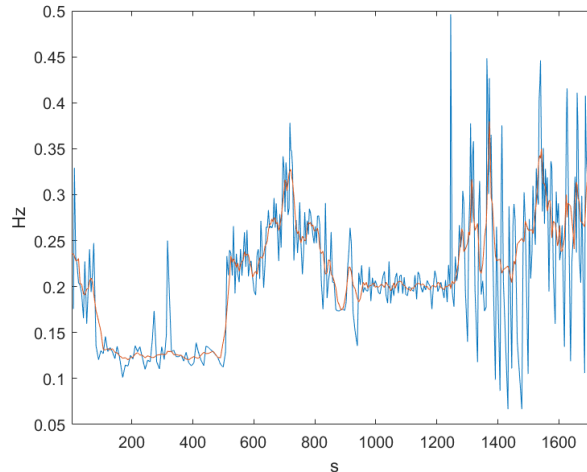


Figure 3.6: Instantaneous respiratory frequency raw and smoothed.

The peaks were identified on the respiratory signal imposing a minimum prominence of 0.3 standard deviations and a minimum distance of 2 seconds. A time series containing the time distance between consecutive breaths was computed from the identified peaks. To remove outliers a Hampel filter of order 10 was applied on the series and a moving average of width 6 was then used to smooth the signal. An example of respiratory frequency obtained from a subject of the N-Back protocol is reported in Figure 3.6.

3.2.5 Feature extraction

The features listed in this chapter were extracted in both protocols. Time-frequency domain features were computed from the spectrograms presented in chapter 3.2.3 while time domain and non-linear features were computed directly from the HRV and respiratory signals.

3.2.5.1 Frequency Domain

The features in the frequency domain were extracted integrating the spectra in the desired frequency range. The values obtained (one for each heartbeat) were then mediated in the time window of interest. Before computing the average value a Hampel filter of order 10 was applied on the obtained series to remove outliers. The filter replaces with the median all the values in the window that lie more than 3 standard deviations away from the median.

The features in Table 3-1 were extracted from $\Phi(1, 1)$.

P Tot	The total power of the tachogram, obtained integrating on all frequencies excluding the VLF, i.e. frequencies from 0 to 0.04Hz
HF	The power in the frequency band that ranges from 0.15 to 0.4Hz
LF NU	The power in the frequency band from 0.04 to 0.15Hz divided by P Tot
LF/HF	The ratio between the power in 0.04-0.15Hz and the power in 0.15-0.4Hz

Table 3-1 Features extracted from $\Phi(1, 1)$.

The following features (Table 3-2) were calculated from the product of $\Phi(1, 1)$ with C

P Coer	The power computed integrating the product of $\Phi(1,1)$ with C over $f > 0.04$
P_Coer_NU	P Coer divided by the power obtained integrating over all frequencies of $\Phi(1, 1)$ excluding VLF

Table 3-2 Features computed from the product of $\Phi(1, 1)$ with C

The following features (Table 3-3) were extracted from the partial spectra

HF RSA	The power obtained integrating PSD12 on a frequency band of width 0.25Hz centred at the instantaneous respiratory frequency. The rationale underlying this choice is that this feature is meant to capture only the RSA.
LF NRSA	The power obtained integrating PSD11 in the classical frequency band 0.04-0.15Hz. This feature was extracted as an attempt to expurgate LF computed on the total spectrum from the effects of the respiration, which in the case of slow but still physiological breathing can overlap with the Low Frequency band.

Table 3-3 Features computed from partial spectrograms

The BASE protocol does not have a specific section of sufficient length to be used as the baseline, therefore the data of the first protocol were not normalized.

HR, LF NU, LF/HF, LF NRSA were normalized in the N-back protocol subtracting the baseline value. The only effect of the normalization is to enhance the visualization of the data and does not affect the results of the statistical analysis, as will be discussed later (Chapter 3.5).

3.2.5.2 Time Domain and non-linear

HR: The heart rate was straightforwardly extracted from the tachogram multiplying by 60 the inverse of the time distance between heartbeats to obtain a value in beats per minute (bpm).

Respiratory Frequency: The respiratory frequency was computed multiplying by 60 the inverse of the time distances of the instantaneous respiratory frequency discussed before. For this purpose, the moving average was not applied.

SDNN, RMSSD and pNN50 were extracted only in time intervals of at least 5 minutes of length.

SampEn was computed according to the formula “Eq12”:

$$\text{SampEn}(m, r, N) = -\ln \frac{\sum_{i=1}^{N-m} \sum_{j=1, j \neq i}^{N-m} \{\text{number of times that } d[|x_{m+1}(j) - x_{m+1}(i)|] < r\}}{\sum_{i=1}^{N-m} \sum_{j=1, j \neq i}^{N-m} \{\text{number of times that } d[|x_m(j) - x_m(i)|] < r\}} \quad \text{Eq12}$$

Where d is the Chebyshev distance, m is the length of the segment to be compared, N is the length of the time series and r is the tolerance [87]. The parameter m was set at 2 and r at $0.2 \cdot \text{SDNN}$ in accordance with [88].

3.3 EDA Analysis

As previously mentioned, the skin conductance was analysed only for the N-Back protocol.

The analysis was conducted using model-based methods that enhance the information contained in the signal using a-priori physiological knowledge.

The signal was decomposed into phasic and tonic components with a method already validated [47]. From the identified components the most common time-domain features were computed.

The phasic component was then used for the more innovative time-frequency analysis. Along with the batch methods commonly used in the literature a time-varying RLS algorithm inspired by the HRV analysis was implemented and compared to the existing methods. The advantage of the time-varying method is that it is expected to reach better time-frequency resolution and can be easily adapted for online applications.

3.3.1 Phasic and Tonic Decomposition

The decomposition of the EDA signal into its tonic and phasic components was performed using the continuous decomposition analysis implemented in Ledalab [47]. The estimation of the optimal impulse response function is performed through the minimization of a cost function that depends on the negativity of the phasic driver and its distinctness by means of a gradient descent method. Then, a standard deconvolution is applied. The obtained phasic driver is a continuous measure of phasic activity. The signals of interest obtained are presented in [Table 3-4](#).

Driver	the phasic driver smoothed by convolution with a gauss window with $\sigma = 200\text{ms}$ on which the peaks are detected
Phasic Data	the reconstructed phasic signal obtained convolving the phasic driver with the impulse response function (IRF), i.e. the SCR resulting from an unit impulse
Tonic Data	the reconstructed tonic signal obtained convolving the tonic driver with the IRF. The tonic driver is obtained interpolating the inter-impulse sections using a cubic spline

Table 3-4 Ledalab output signals

In addition, for each impulse identified in the driver function were extracted the information reported in Table 3-5.

Impulse Onset	the time at which the impulse identified in the driver function begins
Impulse Peak Time	the time at which the identified impulse reaches the maximum amplitude
Impulse Amplitude	the maximum value reached by the impulse in the driver function

Table 3-5 Ledalab impulse characteristics

It should be noted that the term “impulse” refers to a peak in the driver of short duration (generally less than 2 seconds) and not a unit impulse.

3.3.2 Time-frequency analysis

3.3.2.1 Pre-processing

The slow variations of the EDA signal are not of interest in this contest. Therefore only the phasic component, obtained as previously discussed, was used.

Before proceeding with the time-frequency analysis the phasic signal had to undergo further processing.

The data were low passed and resampled to 8Hz to avoid oversampling and reduce future computational load, normalized using the standard score to make the results obtained on different subjects comparable, and low passed with a FIR filter with cut-off frequency at 1Hz.

3.3.2.2 Non-parametric approach

For the estimation of the EDA spectrogram a variation of the Fast Fourier Transform was used. The signal was divided into windows with a duration of 90 seconds and an overlapping of 89 seconds (the window is moved with a step of 1 second). Inside each window the spectrum was computed using the Welch algorithm with Hamming windows of 60 seconds and overlapping of 45 seconds. The spectrum

computed is then assigned to the time instant at the middle of the window. Thus, a spectrogram with a time definition of 1 second was obtained, excluding the first and last 45 seconds.

3.3.2.3 *Batch parametric approach*

A Blackman window of 90 seconds was shifted along the signal with a step of one second. Inside the window the spectra were calculated using the Yule-Walker method [89], which finds the optimal parameters minimizing the squared prediction error. The order was selected inspecting the error variance, i.e. using the lower value of the order after which it does not significantly decrease. The spectrogram obtained should have a similar resolution compared to the previous one since it provides a spectrum for each second of the signal (excluding the borders) and calculates the spectra on windows of 90 seconds.

3.3.2.4 *Time-variant parametric approach*

A time-variant autoregressive algorithm (ARTVAR) inspired by the HRV analysis was developed. The phasic signal was down-sampled to 2Hz to make the results comparable with those obtained from the HRV analysis. Since the useful band does not exceed the 0.25Hz [90] no information should be lost.

The algorithm takes as input the EDA signal and computes as many parameters as the selected order and the variance of the prediction error for each sample of the signal (which is sampled at 2Hz). For the initialization of the algorithm, a copy of the five minutes of the baseline was concatenated twice at the beginning of the signal.

The signal is highly non-stationary, which means that the model should be able to adapt quickly to the dynamics of the signal. However, simply reducing the forgetting factor makes it less stable. For this reason the Fortescue method was applied [91]. The method varies the forgetting factor at each sample to keep an estimation of the information content constant, making it smaller when the signal changes rapidly and close to 1 when more closely resembles a stationary signal.

The recursive formulation of the information content Γ_t is reported in “Eq13”:

$$\Gamma_t = \lambda_t \Gamma_{t-1} + (1 - \varphi_t^T K_t) e_t^2 \quad \text{Eq 13}$$

Where φ is the vector of the observations, K the gain matrix and e the prediction error. Therefore, substituting to Γ_t and Γ_{t-1} the constant value Γ_0 , the adaptive forgetting factor can be formulated as in “Eq14”:

$$\lambda_t = 1 - \frac{1 - \varphi_t^T K_t}{\Gamma_0} e_t^2 \quad \text{Eq 14}$$

The information content was estimated as in “Eq15”:

$$\Gamma_0 = \sigma_0^2 N_0 \quad \text{Eq 15}$$

Where N_0 is the memory of the algorithm, defined as $1/(1 - \lambda_0)$, and σ_0^2 is the variance of the prediction error. To estimate σ_0^2 the time-varying algorithm was first applied with a fixed forgetting factor λ_0 , which was chosen a priori to be 0.987. The time-varying algorithm was then applied again with the new formulation of λ_t .

The condition on the error was also applied, meaning that the parameters were only updated when the error was lower than a certain threshold, according to “Eq16”

$$|E_{eda}| < (F_{eda} \sqrt{v_{eda}^{old}} + E_{eda}^{old}) \quad \text{Eq 16}$$

Where F_{eda} is a tuneable hyperparameter.

Similarly to the batch parametric analysis, the order was chosen by inspecting the variance of the prediction error.

The spectrogram was calculated computing the PSD at each sample from the parameters returned by the algorithm with the formula “Eq17”:

$$PSD(f) = \frac{\sigma^2}{F_s} \left| \frac{1}{A_z} \right|_{z=e^{-j\omega T_s}}^2 \quad \text{Eq 17}$$

Where σ^2 is the variance of the prediction error, A is the vector of the coefficients, F_s is the sampling frequency and T_s is its inverse.

3.3.3 Features extraction

Features related to the electrodermal activity signal were computed relying on the models previously described. In time domain were computed on the extracted tonic and phasic components and considering the impulses obtained from the phasic driver. In the time frequency domain were computed from the spectrograms of the phasic component.

3.3.3.1 Time Domain

The peaks were identified by Continuous Decomposition Analysis on the smoothed phasic driver. Only peaks with amplitude greater than a threshold value set at 0.1 standard deviations of the signal were considered.

The features computed are reported in [Table 3-6](#).

Peak Frequency	The number of peaks identified by the decomposition in the window divided by the length of the window
Impulse Amplitude	The average amplitude of the peaks in the window
Rise Time	The average time between impulse onset and impulse peak
ISCR	Integrated Skin Conductance Response: the time integral of the smoothed phasic driver
Tonic Mean	The average value of the tonic component in the window

[Table 3-6](#) EDA time-domain features

All the features except “Rise Time” were normalized subtracting the mean computed during the baseline.

3.3.3.2 Time-Frequency Domain

From the spectrograms computed with all the methods mentioned before the following features were computed ([Table 3-7](#)):

TVSymp	The power obtained integrating in the frequency band that ranges from 0.045 and 0.25Hz and averaging in the time window of interest
TVTot	The power obtained integrating in all frequency bands and averaging in the time window of interest
TVSympStd	The standard deviation of TVSymp in the time window (before averaging)

Table 3-7 EDA time-frequency domain features

3.4 Analysis of interactions: HRV-EDA

The sympathetic branch of the ANS innervates both the heart and the skin. A study of the coherence between signals related to the two organs was performed in order to identify a common source.

Since the expected effect of the SNS is to lower the value of RR series but to increase the value of the skin conductance, to obtain a positive correlation the inverse of the RR series (the heart rate) was computed and used for further analysis.

Regarding the EDA signal, only the phasic component extracted using Continuous Deconvolution Analysis was considered, since it is the component that better reflects the activity of the SNS. To reduce their skewness the data were transformed using the logarithm in base 10, summing 1 to the argument to obtain only positive numbers. Both signals were then high passed with a cut-off frequency of 0.02Hz. To make them comparable, the Standard score was computed on both.

The cross-correlation in the time domain was performed as reported in formula “Eq19”.

$$R_{xy}(m) = E\{x_{n-m}y_n\} \quad \text{Eq 19}$$

The expected value was calculated as in “Eq 20”

$$R_{xy}(m) = \begin{cases} \sum_{n=0}^{N-m-1} x_{n+m}y_n^T, & m \geq 0 \\ R_{xy}(-m), & m < 0 \end{cases} \quad \text{Eq 20}$$

and then corrected to avoid bias due to the fact that the sequences have finite length (“Eq21”).

$$R_{xy}^{unbiased}(m) = \frac{1}{N - |m|} R_{xy}(m) \quad \text{Eq 21}$$

Finally, for the sake of a more intuitive representation, the value was divided by the maximum of the absolute value of the cross-correlation in a window of 1 minute around 0 lag (“Eq22”).

$$R_{xy}^{normalized}(m) = \frac{R_{xy}(m)^{unbiased}}{\max(|R_{xy}^{unbiased}|)} \quad Eq\ 22$$

According to the hypothesis that the signals have a common source that drives the correlation, a maximum in the correlation function is expected around 0 lag. Since the SNS innervates the two organs with different pathways that have different conduction times and take a different time to generate measurable effects it may not be at exactly 0 lag. Identifying the peak allows to measure this time difference simply by looking at the lag.

An analysis in the frequency domain to determine if the two signals have some frequency at which they covary was performed evaluating the magnitude squared coherence, defined as in “Eq23”.

In this context, as shown in [Figure 3.7](#), only the NRSA component, obtained using the model introduced in chapter 3.2.1 as the output of A11, was considered. This choice was made to remove the effect of the Respiratory Sinus Arrhythmia on the RR series. Indeed, the respiration has an effect on both the HRV and the EDA signals but is not of interest in this analysis, since its effect is mostly related to the PNS. This was not done for the assessment of the cross-correlation in time-domain because the filter introduces a delay that biases the computation of the time lag between the two signals.

$$K_{xy}^2(f) = \frac{|PSD_{xy}(f)|^2}{|PSD_x(f)||PSD_y(f)|} \quad Eq\ 23$$

The cross-spectrum PSD_{xy} was calculated as in “Eq24”

$$PSD_{xy}(f) = PSD_{yx}(f) = X(f) * Y(f)^T \quad Eq\ 24$$

For its computation were used Hamming windows of 100s with an overlapping of 10s.

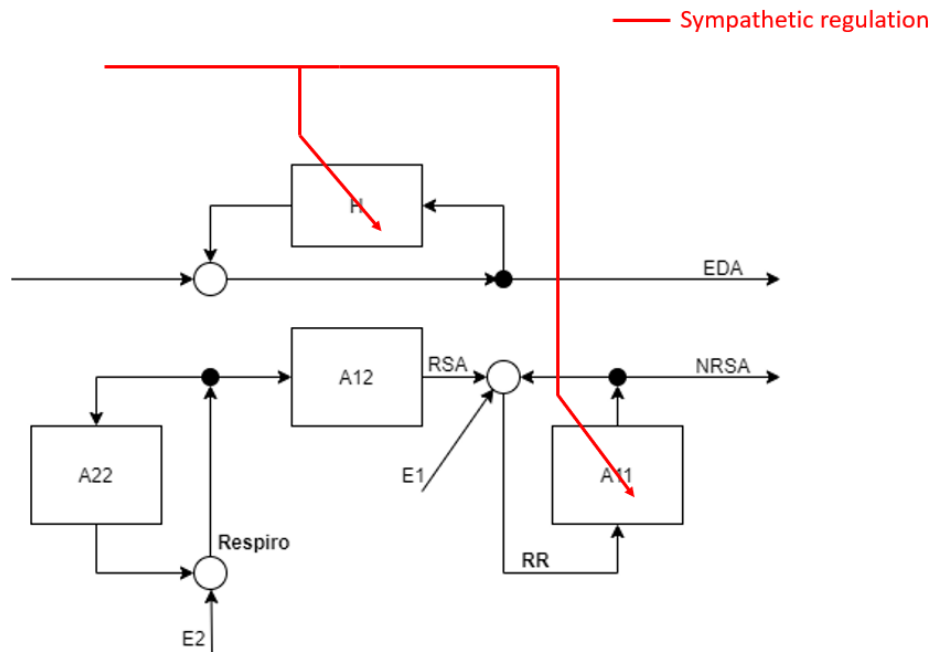


Figure 3.7 Block diagram. Sympathetic regulation over EDA and NRSA.

3.5 Statistical analysis

Several methods for computing quantitative indices have been presented. The goal of the statistical analysis is to answer the following research questions:

1. Do the features vary significantly during the different tasks of the protocols?
2. Do they correlate with objective measures of performance and the scores provided in the questionnaires?
3. What is the correlation between indices extracted from the EDA signal and the HRV-Respiratory signals?

3.5.1 Differences across tasks

To answer the first question differences among features computed on different time windows were evaluated using the Friedman test. The Friedman test is a non-parametric test, i.e., it does not assume that data come from a specific distribution but rather only assumes that data come from populations that have the same continuous distribution. It also corrects for intra-subjects variations, looking only for common trends. The null hypothesis of the test is that measures obtained in different moments are equal. This hypothesis was rejected when the returned p-value was lower than 0.05.

When the p-value was significant, a post-hoc multicomparison Bonferroni test was applied to determine which groups differs from each other through pairwise comparison.

3.5.1.1 BASE protocol

The two runs (RLE – SPLIT) were kept separate to investigate if differences in difficulty affect the results. The segments reported in the protocol definition were compared. In order to use windows of the same lengths the Writing and Read problem tasks were defined as follow:

Code Writing: 5 minutes extracted from the Writing task in which the participant was continuously writing code (without significantly long stops, that would be labelled as “thinking”). If 5 minutes were not available, the longest available session was chosen.

Read problem – this window was considered only when longer than 1 minute. Since for the majority of the subjects it took less than 1 minute to read the instruction of the SPLIT session (the easy one) this window was only considered for the RLE task.

Time-domain features and SampEn were tested against five minutes of Code Reading and five minutes centred at the longest Code Writing session, defined as stated before. No other windows could be tested since time-domain features of different lengths are not comparable and the conventional minimum recordings for this kind of measurement are 5 minutes [20].

Regarding frequency-domain features, even if the time-variant approach selected makes it possible to compute features for each heartbeat, only features mediated over windows of at least 1 minute were considered. The choice of this window length was due to the time limitation imposed by the Text Reading task of the protocol.

The following windows were tested for differences: Text reading, Read problem, Code writing and Code reading.

3.5.1.2 *N-Back protocol*

The segments were divided following the tasks of the protocol.

As mentioned before, the Demo task was not analysed. The first 15 seconds of each task were also discarded since they are considered transition periods.

The beforementioned windows were tested for significance except for the relaxation, that was used as the baseline.

3.5.2 Correlations

To perform a more comprehensive analysis of the features extracted from the three signals analysed, their link and their relationship with the categorical outcomes provided by the participants in the questionnaires or in the evaluation, multiple correlation analyses were performed.

The correlation was measured using the Spearman correlation coefficient, which tests for monotonic relationships according to the formula “Eq18”:

$$\rho = 1 - \frac{6 \sum d^2}{n(n^2 - 1)} \quad \text{Eq 18}$$

where n is the number of samples in the two variables (which has to be the same) and d is the difference between the ranks. The coefficient ρ is 1 (or -1, if the correlation is negative) when the relationship is perfectly monotonic, even when it is not linear.

The Spearman coefficient was preferred over Pearson because it does not assume normality of the data, which cannot be properly assessed in the data presented because the number of subjects is too low, especially for the BASE protocol. It should be noted that this type of analysis does not say much about possible non-monotonic relationships among the variables considered, that were not investigated.

The p-value was calculated for each coefficient using the permutation distribution. To obtain the value for the two-tailed test (i.e., testing against the null hypothesis that the coefficient is different from 0 without assuming a specific direction) the most significant value for a one-tail test was multiplied by two [92],[93]. The significance level was set at 0.05.

3.5.2.1 BASE protocol

HRV features

In order to reach a higher numerosity and a more robust evaluation the data from RLE and SPLIT were merged (i.e. to each subject correspond 2 points, one for each run).

Only the Code writing and Code reading segments were considered. HRV features related to the coding task were correlated with each other and with the categorical variables (effort, pressure, score, discomfort, completion). For Code Reading the features were only correlated with each other and the score and performance obtained during the coding task.

HRV-EEG

The EEG spectral power density calculated in different frequency bands and for different channels was correlated with the HRV features to investigate links between central and autonomic signals.

The frequency bands considered are 'Theta' and 'Alpha'. These bands were chosen

because are the ones that gave the most significant results in a previous study conducted specifically on the EEG signals recorded in this study [80]. The channels were grouped in different functional and anatomical areas: “Frontal”, “Central” and “Parieto-occipital”.

The computation of the features related to the electroencephalographic signal is not explained here since it was not an objective of the present work.

3.5.2.2 *N-Back protocol*

All the variables extracted from the HRV and the EDA signals were correlated with each other and the final score. The purpose of this correlation analysis is:

- Test if the features extracted from the HRV and from the EDA change together, due to the common sympathetic drive.
- Test how much the features extracted from the EDA are correlated with each other, in order to assess redundancy and identify the independent variables.
- Test if some variables covary with the final score and average time to answer, to test if they could be used as predictors of performance.

4. Results and Discussion

4.1 TVAR Model validation

4.1.1 Model order

The proportion of values of the ACF that exceed the 99% confidence interval computed for a white Gaussian noise as explained in chapter 3.2.2.2 is reported in Figure 4.1. The image shows the average percentage value and the standard error in function of the model order, computed over all subjects and runs of the BASE protocol. Since the average is always higher than 1% (shown as a red line in figure), it can be concluded that none of the orders tested satisfied the whiteness of the prediction error.

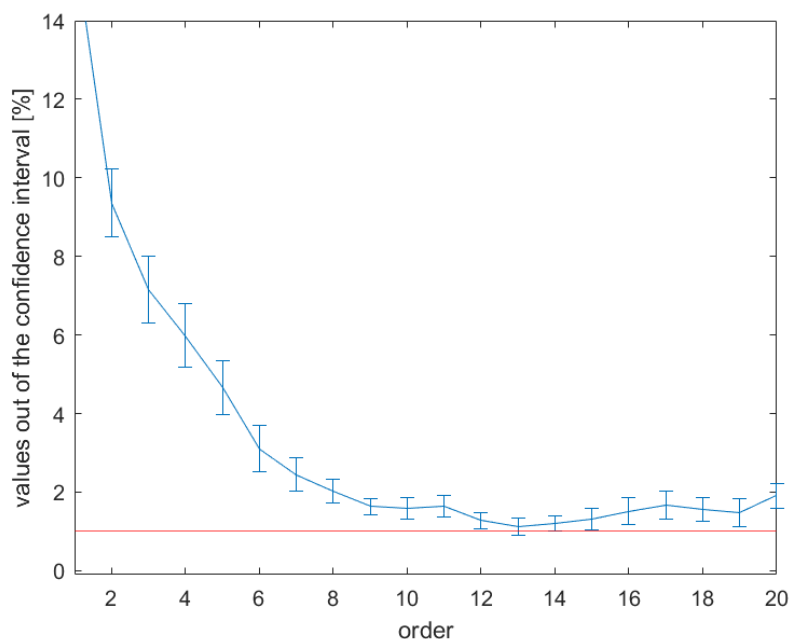


Figure 4.1: Percentage of values outside the confidence interval.

A possible explanation is that the condition of stationarity of the signal is not satisfied. Ultimately the order 9 was chosen basing also on the inspection of the spectra and other works in the literature. Figure 4.2 shows the prediction error obtained from the first run of subject 1 (BASE protocol), which was picked as an example representative of the general trend observed in all subjects.

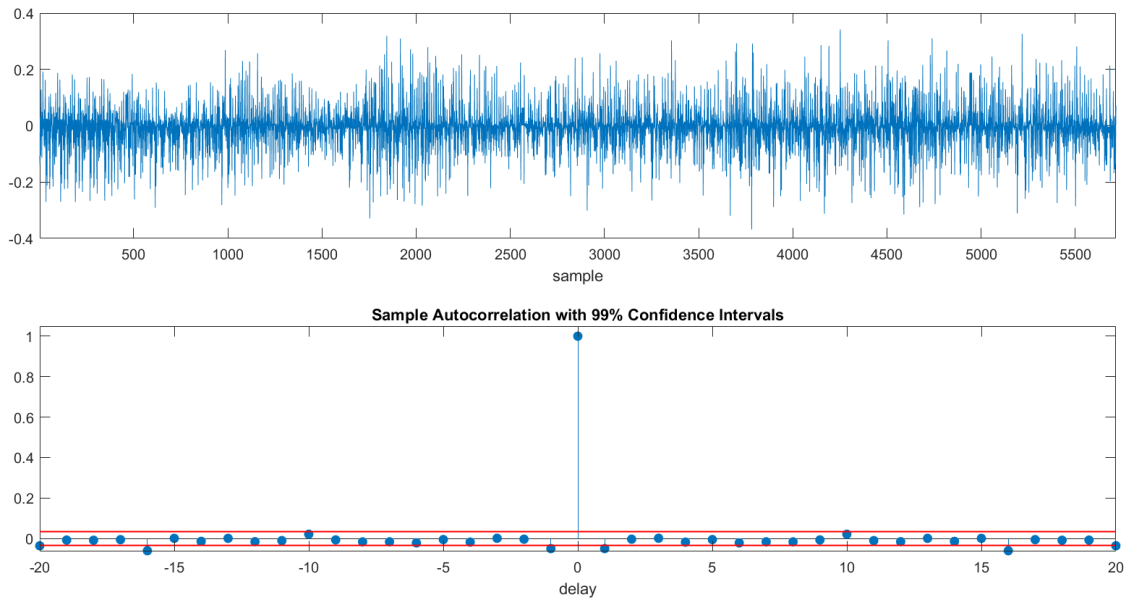


Figure 4.2: Prediction error with spectrum and ACF.

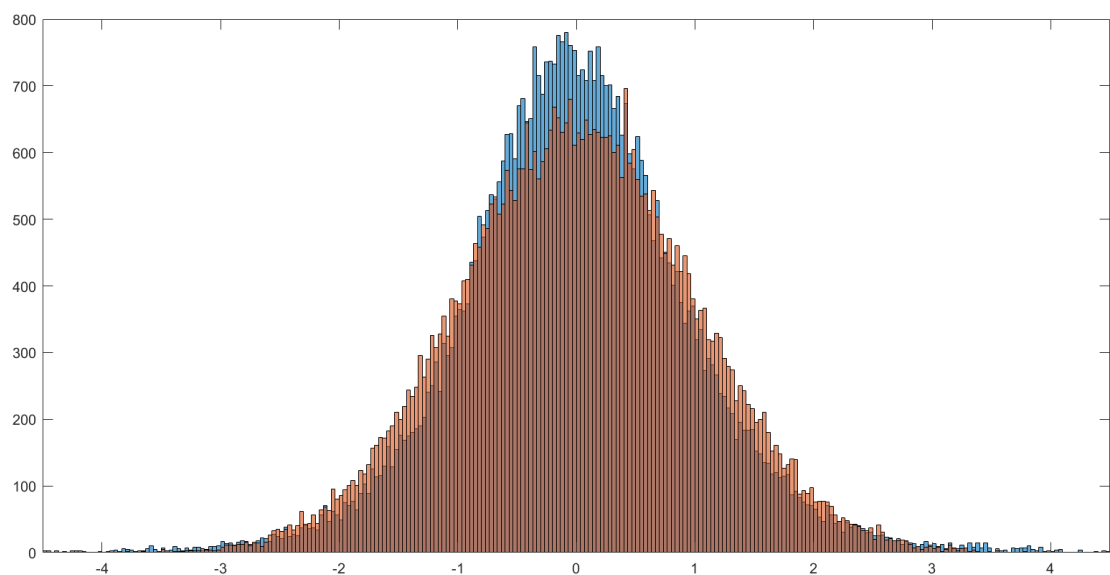


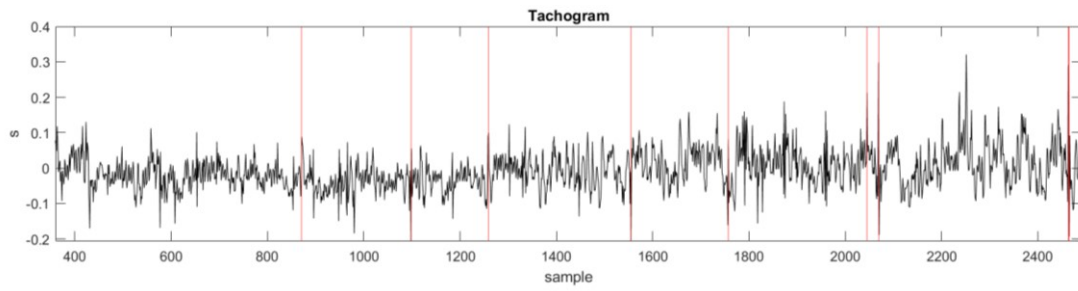
Figure 4.3: Histogram of the standard score of the error (blue) and normal distribution (orange).

The prediction error can still be considered at least approximately white as suggested by its autocorrelation function. Indeed, as expected, almost all the values of the ACF lie inside the confidence interval or very close to the margin.

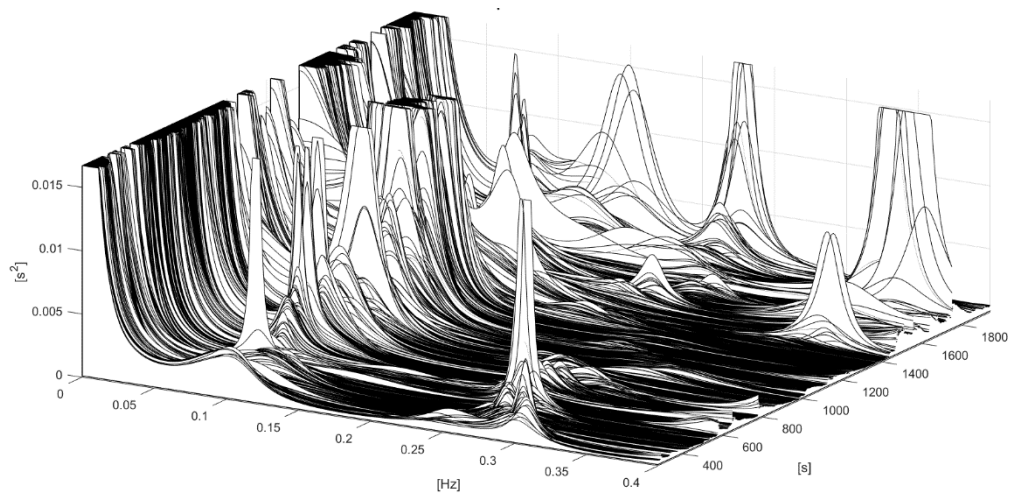
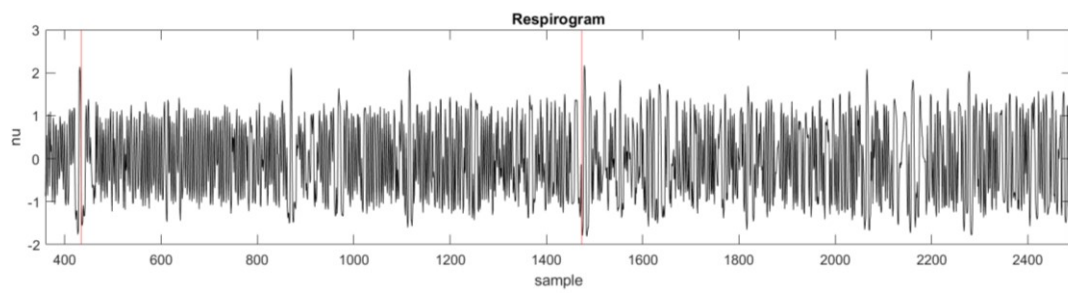
The distribution of the prediction error values observed in all the subjects of the BASE protocol, depicted in blue in [Figure 4.3](#), shows an excessive kurtosis compared to the normal distribution (in orange), thus explaining the non-normality. However, this is consistent with the functioning of the model in non-stationary conditions: when the signal quickly changes its dynamics the algorithm produces large errors (long tails in the distribution) while it returns an error very close to 0 when it has adapted to the dynamic (high peak in zero).

4.1.2 Control on the error

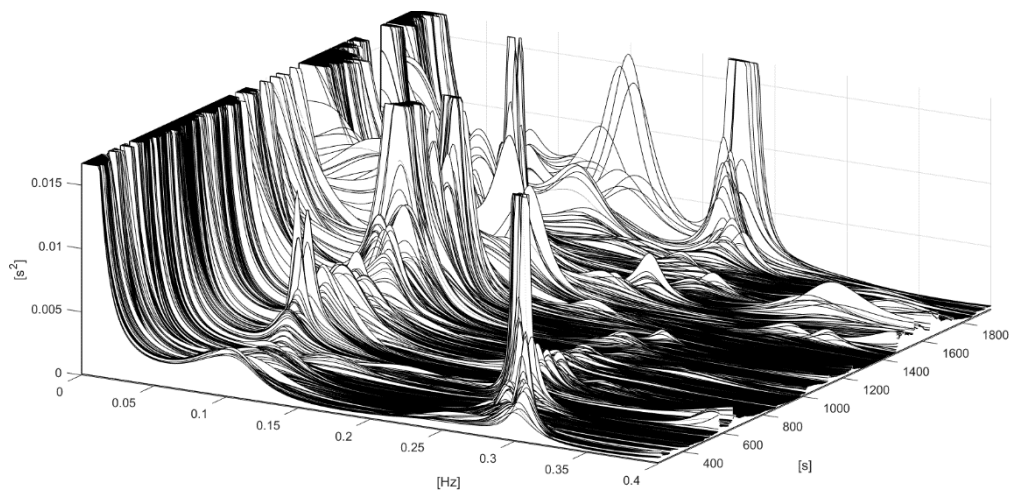
The control on the error has the effect to prevent the update of the model parameters when the error is considered too big according to “Eq8”. The control makes the algorithm more robust by removing dependence on outliers. Specifically, the value of F_{RR} and F_{RESP} were set at 4 and 3, respectively. These values appear to be a reasonable trade-off between the need to avoid outliers and the requirement to follow fast variations, as was confirmed by inspection of the signals. [Figure 4.4a](#) shows an example of the identification of outliers on HRV and respiratory signal for subject 11 of the BASE protocol during the first run. This subject was selected because relatively many samples did not pass the control on the error. [Figure 4.4b](#) and [Figure 4.4c](#) show the total spectrogram of the tachogram before and after applying the error control, respectively. As can be seen in figure, the spectrogram after the error correction presents the typical VLF, LF and HF peaks, without the unexpected third peak at the limit of the HF band, which was assumed to be noise.



a



b



c

Figure 4.4: Input signals and $\Phi(1,1)$ before and after the control on the error.

4.1.3 Initialization

Figure 4.5 shows the sum of the absolute values of the gain matrix related to the tachogram samples. Once again, subject 11 of the BASE protocol was chosen as an example in figure but a similar trend was observed in all subjects. A moving average, marked in red, was also superimposed for clarity. The blue line marks the end of the initialization period. As required, the transient part during which the values of the gain matrix present a ramp-like dynamic finishes before the end of the initialization period.

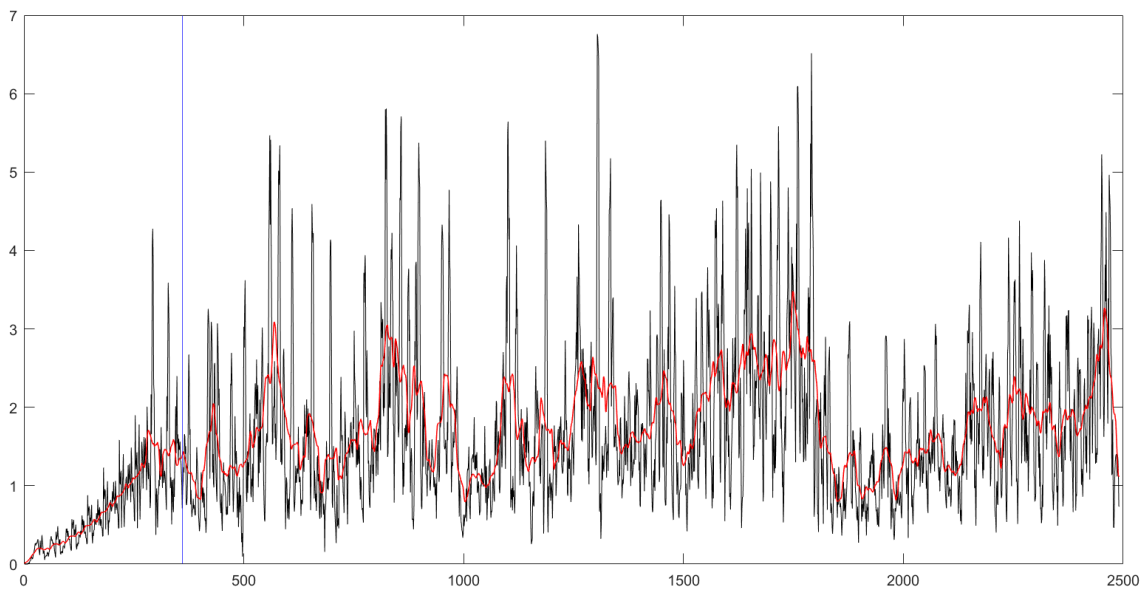


Figure 4.5: Dynamics of the gain matrix K.

4.2 Spectrograms and features extraction

4.2.1 Spectrograms

The advantage of using the time-variant algorithm is that non-stationarities in the signals can be tracked in time to highlight variations during the protocol tasks.

Figure 4.6 and Figure 4.7 show the HRV and respirogram with their spectrograms, respectively. On the tachogram one, the fixed frequency bands were superimposed, while on the respirogram the adaptive respiratory frequency band was superimposed.

Vertical lines represent the tasks and the 30s fixation periods. In order: first fixation, text reading, second fixation, coding, third fixation, code reading.

Figure 4.8 shows the spectrum of the coherence. Subject 4 was picked as an example for the BASE protocol since the respiratory frequency is lower than the classical HF band (0.15-0.4Hz) and varies in time.

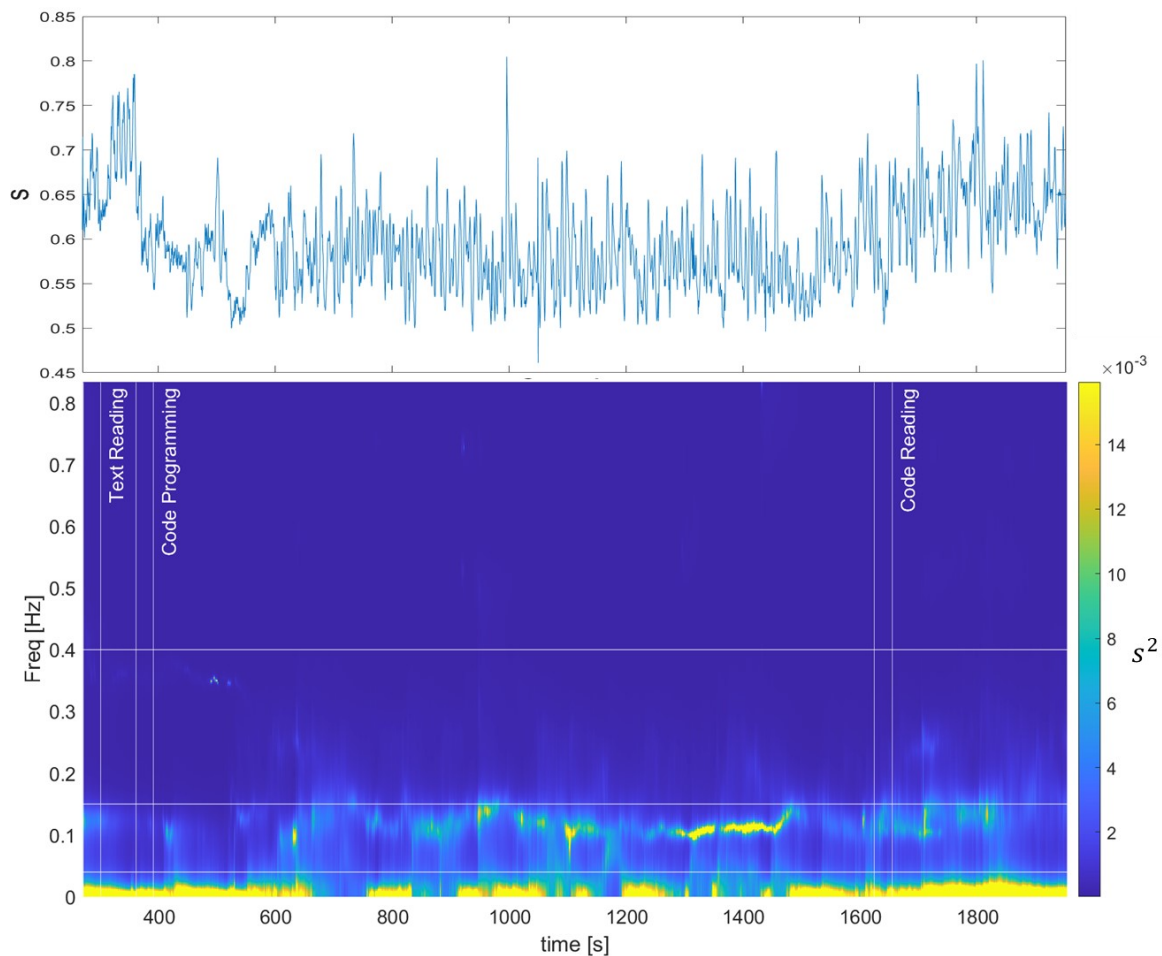


Figure 4.6 Tachogram and its spectrogram

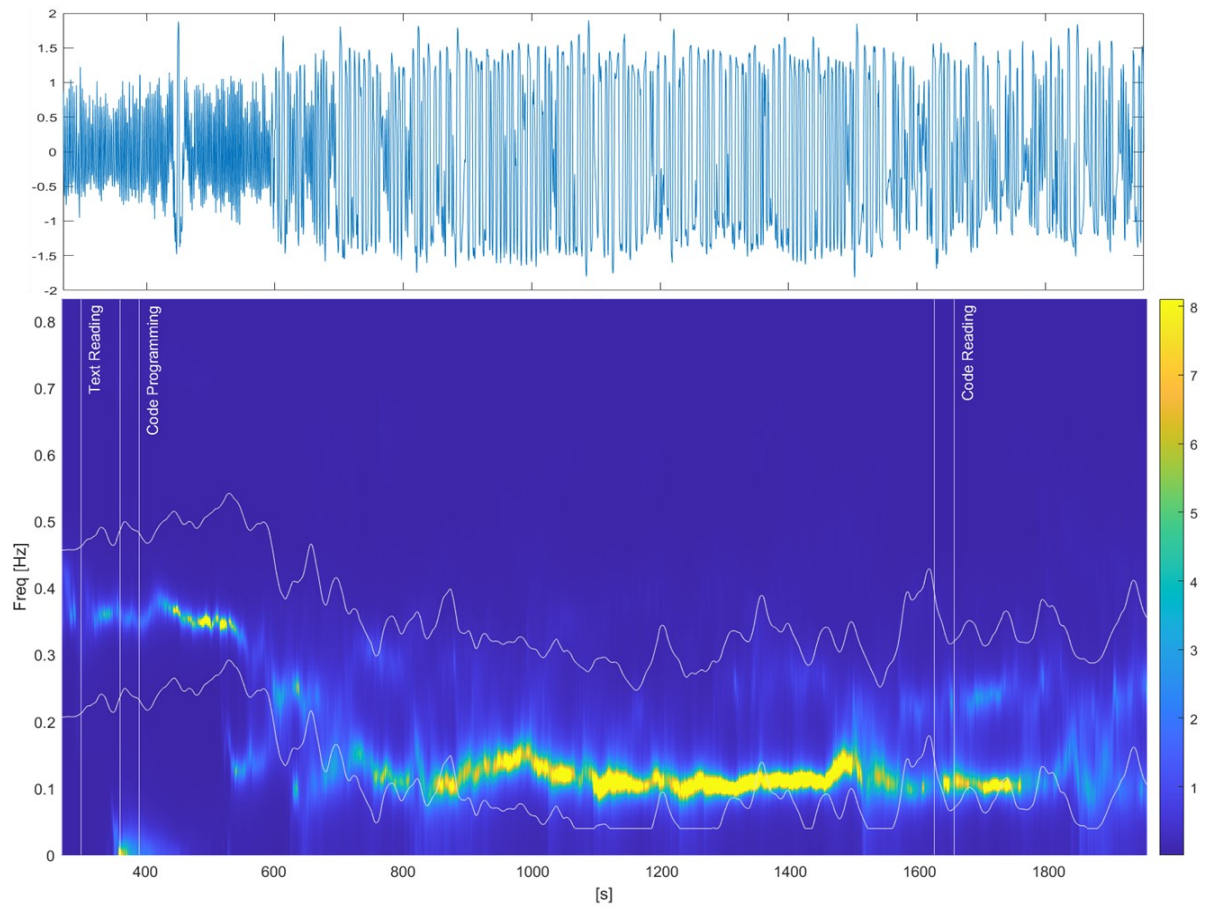


Figure 4.7 Respirogram and its spectrogram

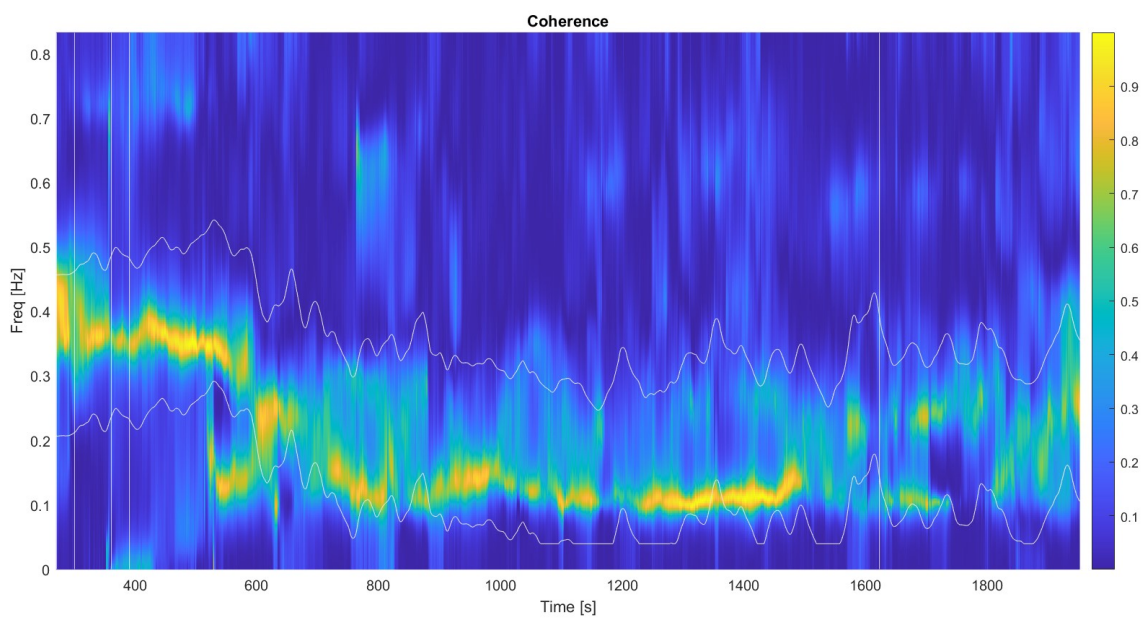


Figure 4.8: Spectrum of the coherence. Run 1 subject 4

As expected, most of the coherence between the two signals (Figure 4.8) is contained in the adaptive frequency band, as an effect of the RSA. This result highlights the advantage of a bivariate time-variant approach, which allows to measure the coherence between the two signals at every sample and take into account non-stationarities.

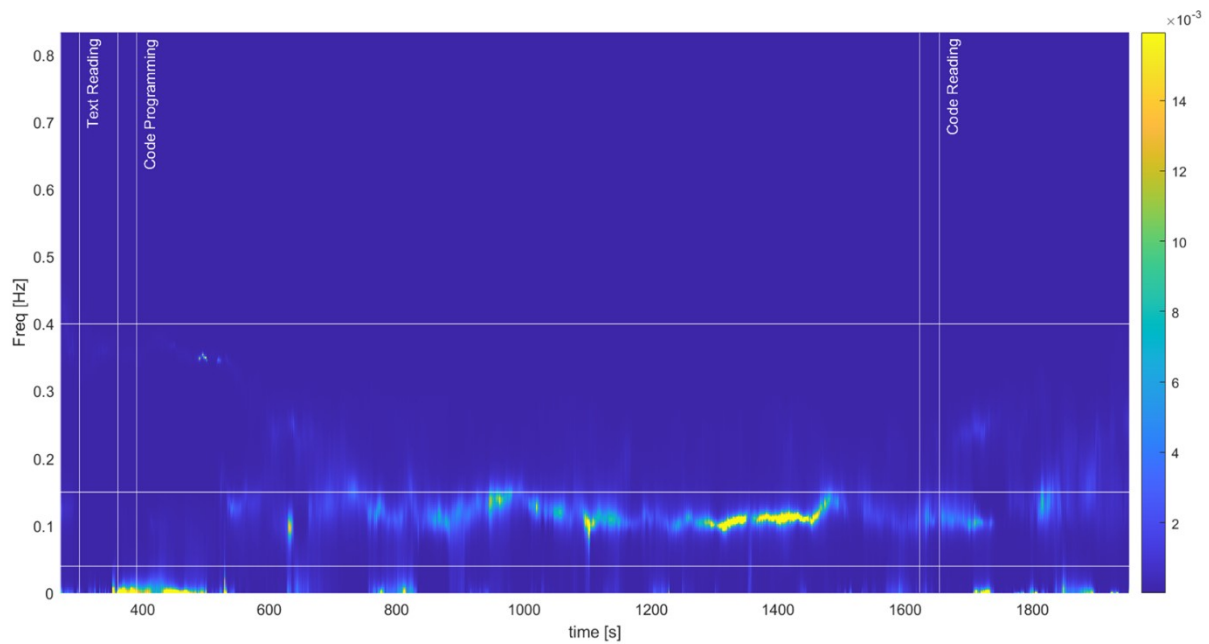


Figure 4.9: Partial spectrogram PSD12

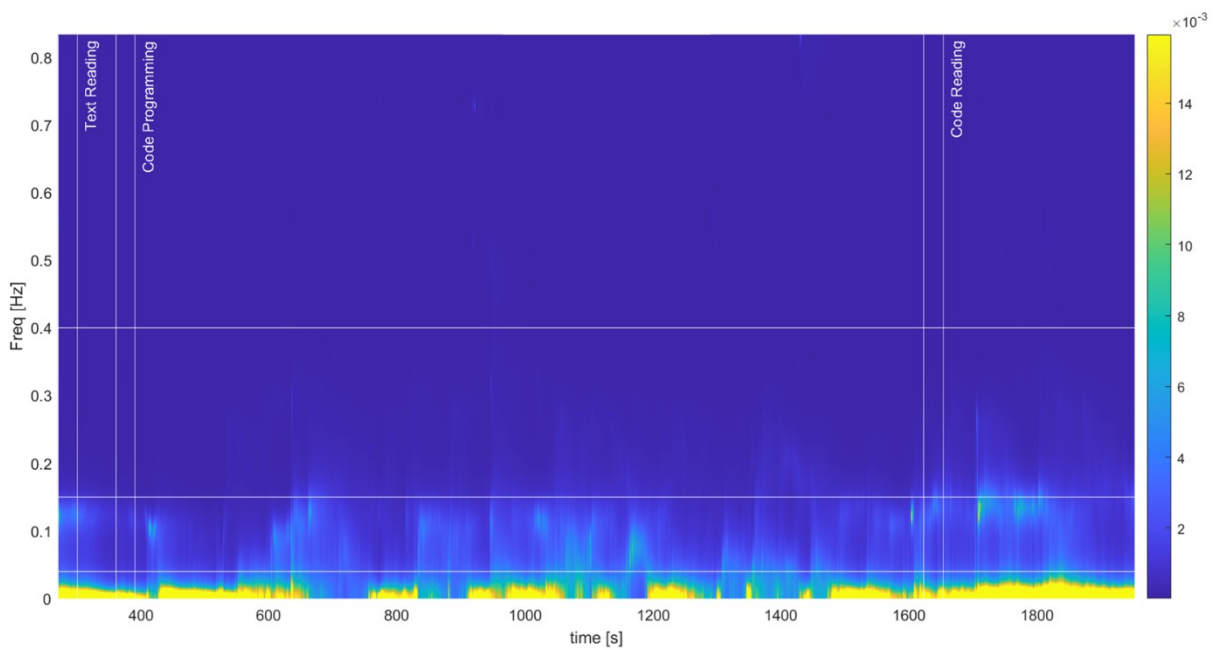


Figure 4.10 Partial spectrogram PSD11

Figure 4.9 shows the partial spectrogram representing the effect of the respiration on the tachogram. Comparing this figure with the total spectrum (Figure 4.6), it can be observed how only the RSA is retained in the partial spectrogram. Figure 4.10 shows the autospectrum of the tachogram, i.e., the component that is not dependent on the respiratory signal. As expected, most of its power falls in the LF band. Indeed, even though the bands overlap in the total spectrum, the bivariate time-variant approach allows to remove the RSA component from the autospectrum of HRV.

The advantage of the spectral decomposition is also evident in the first subject of the N-Back protocol, chosen as an example, whose respiratory frequency falls in the standard LF frequency band during both the Relaxation and Sit phases of the protocol, as can be noticed in Figure 4.11.

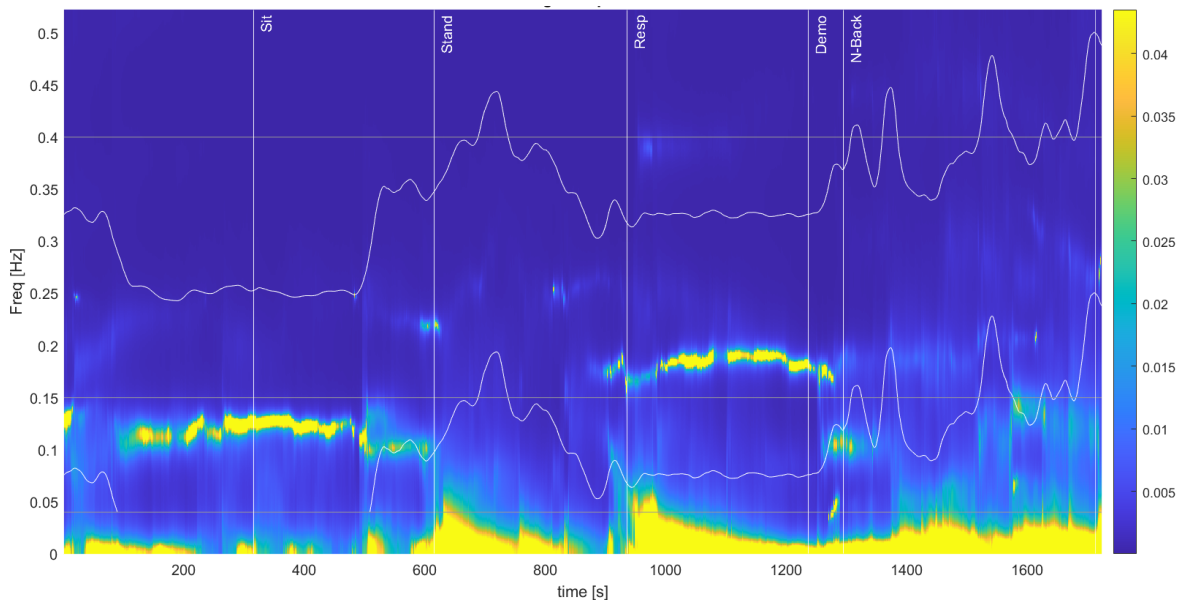


Figure 4.11: Spectrogram of the tachogram

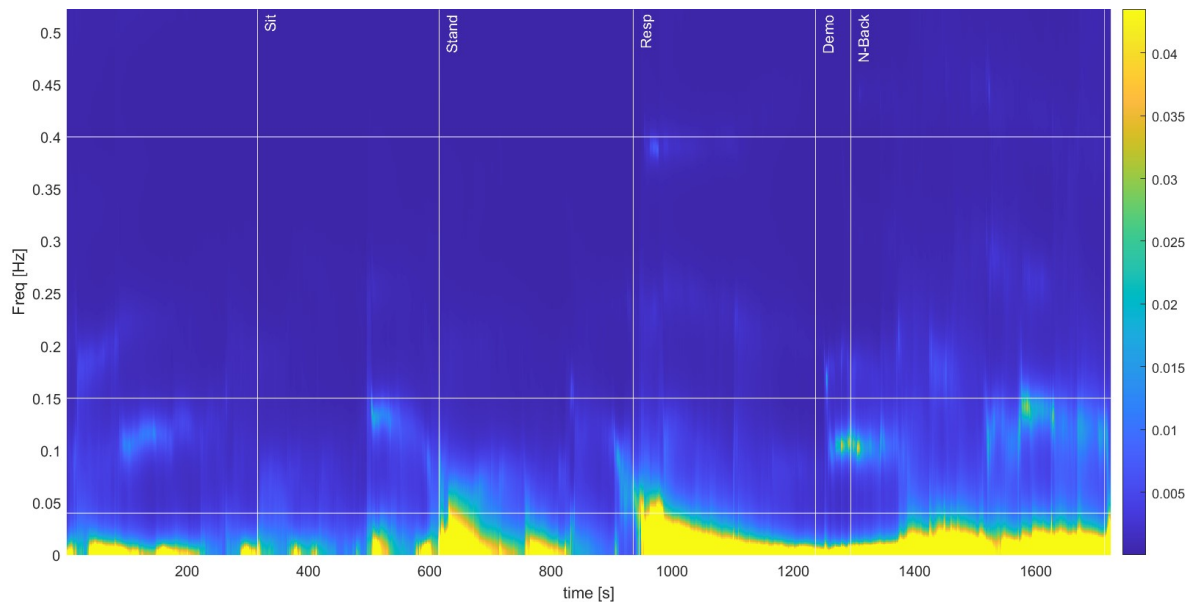


Figure 4.12: Partial Spectrogram PSD11

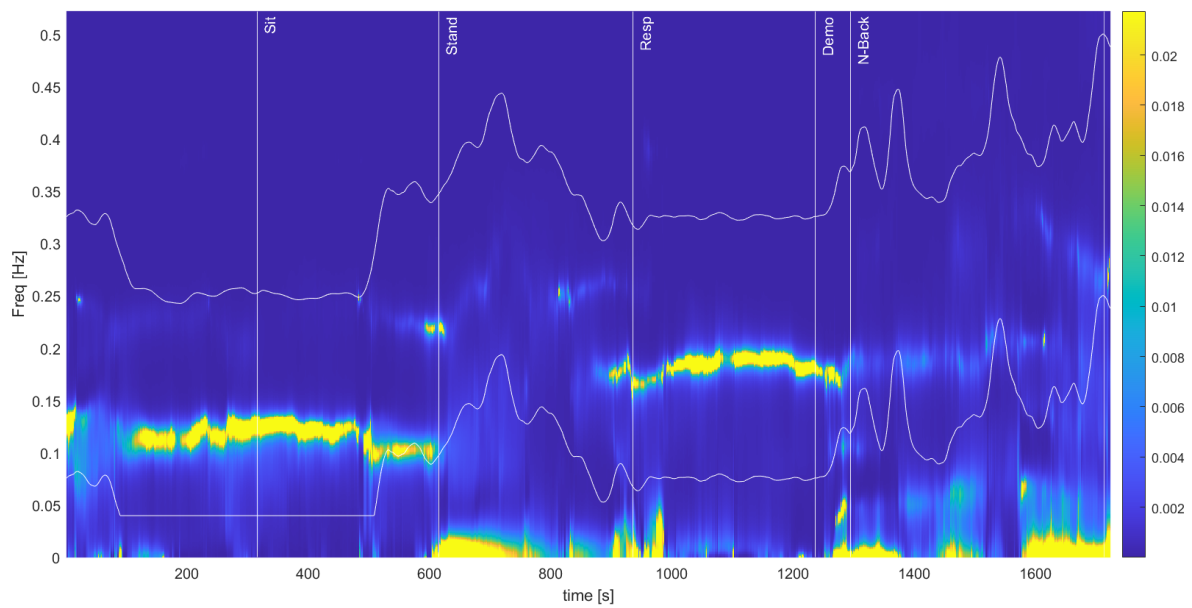


Figure 4.13: Partial spectrogram PSD12

Therefore, the computation of the features in the total spectra results in misclassification of the RSA in the LF band. The partial spectrogram PSD11 shown in Figure 4.12, on the other hand, can be used for a less biased computation of LF, as in the previous example.

4.2.2 Time-Frequency domain features

Time-frequency domain features were extracted directly from the spectra integrating in the respective frequency bands, as explained in chapter 3.2.5.1.

Figure 4.14 shows the features calculated from the spectra presented in Figure 4.6 and Figure 4.9 which are reported as an example. Different colours are used to differentiate among the sub-classes of coding: Read problem is marked in green, while Writing is red. The scale of the plots have been fixed between 0 and 0.005 s^2 for non-normalized features and between 0 and 1 (or 100) for the normalized ones.

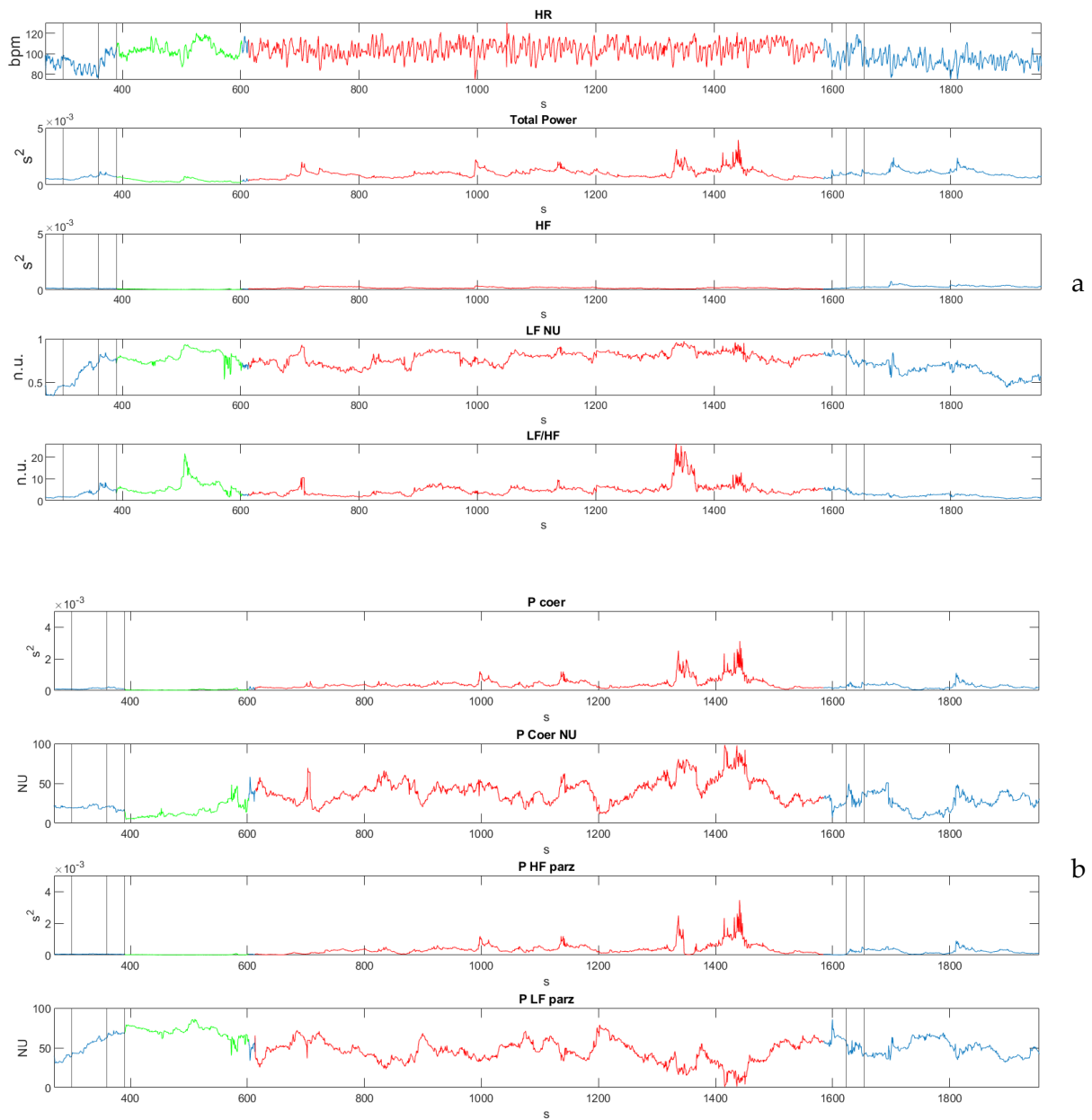


Figure 4.14: HRV time-frequency features with and without respiratory information. Writing in red and Read problem in green.

The features presented in Figure 4.15 are referred to the spectrograms presented in Figure 4.12 and Figure 4.13. The scale of the plots is reported on the axis and was adapted to optimize the visualization.

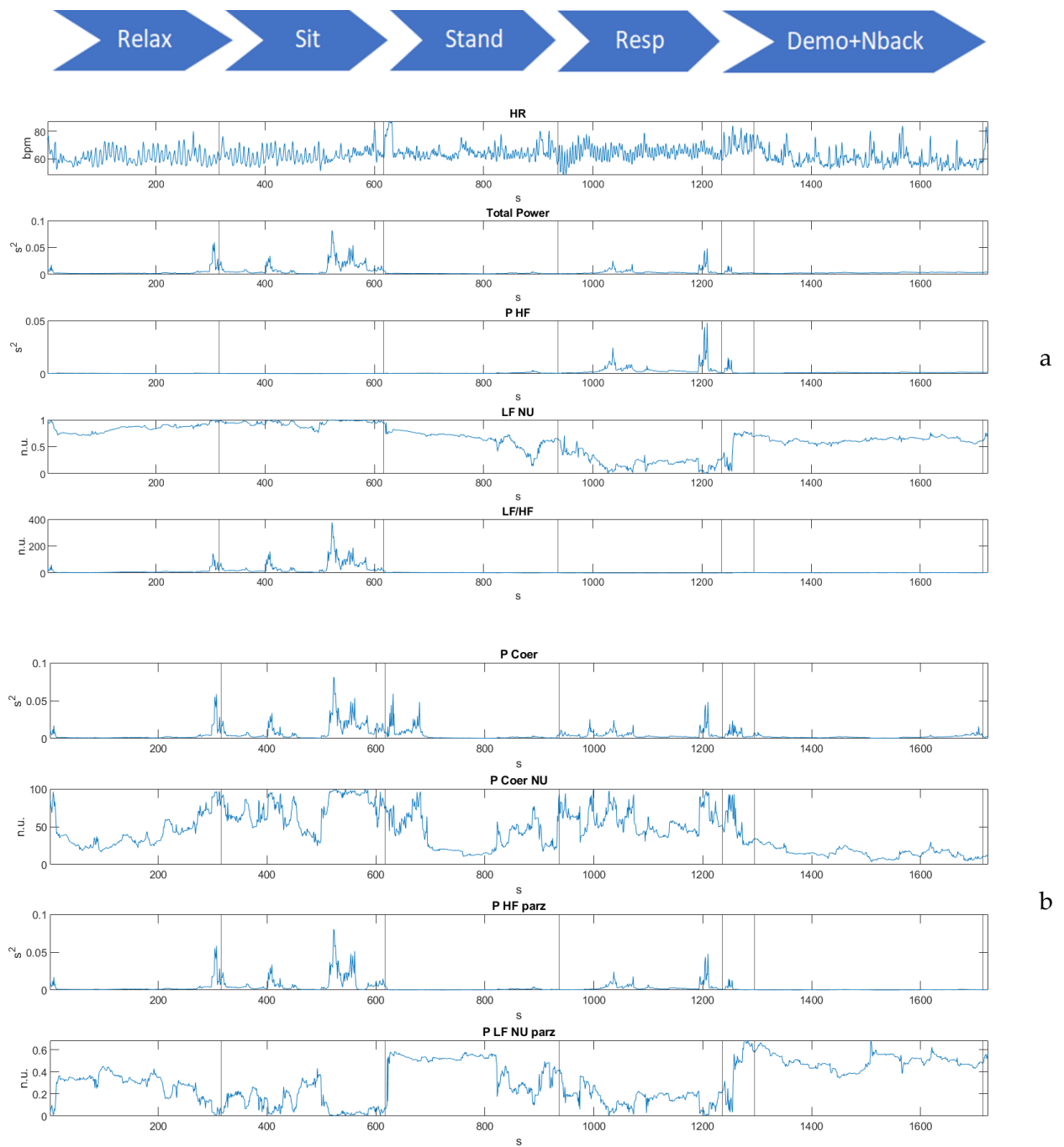


Figure 4.15: HRV features without and with respiratory information.

The difference in the LF computed on the total and partial spectra for this subject can be visualized in Figure 4.15a and Figure 4.15b. The misclassification of the RSA in the computation of LF from the total spectrum resulted in an overestimation of the sympathetic activation during the first two tasks, which is inconsistent with the experimental condition (relaxation and sit). The computation of LF from the partial spectrum allowed to remove the RSA component, leading to a time trend of this feature in line with the expectations. In particular, the increase in LF and the decrease in HF during the stand phase is clear, which is a well-known phenomenon that has been extensively studied in the literature and reflects the sympathetic activation induced by the orthostatic stressor.

Figure 4.16 shows how LF NU and HF computed on the total and partial spectrograms differ for all the subjects in the sit-to-stand phase. It can be noticed that computing LF on the partial spectrogram removes some power, which is assumed to be due to the RSA and increases the separation between the two conditions. The difference between sit and stand is also more pronounced if HF is computed with the adaptive band on the partial spectrogram compared to the standard definition of HF.

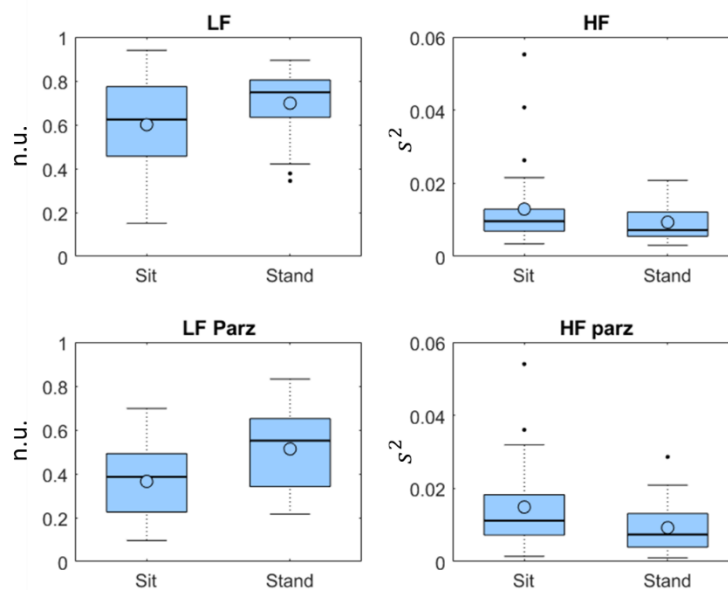


Figure 4.16: LF and HF computed on total and partial spectra. Sit to Stand.

4.3 EDA decomposition analysis

The first subject of the N-Back protocol was selected as the example for all the analyses concerning the EDA signal. The decomposition of the EDA signal into its phasic and tonic components explained in chapter 3.3.1 is shown in Figure 4.17.

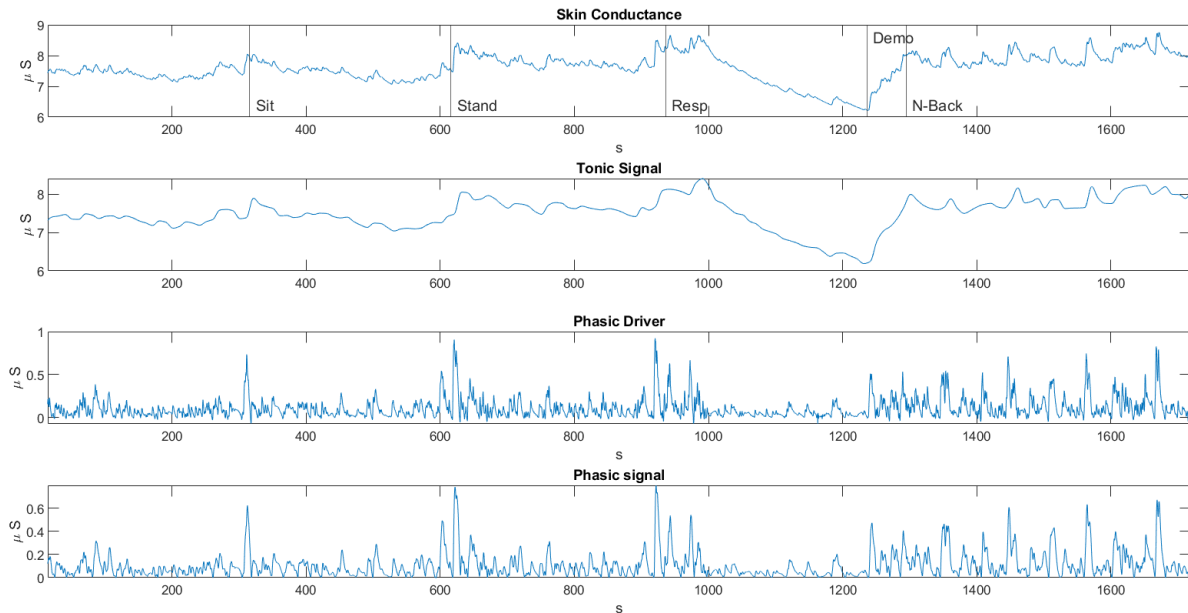


Figure 4.17: Ledalab Decomposition of EDA

The observed results are consistent with the expectations. During the first 10 minutes, that correspond to the baseline and sit phases, the tonic signal is lower compared to the stand and cognitive phases. This effect was identified in almost all the participants, as will be discussed in chapter 4.6.2.2. During the 5 minutes of controlled respiration the skin conductance decays quickly. However this effect, which is consistent with the reduced sympathetic activation expected from this task, is not conserved in all subjects. The frequency and amplitude of the peaks identified on the phasic component follow the same trend, as was confirmed by the correlation analysis in chapter 4.7.2.1. This effect is also physiologically well justified, since the average conductivity of the skin, which is quantified by the tonic component of the signal, depends directly on the number of sweat glands that open and the amount of sweat they release, which corresponds to the phasic component.

Figure 4.18 illustrates the advantage of the decomposition approach over standard peak-detection algorithms with threshold. The algorithm is able to reliably detect overlapping peaks and label them independently. Only peaks that overcome the threshold of 0.1 standard deviations are considered. In the image can also be seen the

phasic signal sometimes falls below 0. This effect is not physiologically justified and is considered noise.

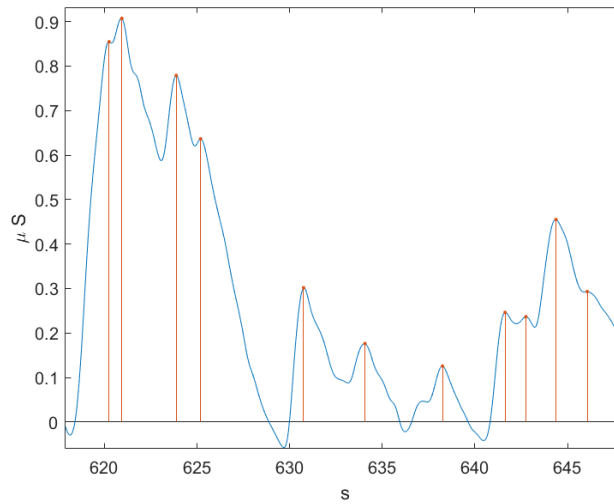


Figure 4.18: Identified peaks on phasic signal.

4.4 EDA Time-frequency analysis

Figure 4.19 reports the error variance as a function of the model order for all subjects obtained for the batch parametric time-frequency analysis

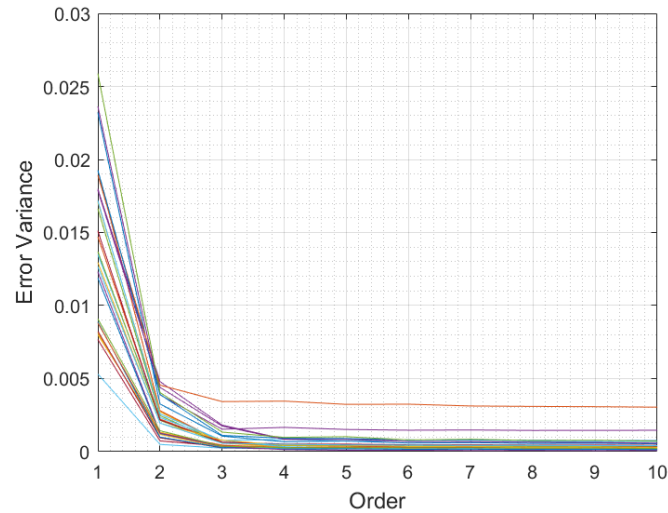


Figure 4.19: Error variance in AR batch analysis of EDA.

The order was set to 4 since after that the error variance remains almost constant. Concerning the time-varying AR model, instead, the order 4 is not sufficient to minimize the variance of the prediction error, as shown in Figure 4.20. The order was ultimately set to 7 because it appears to be a valid trade-off between the need to minimize the error variance and avoid overfitting.

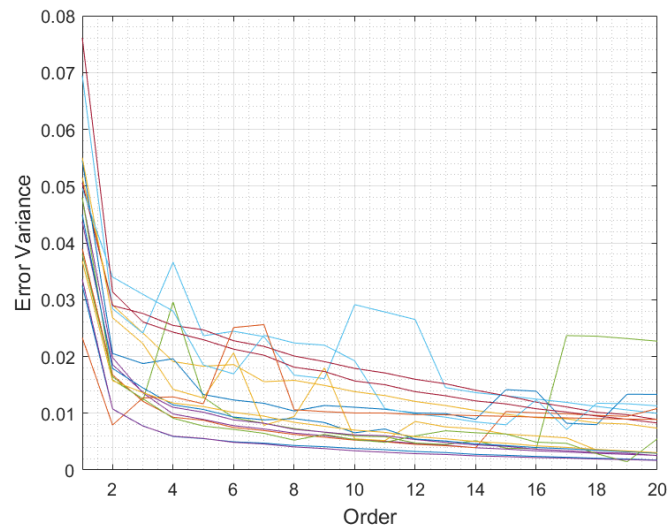


Figure 4.20: Error variance in TVAR analysis of EDA.

The control on the error was applied and the value of F_{eda} ("Eq16") was set to 7, which is higher than the values used for the HRV analysis since a higher prediction error is expected in the EDA signal.

The ARTVAR model was also validated by inspecting the whiteness of the prediction error. Figure 4.21 shows the power spectral density and the autocorrelation function of the prediction error obtained applying the algorithm on the first subject.

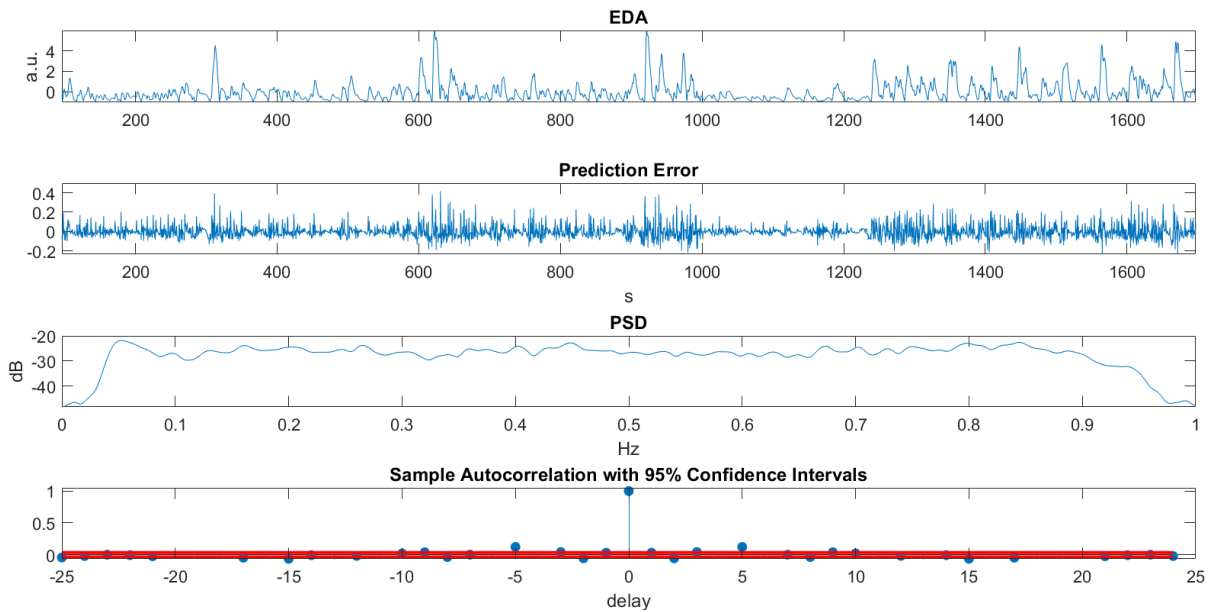


Figure 4.21: The prediction error, its spectrum and ACF from EDA TVAR

Despite the observable high non-stationarity of the EDA signal, the algorithm appears to be able to fit it correctly, as shown by the fact that the prediction error does not retain any dominant frequency.

Figure 4.22 shows how the forgetting factor varied during the protocol. As it can be seen, the forgetting factor quickly adapts and reduce its values when the signal varies its properties and gets closer to unity when the signal is approximately stationary.

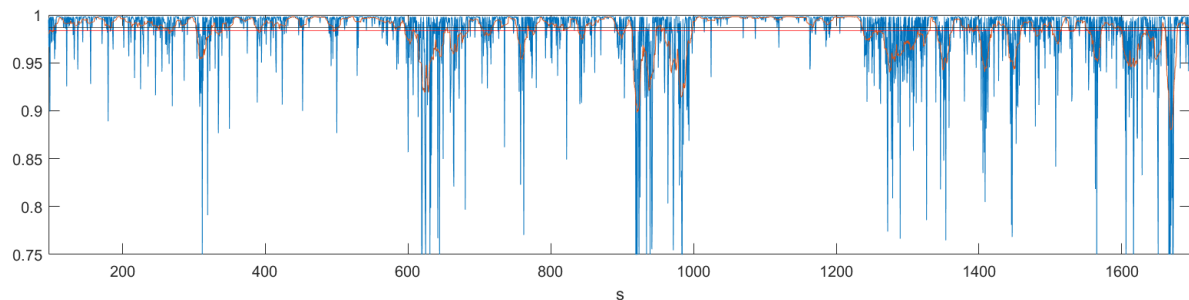


Figure 4.22: Forgetting factor with Fortescue.

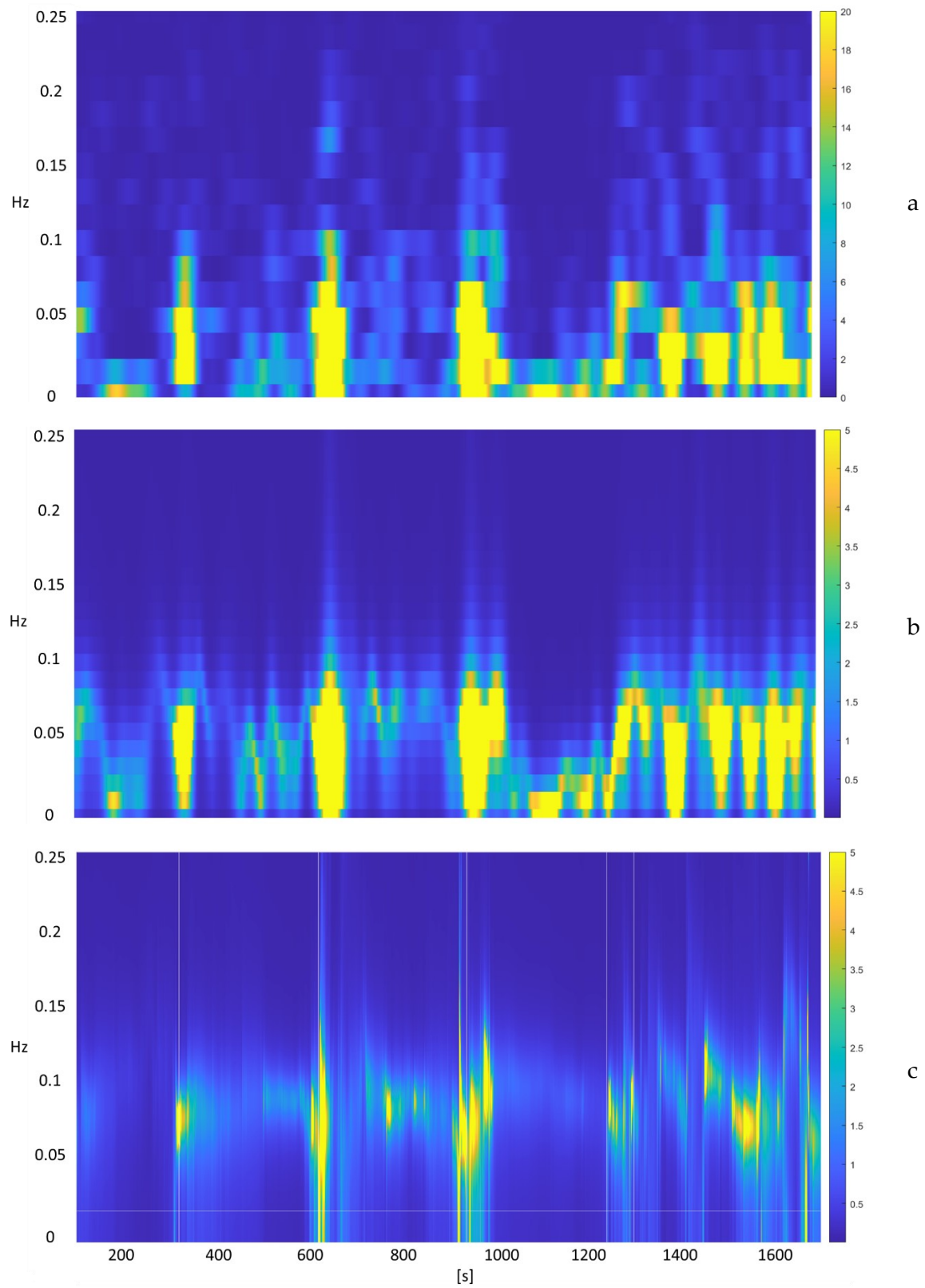


Figure 4.23: EDA Spectrograms. a) non parametric b) parametric batch c) ARTVAR

The spectrograms computed with the three time-frequency methods presented in chapter 3.3.2 are presented in Figure 4.23. The most relevant difference among the three approaches is the higher temporal definition of the ARTVAR algorithm.

4.4.1 Time-Frequency domain features

The total power and the power in the frequency band of interest according to literature (i.e. 0.045 – 0.25Hz) were computed integrating over the frequency in the spectrograms, similarly as it has already been reported for the HRV.

Figure 4.24 shows TVSymp computed with the three different methods. As it can be seen in image, the time-variant feature is associated with a much higher temporal resolution. Indeed, compared to the other methods tested, the time-variant autoregressive algorithm has the advantage of being able to capture fast variations in the statistical properties of the signal.

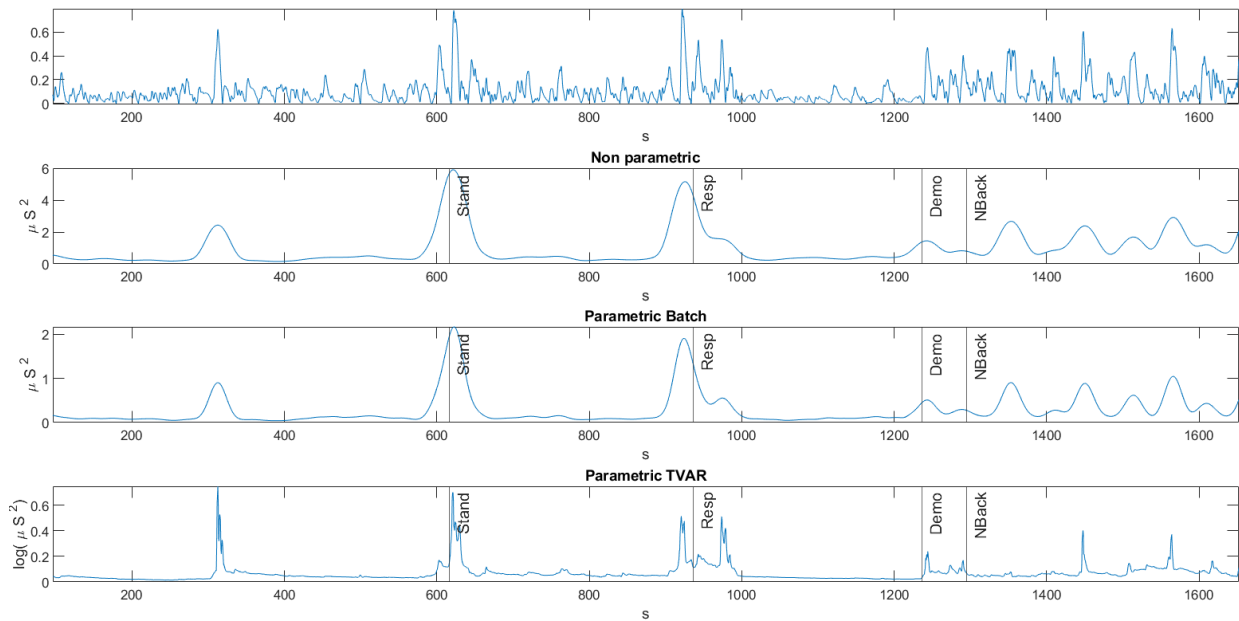


Figure 4.24: Phasic signal and TVSymp computed with the 3 methods.

On the basis of these results and in order to be consistent with the approach used for the HRV analysis, the time-variant algorithm was selected for the extraction of the time-frequency descriptors of EDA and further statistical analysis.

Figure 4.24 also shows that TVSymp is especially sensible to fast variations in the dynamic of the signal, that produce high prediction errors and therefore result in a lower power in the spectral estimation ("Eq17").

Since almost all the power of the signal falls in the frequency range of TVSymp, it can be considered an estimation of the power of the filtered signal and is almost identical to TVTot, which was therefore not considered in further analyses.

4.5 EDA - HRV Cross-Correlation

The normalized cross-correlation between the inverse of the tachogram and the phasic component of the EDA signal was used to evaluate if the two signals present some common patterns. As can be seen in Figure 4.25., almost all subjects present a peak at few seconds after the 0 delay. This observation suggests that the EDA signal is delayed with respect to the tachogram, which is consistent with [94], in which is reported that the EDA signal has significant latency, of around 1.60 -2.23.

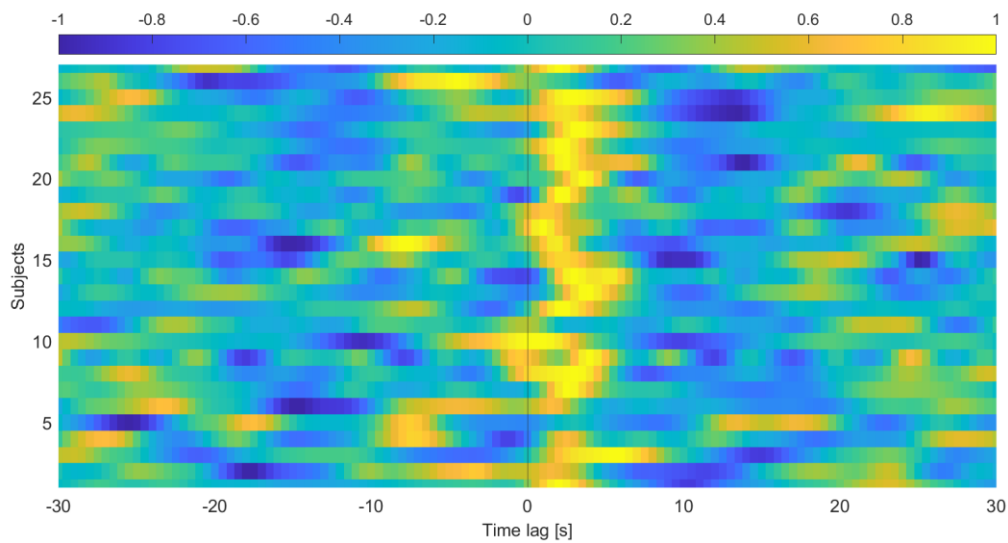


Figure 4.25 Cross-correlation EDA-RR

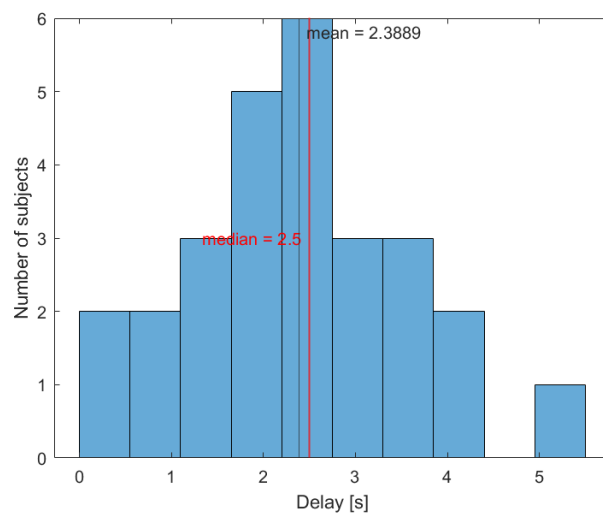
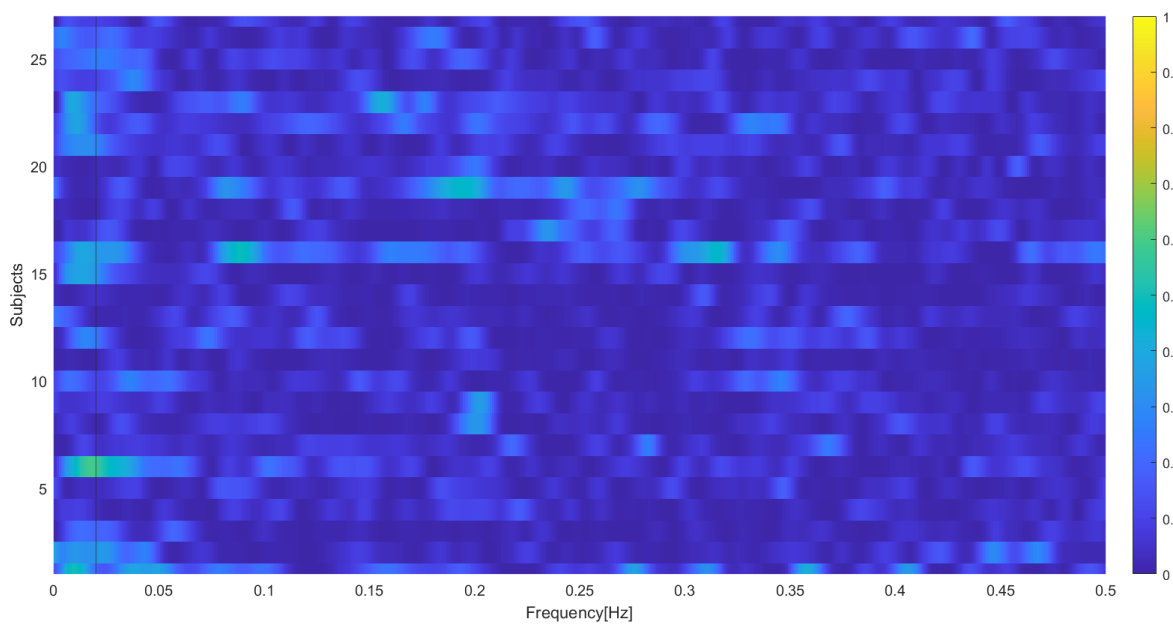


Figure 4.26 Estimated time delay EDA-RR

To quantify the delay, the lag corresponding to the maximum cross-correlation in the range from 0 to 6 s was considered. These values were selected as a reasonable lag between the two signals. The result is reported in [Figure 4.26](#)

The median delay is around 2.5s. The method adopted allows to obtain only a rough estimate, since the signals were resampled at 2Hz. Furthermore, the RR series has a time resolution that depends on the hearth frequency and is typically only slightly higher than 1Hz (to cross-correlate the two signals EDA was downsampled and the tachogram was resampled).

In the frequency domain only the component independent from the respiration of the tachogram was used (NRSA). As can be seen in [Figure 4.27](#), the magnitude squared coherence is quite low for all subjects and no dominant frequency band in which the two signals interact could be identified. In the image the rows represent subjects, the columns the frequency intervals, and the colour the coherence value.



[Figure 4.27](#) Magnitude squared coherence EDA Phasic-NRSA

The lack of strong correlations between the two signals in frequency suggests that they do not significantly covary at any frequency analysed but rather bring heterogeneous information. However, the two signals are non-stationary, especially the phasic component of EDA, which may affect the quality of this estimation.

4.6 Statistical Analysis: Differences Across Tasks

This chapter reports the results of the statistical analysis presented in chapter 3.5.1. The goal is to investigate how the various indices vary in response to the different experimental conditions and to identify, among them, the autonomic features that better reflect cognitive load.

4.6.1 BASE protocol

In this chapter the distributions of the features extracted during the phases of Read problem –(RP), Code writing (WR), Code reading (RC) and Text reading (RT) are reported and compared by means of boxplots. Moreover, statistical significant differences identified by the Friedman test are highlighted on the boxplots using a red line. p-values lower than 1% are marked with two asterisk, p values between 1 and 5% with one.

As can be observed in Figure 4.28, the heart rate is significantly higher during the Writing task in both difficulty levels (i.e., SPLIT and RLE). This effect can be explained as the result of the higher metabolic demand induced by the cognitive effort of this task.

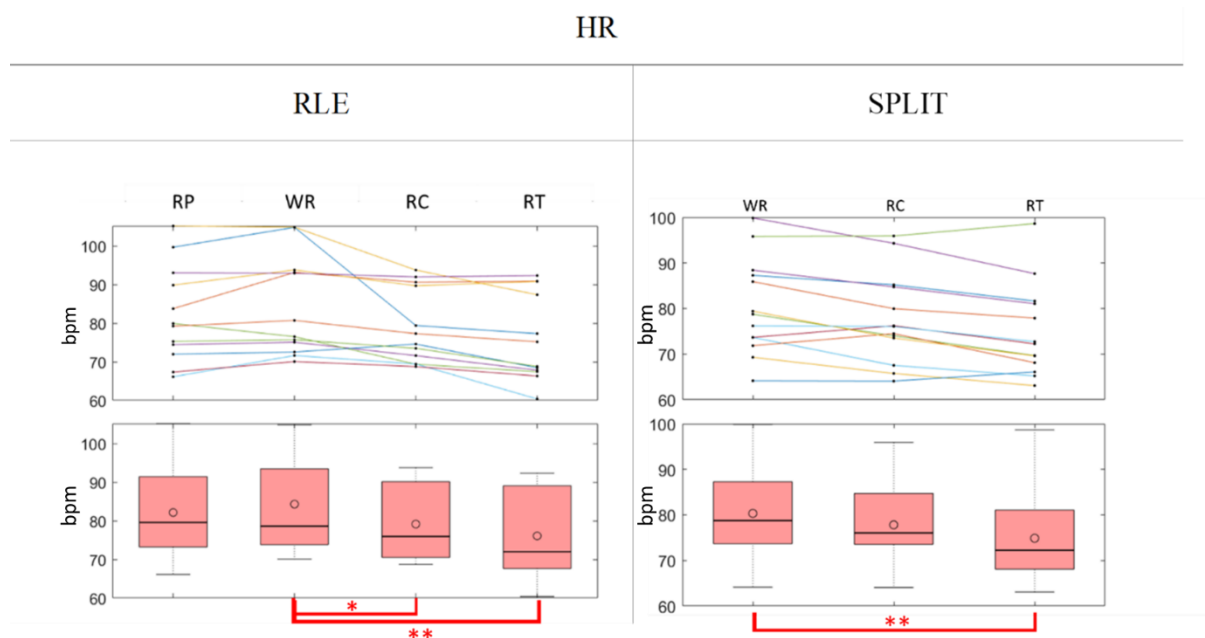


Figure 4.28 Heart Rate across tasks of BASE

Intra-subject variability in the resting heart rate, that could not be corrected due to the lack of a sufficiently long baseline, make it difficult to clearly visualize the

existing differences of HR values among the compared tasks. However, from the upper plot it can be observed that most subjects show a common trend: increasing HR with increasing task demand. Furthermore, the increase in heart rate is accompanied by a significant reduction in the total power in both RLE and SPLIT (Figure 4.29). Consistently, SDNN is lower during Writing compared to Code reading. However, the difference in SDNN is only significant in RLE, which is the most difficult task (Figure 4.30). The difference between P Tot and SDNN, besides the method applied for the computation, is that SDNN also considers very low frequencies, that have been discarded from the computation of the time-frequency HRV features.

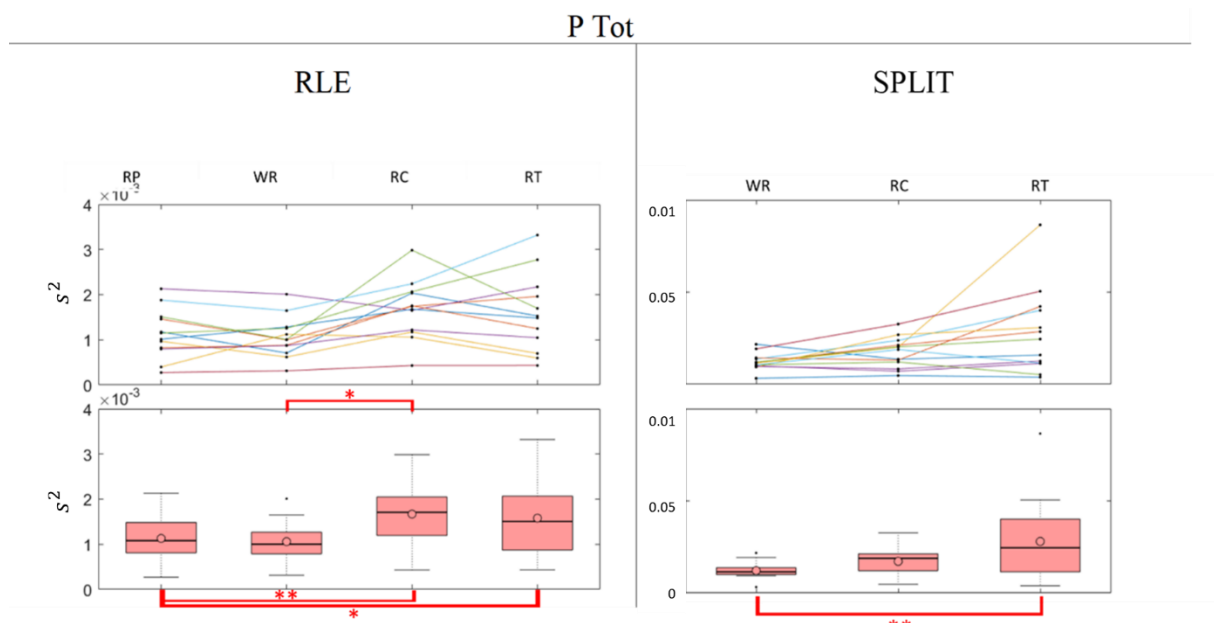


Figure 4.29 P Tot. BASE protocol

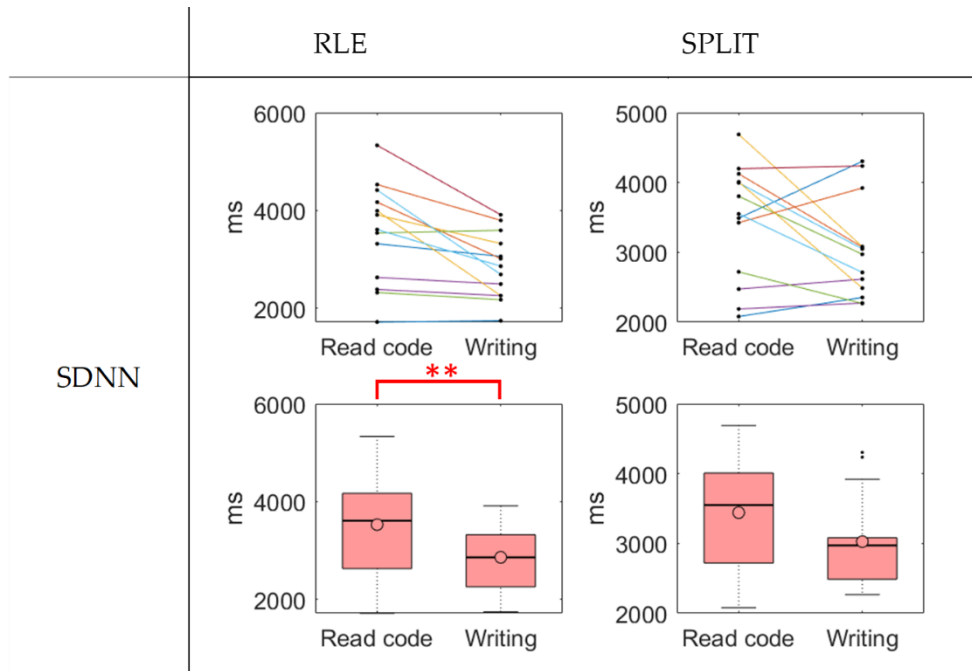


Figure 4.30 SDNN. BASE protocol

The observed reduction in total power during more demanding cognitive tasks is consistent with other works in the literature [59],[3].

Moreover, HF (Figure 4.31), the Power Coherent with the respiration (Figure 4.32), and the respiratory rate (Figure 4.33) are all significantly lower during the Writing task in RLE but not in SPLIT. The reduction of the respiratory rate during Code writing is expected and consistent with most works in the literature [64].

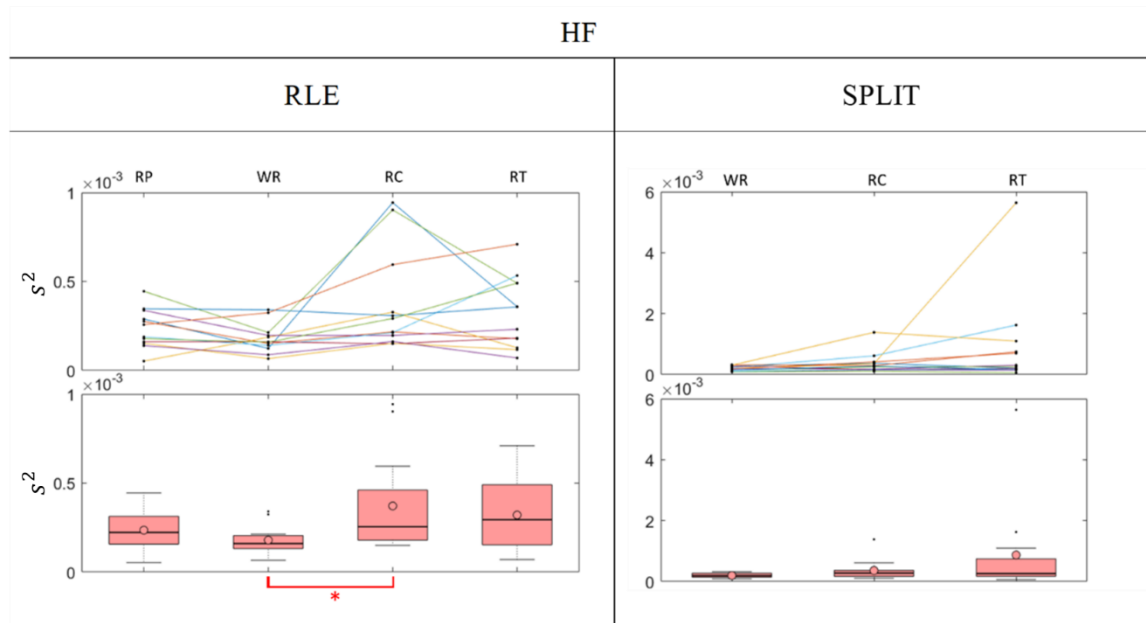


Figure 4.31 HF. BASE protocol

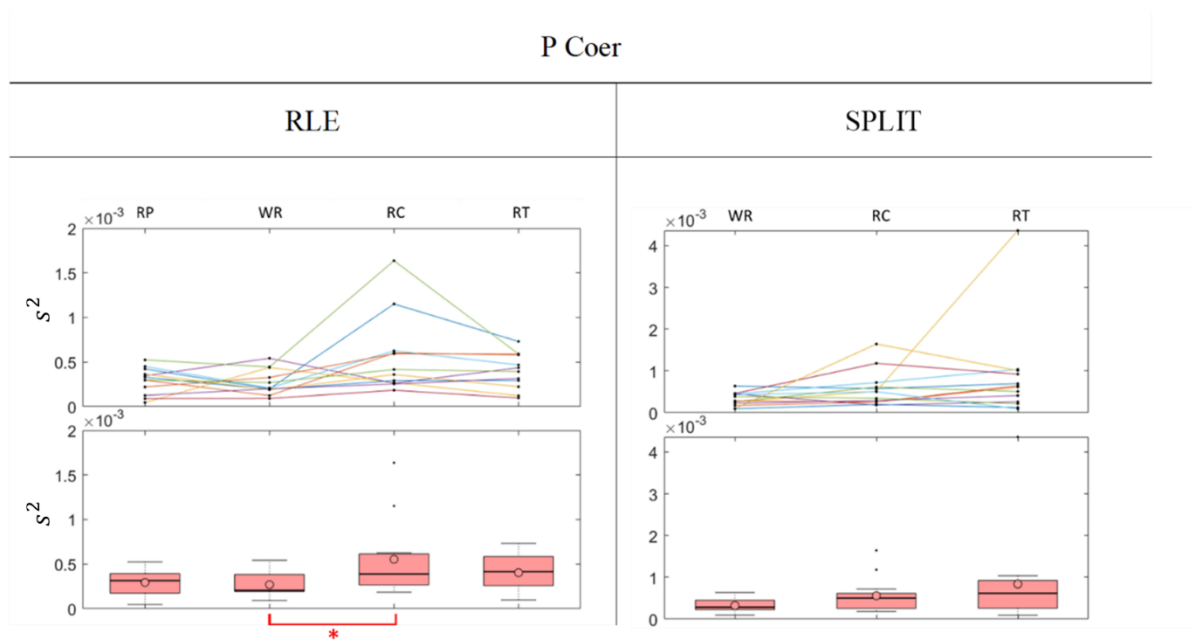


Figure 4.32 P Coer. BASE protocol

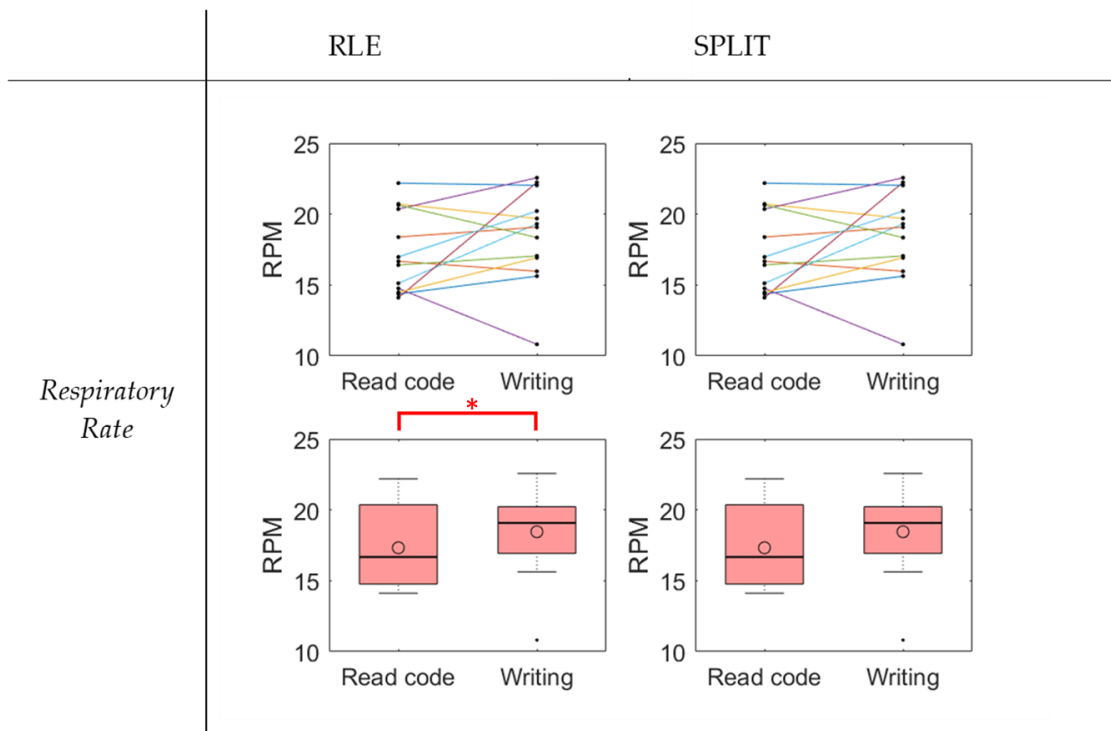


Figure 4.33 Respiratory Rate in Resp Per Minute

No significant differences were identified considering the normalized power in the LF band, neither if calculated from the partial (Figure 4.35) nor the total spectra (Figure 4.34). For most subjects, it maintained relatively high values during the entire protocol. A possible explanation could be related to the stressing nature of the protocol, probably also accentuated by the uncomfortable instrumentation, and the consequent difficulty for the participants to relax.

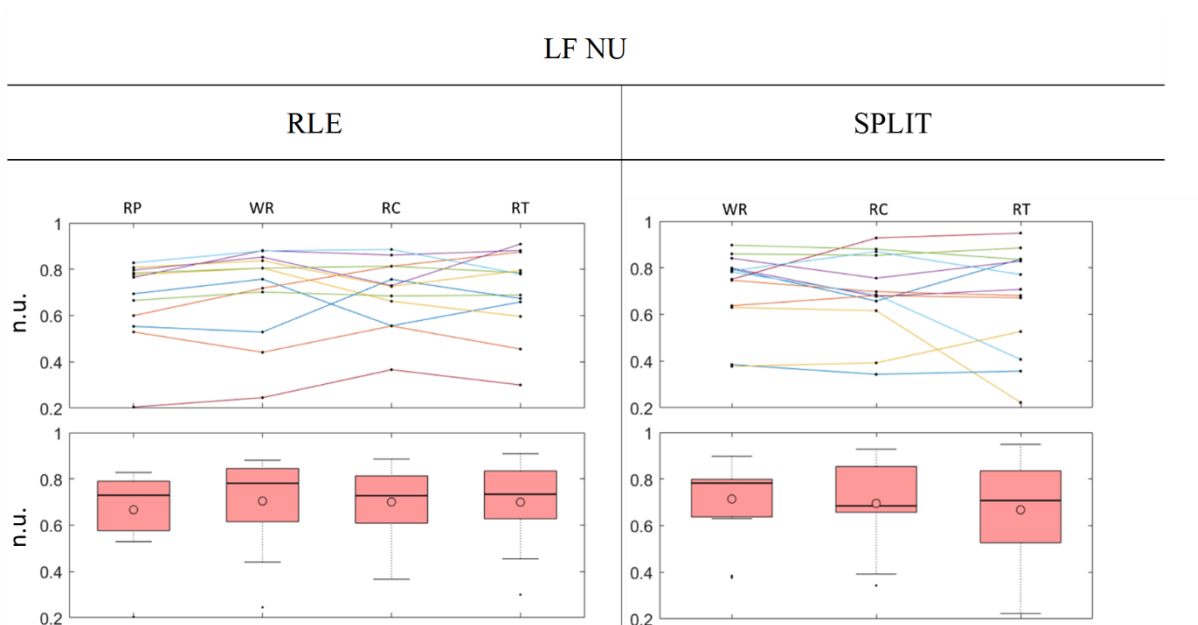


Figure 4.34 LF NU. BASE protocol.

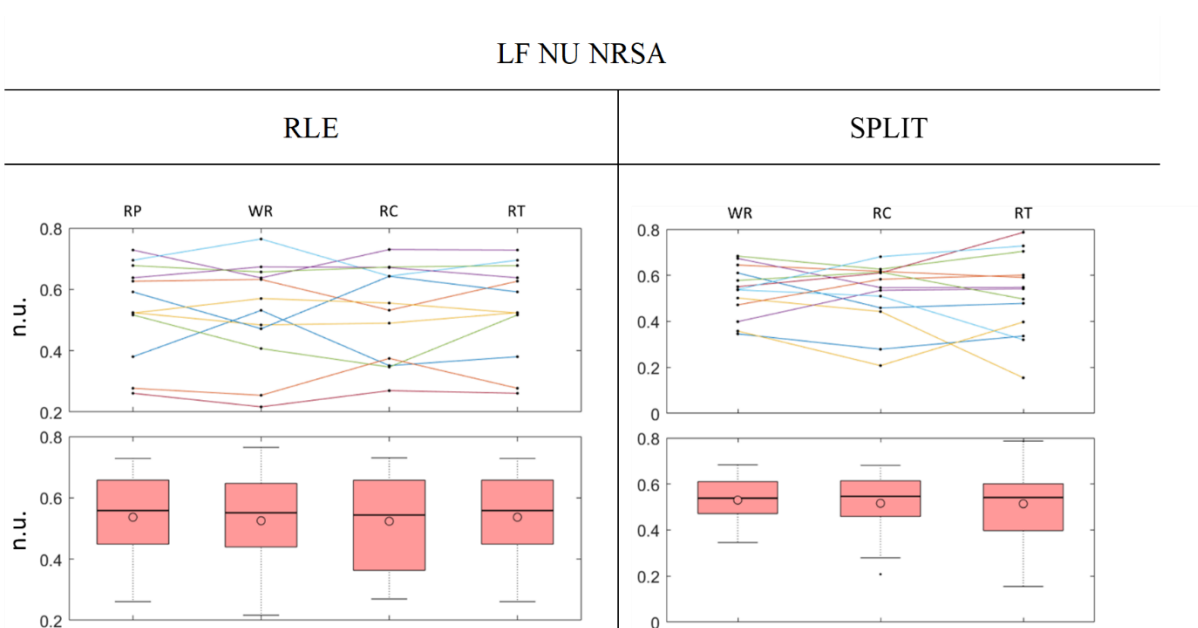


Figure 4.35 LF NU NRSA. BASE protocol

Altogether, reading code and reading natural text appear to produce similar autonomic activations while the coding task significantly increased the heart rate and reduced the total power of the HRV signal.

The adaptation of the frequency band to the respiratory rate and the decomposition of the spectra did not improve the ability of the indices to discriminate between tasks in this protocol.

Table 4-1, Table 4-2 and Table 4-3 summarize the significant results obtained in the BASE protocol. The complete tables can be found in Appendix (Table A-1, Table A-2, Table A-3, Table A-4).

RLE

	FRIEDMAN	PAIRED COMPARISONS					
		RP-WR	RP-RC	RP-RT	WR-RC	WR-RT	RC-RT
HR	<0.01	0.4919↑	1	0.0684↓	0.0265↓	<0.01↓	0.9283↓
P TOT	<0.01	1	<0.01↑	0.0159↑	0.0159↑	0.0265↑	1
HF	0.0129	0.3466↓	1	1	0.0265↑	0.0265↑	1
P COER	<0.01	1	0.0684↑	0.4919↑	0.0159↑	0.1611↑	1

Table 4-1 Significant p-values in RLE

RLE

	SDNN	Resp Rate
WR-RC	<0.01↑	0.0215↓

Table 4-2 Significant p-values in RLE

SPLIT

	FRIEDMAN	PAIRED COMPARISONS		
		WR-RC	WR-RT	RC-RT
HR	<0.01	0.5094↓	<0.01↓	0.1495↓
P TOT	0.0125	0.7179↑	<0.01↑	0.2326↑

Table 4-3 Significant p-values in SPLIT

4.6.2 N-Back Protocol

4.6.2.1 HRV features

As reported in Figure 4.36, the results obtained in the N-back protocol show a reduction in the total power of the HRV during the cognitive task compared to Sit, which is consistent with the results obtained in the BASE protocol. Sit was chosen as the reference task since it does not require a specific cognitive effort, neither is characterized by specific sympathetic or parasympathetic stressors. The total power was also significantly higher during the controlled respiration task, an effect that can be explained by the increased RSA. SDNN, on the other hand, was not able to capture this difference, as shown in Figure 4.37.

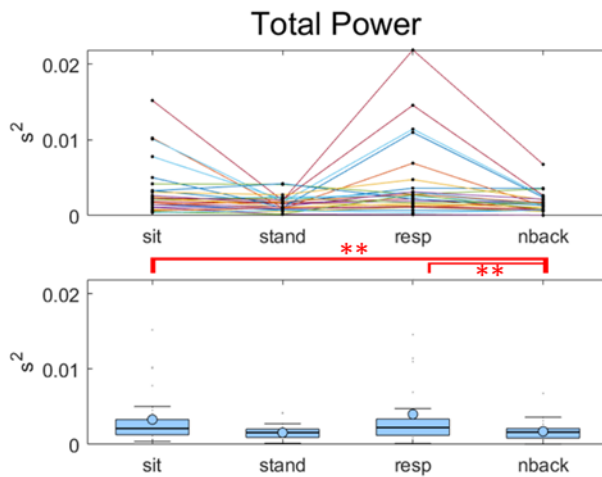


Figure 4.36 P Tot. N-Back Protocol

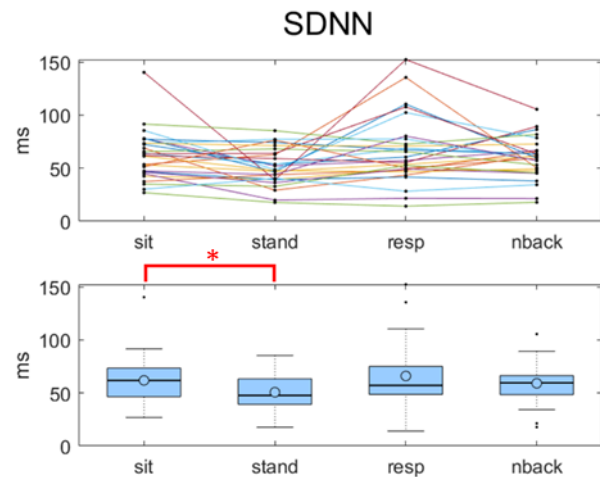


Figure 4.37 SDNN. N-Back Protocol

The coherent power and the power in the HF band showed very similar trends, as presented in Figure 4.38 and Figure 4.39. This was expected since most of the power in the HF band is due to the effect of the RSA. In particular, their values decreased during the cognitive task and increased during the controlled respiration. However, no statistical differences between the Sit and N-back tasks were detected. The data in Figure 4.38 and Figure 4.39 were represented in a logarithmic scale to improve the visualisation.

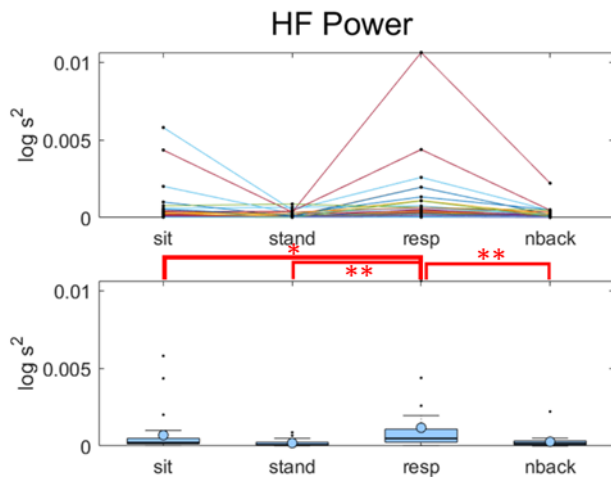


Figure 4.38 HF. N-Back Protocol

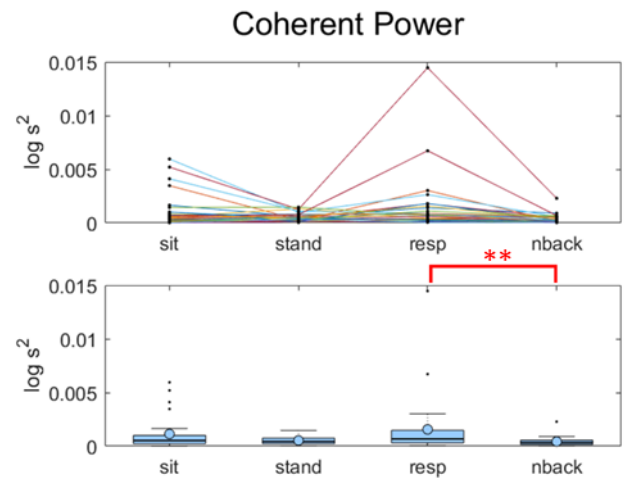


Figure 4.39 P Coer. N-Back Protocol

Differently from what observed on the BASE protocol, in this protocol the heart rate was not significantly higher during the cognitive task compared to the low effort task (Sit). Indeed, the HR increased only during the Stand phase, which is expected due to the higher metabolic demand required by the standing position (Figure 4.40).

The respiratory rate instead increased during the cognitive task and not during the stand phase (Figure 4.41). This effect is probably due to the fact that the respiration was, for most subjects, less regular during the cognitive task. This result is consistent with the results of the BASE protocol and with results obtained in similar works in the literature [64]. The respiratory rate during the controlled respiration task was exactly 12 resp/min as requested by the protocol and was not plotted.

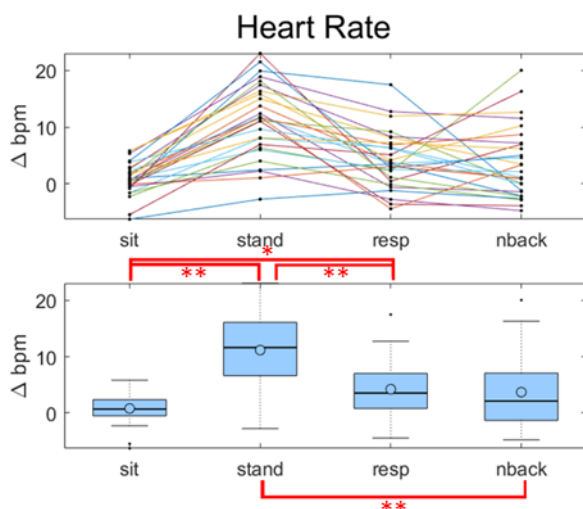


Figure 4.40 HR. N-Back Protocol

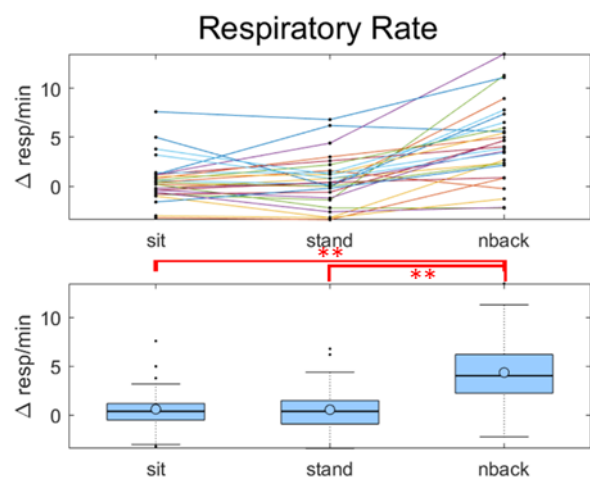


Figure 4.41 Respiratory Rate.

The normalized power coherent with the respiration showed significant differences and reached its minimum during the N-back task (Figure 4.42). The normalized power in the LF band computed on the partial spectra, contrary to the BASE protocol, showed a significant trend consistent with the expectation (Figure 4.43), i.e. higher levels during Stand and cognitive task compared to sit and Controlled respiration. Both these features are significantly different during the cognitive task compared to Sit but not compared to Stand.

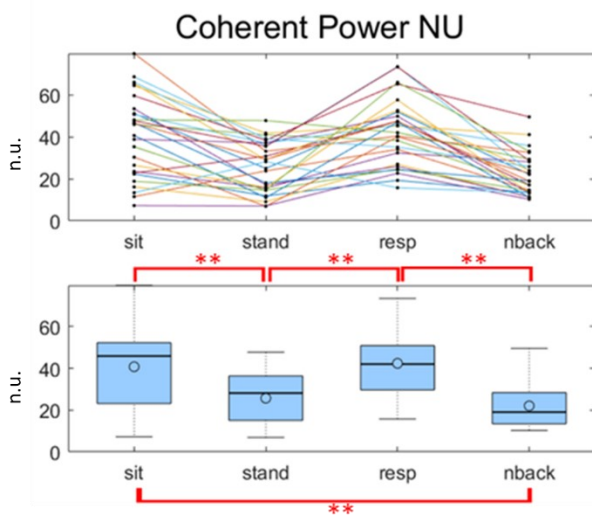


Figure 4.42 P Coer NU as percentage

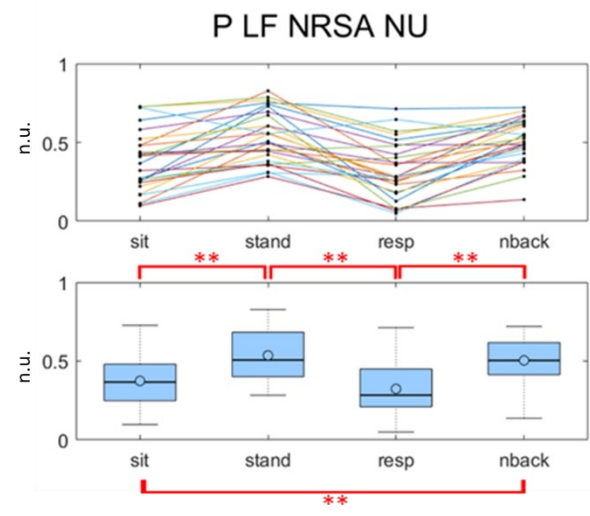


Figure 4.43 LF NU NRSA

In conclusion, these features do not differentiate between the cognitive and orthostatic stressors.

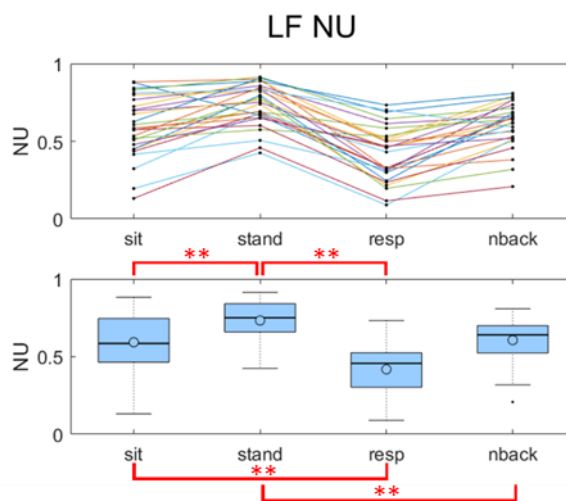


Figure 4.44 LF NU. N-Back protocol

The power in LF computed on the total spectra on the other hand was significantly lower during N-back compared to Stand, as shown in Figure 4.44. It is possible however that this effect is due to the incorrect inclusion of the RSA in its computation, as already discussed in chapter 4.2.

RMSSD, which is a measure strongly correlated with the power in HF, assumed lower values during the Stand phase compared to all the other tasks. Similar results were obtained from SampEn, a measure of information. These two features, depicted in Figure 4.45 and Figure 4.46, did not capture any other significant differences.

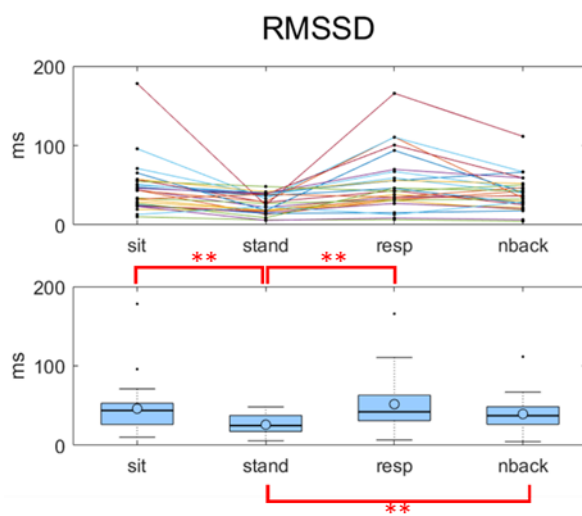


Figure 4.45 RMSSD. N-Back protocol

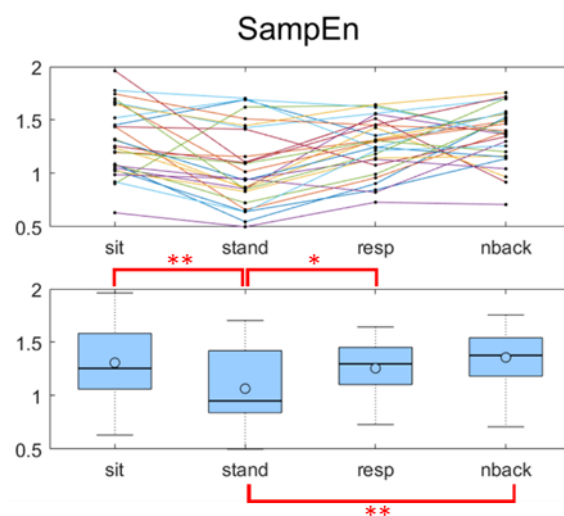


Figure 4.46 SampEn. N-Back protocol

In general, these results suggest that the cognitive task reduced the parasympathetic tone and increased the sympathetic one compared to the Sit task, in which no cognitive effort was required. The Stand and Controlled respiration produced the expected variations, confirming the validity of the methods adopted.

Altogether, despite the same algorithms were used for their computation the features extracted from the HRV and Respiratory signals in the N-Back protocol yielded more significant results compared to the BASE protocol.

A possible reason can be found in the protocol itself. BASE required the participants to wear uncomfortable sensors for a long time (in particular for the acquisition of NIRS and EEG signals) and did not contain a proper relaxation phase.

On the contrary, the N-Back protocol only required the acquisition of autonomic signals, that for their very nature are easier to acquire with more comfortable instrumentation. In addition, the tasks proposed have been selected specifically for the analysis of the autonomic system. The Relaxation and Sit phases allowed the

subjects to relax. The Respiration phase required participants to take long controlled breaths, an action that is known to elicit a parasympathetic activation and induce Respiratory Sinus Arrhythmia. The Stand phase, on the other hand, is a common stressor used to stimulate the sympathetic system.

All the significant features and the p-values obtained from paired multi comparisons are reported in Table 4-4. The complete table is reported in Appendix (Table A-5).

	FRIEDMAN	PAIRED COMPARISONS					
		Sit-Stand	Sit-Resp	Sit-NB	Stand-Resp	Stand-NB	Resp-NB
HR	<0.01	<0.01↑	0.0504↓	0.8401↑	<0.01↓	<0.01↓	1
P TOT	0.0159	0.2101↓	1	<0.01↓	0.2101↑	1	<0.01↓
HF	<0.01	0.0368↓	0.0504↑	0.4388↓	<0.01↑	1	<0.01↓
HF RSA	<0.01	0.0368↓	1	<0.01↓	<0.01↑	1	<0.01↓
LF NU	<0.01	<0.01↑	<0.01↑	1	<0.01↑	<0.01↑	<0.01↑
LF NU NRSA	<0.01	<0.01↑	1	<0.01↑	<0.01↓	1	<0.01↑
LF/HF	<0.01	<0.01↑	<0.01↓	0.5501	<0.01↓	0.6831↓	<0.01↑
P COER	<0.01	1	1	0.1611↓	0.6831↑	0.2712	<0.01↓
P COER NU	<0.01	<0.01↓	1	<0.01↓	<0.01↑	1	<0.01↓
RMSSD	<0.01	<0.01↓	1	0.5501↓	<0.01↑	<0.01↑	0.6831↓
SDNN	0.0293	0.0266↓	1	1	0.1611↑	0.8401↑	1
PNN50	<0.01	<0.01↓	1	0.8775↓	<0.01↑	0.3579↑	0.1074↓
SAMPEN	<0.01	<0.01↓	1	1	0.0368↑	<0.01↑	1
RESP. RATE	<0.01	0.9122		<0.01↑		<0.01↑	

Table 4-4 p-values N-Back, HRV features

The features computed on the partial spectra discriminate better between Sit and the N-back task, probably because during Sit the respiratory rate often fell into the LF

band. The decomposition allows to better capture the increase in sympathetic tone in the cognitive task compared to the neutral task. However, they do not identify significant variations between the Stand task and the cognitive one.

4.6.2.2 EDA features

Features computed on the phasic driver show a modest increase during the Stand phase and a more significant increase during the cognitive task. The trends of ISCR and Peak Frequency are very similar, as shown in Figure 4.47 and Figure 4.48. This was expected since the two measures are strongly correlated.

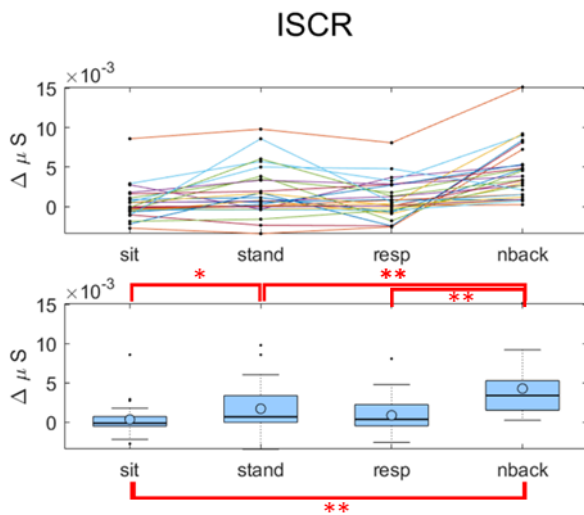


Figure 4.47: ISCR. N-Back Protocol

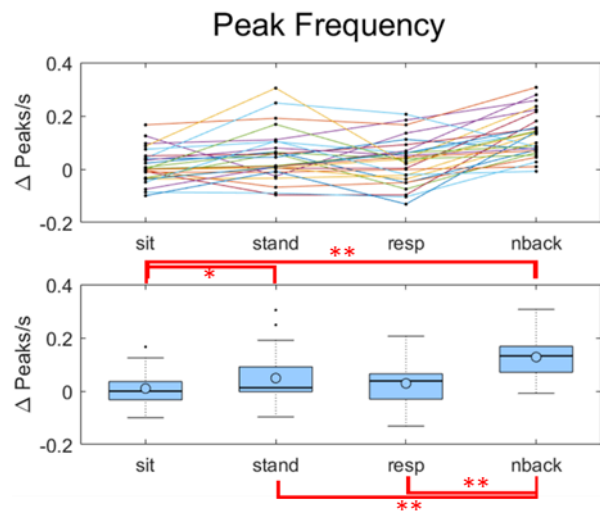


Figure 4.48: Peak Frequency. N-Back Protocol

Considering the tonic component (Figure 4.49) the trend is similar but less significant, in accordance with the result already reported in the literature [68]. Noticeably, the cognitive task is the only one that induces significant variations in the tonic component.

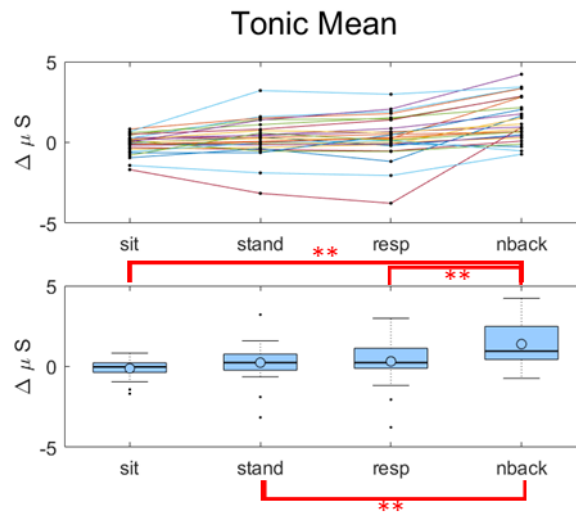


Figure 4.49: Tonic Mean. N-Back Protocol

The results obtained in the time-frequency domain are similar to those obtained in the time domain, as shown in Figure 4.50 and Figure 4.51.

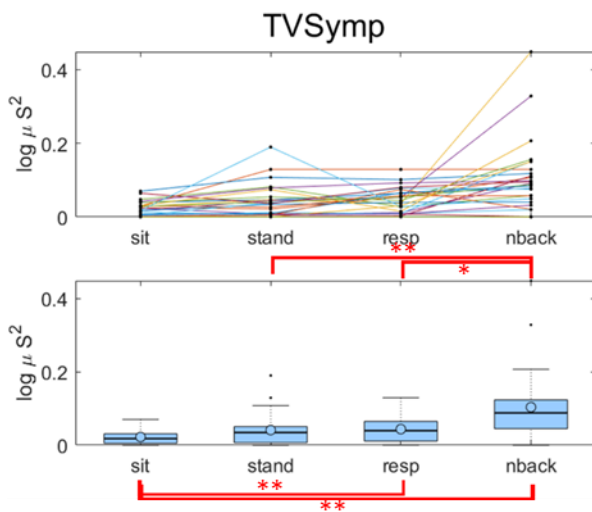


Figure 4.50 TVSymp. N-Back Protocol

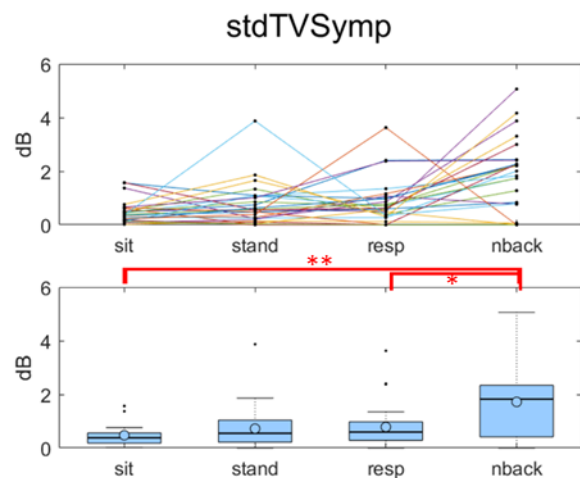


Figure 4.51 StdTVSymp. N-Back Protocol

All the indices extracted from the EDA signal, which is known to be dependent only on the sympathetic branch of the autonomous nervous system, significantly increased during the cognitive task compared to relaxation. All of them maintained the trend also compared with the Stand task, which was expected to elicit a sympathetic activation, even though it is generally less significant. A possible explanation is that, while the cardiorespiratory parameters need to adapt to the standing position to control the blood pressure and find a new equilibrium, the EDA

parameters only react to the transition from Sit to Stand and rapidly recover. On the other hand during the cognitive task, that provides continuous stimuli, the sympathetic activation measured through the EDA parameters remain high. This hypothesis can be confirmed by exploiting the advantage of the features extracted in time frequency domain, that allow tracking variations in time, as shown in [Figure 4.52](#). that shows the trend of TVSymp on an example subject.

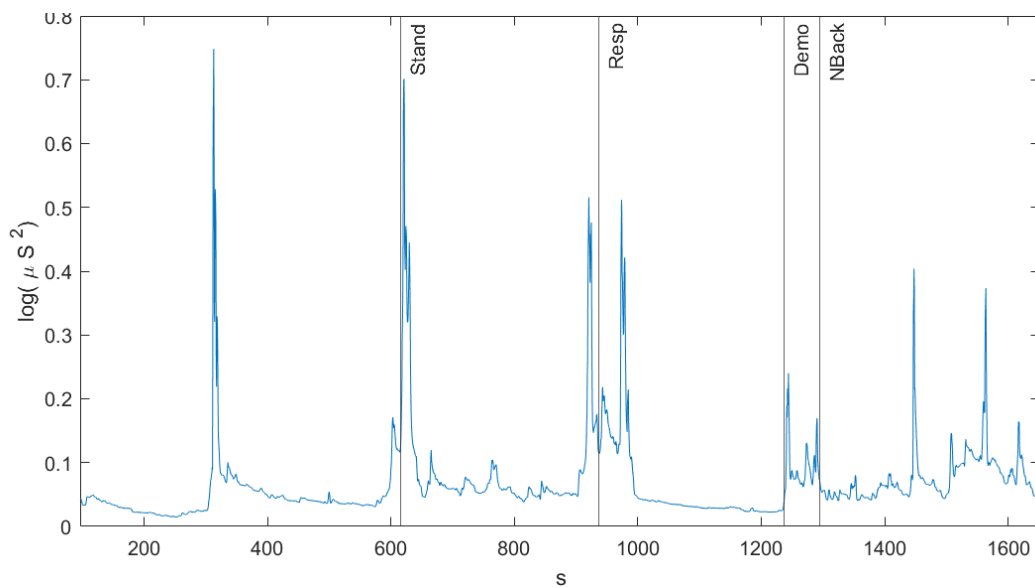


Figure 4.52: TVSymp. First subject of the N-Back Protocol

The Controlled respiration, which is known to suppress indices of sympathetic activation in the HRV, produced an increment in most EDA indices compared to the resting state. This apparent contradiction can be explained by some work in the literature. Indeed, EDA has been shown to be influenced by controlled, volitional respiration that requires cortical participation [95]. The response seems generated centrally, by an interaction of the respiratory neurons and the central autonomic system [96]. [Table 4-5](#) reports the p-values of the significant features. The table complete also with the non-significant results is reported in [Appendix \(Table A-6\)](#).

	FRIEDMAN	PAIRED COMPARISONS					
		Sit- Stand	Sit-Resp	Sit-NB	Stand- Resp	Stand- NB	Resp-NB
PEAK FREQ.	<0.01	0.0154 ↑	0.4325↑	<0.01↑	1	<0.01↑	<0.01↑
PEAK AMP.	<0.01	0.1375↑	0.0490 ↑	<0.01↑	1	0.0667↑	0.1805↑
ISCR	<0.01	0.0190 ↑	0.2101↑	<0.01↑	1	<0.01↑	<0.01↑
TONICMEAN	<0.01	0.2101↑	0.0504↑	<0.01↑	1	<0.01↑	<0.01↑
TVSYMP	<0.01	0.2061↑	<0.01↑	<0.01↑	0.8313	<0.01↑	0.0357 ↑
STDTVSYMP	<0.01	1	1	<0.01↑	1	0.1787↑	0.0483 ↑

Table 4-5: p-values N-Back, EDA features

4.7 Statistical Analysis: Correlations

In this chapter the correlations obtained between indexes of the autonomic nervous system, the outcome measures, and the indexes of the central nervous system computed from the EEG signal are discussed.

The ρ Spearman coefficients are represented using colours: positive correlations in red and negative in blue. Significant results are highlighted in yellow on the images.

4.7.1 BASE

4.7.1.1 Correlations among HRV features

Figure 4.53 shows the correlations obtained among HRV features. P Tot and SDNN, as expected, are highly correlated with each other, but also positively correlate with parasympathetic indices (P Coer, HF computed on the partial spectrum, RMSSD) and negatively with the heart rate but not with LF NU, which was also computed on the partial spectrum. Noticeably, LF NU does not significantly correlate with any feature.

All the others correlations identified are consistent with the expectations.

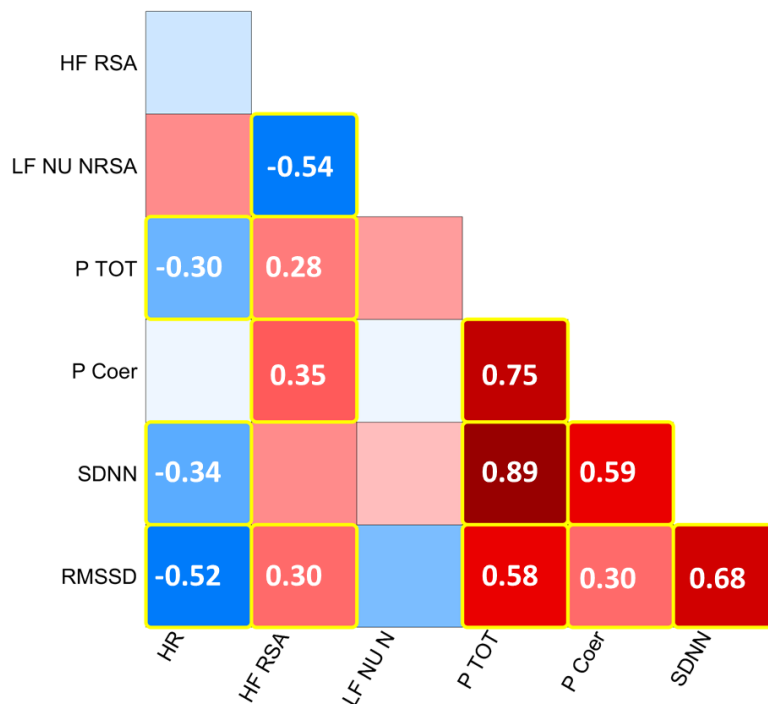


Figure 4.53: Correlation matrix. HRV features. Significant ρ are framed in yellow

4.7.1.2 Correlations with EEG features

The correlations between indices of the CNS and ANS are reported in Figure 4.54 and Figure 4.55, which are referred to the features computed in the Writing phase.

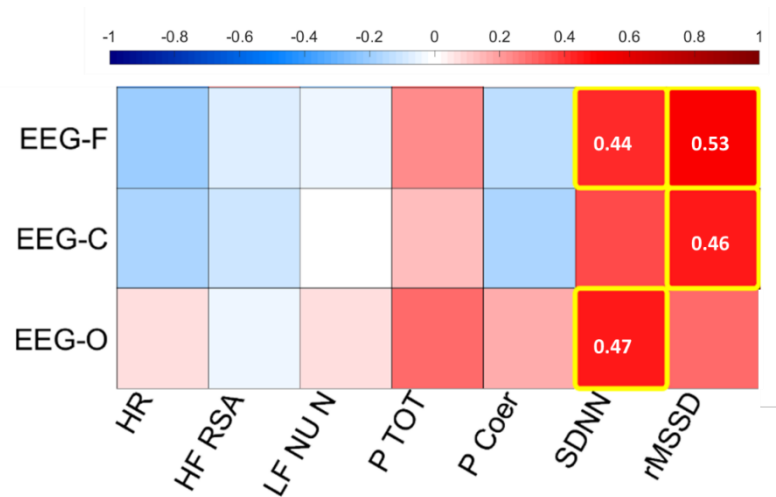


Figure 4.54 Correlation matrix. Theta band. Code writing

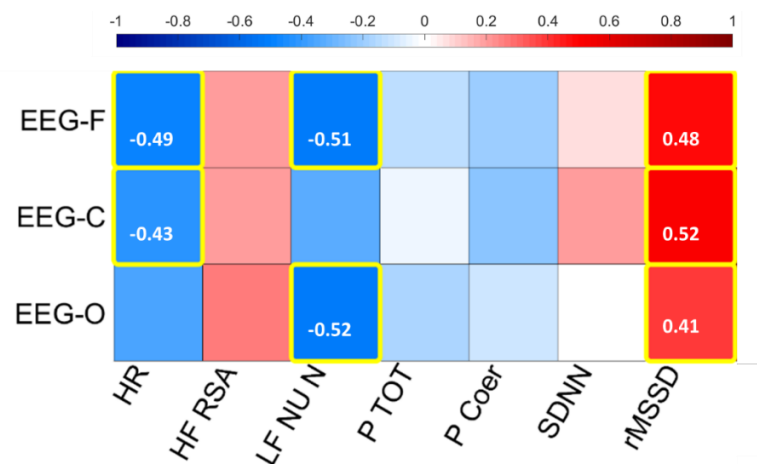


Figure 4.55 Correlation matrix. Alpha band. Code writing

The power in the alpha frequency band positively correlates with RMSSD. The scatterplot of the power in the alpha band in the frontal area and the RMSSD is also shown in Figure 4.56 with a linear interpolation line and the significance of the correlation coefficient. RMSSD is an index of vagal control on the hearth [20]. Higher levels of alpha are usually reported in resting conditions and have been interpreted as an inhibitory mechanism. Higher levels of alpha were here found to be linked to higher levels of vagally mediated control of the heart computed as RMSSD, but not with the component synchronous with the respiration, computed as P Coer and HF RSA, which was computed on the partial spectra that captures the effect of the

respiration on the variability of the heart rate. Consistently, alpha is negatively correlated with LF (Figure 4.57 shows its correlation considering the frontal area) and the Heart Rate, both measures of sympathetic control of the heart.

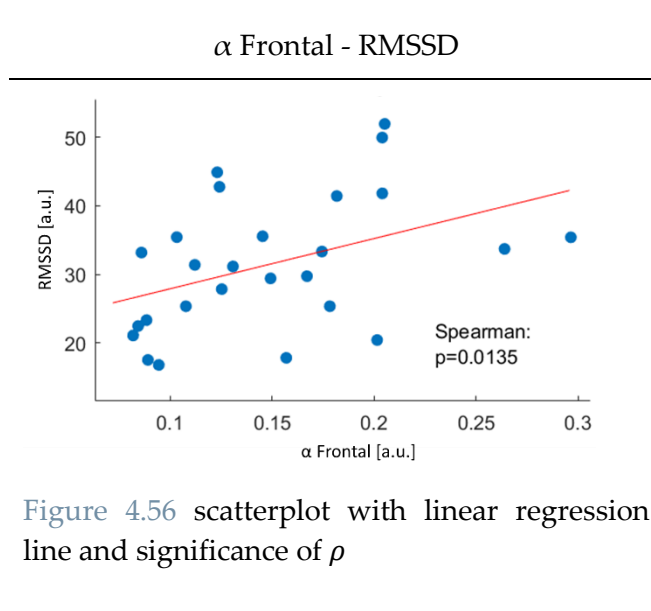


Figure 4.56 scatterplot with linear regression line and significance of ρ

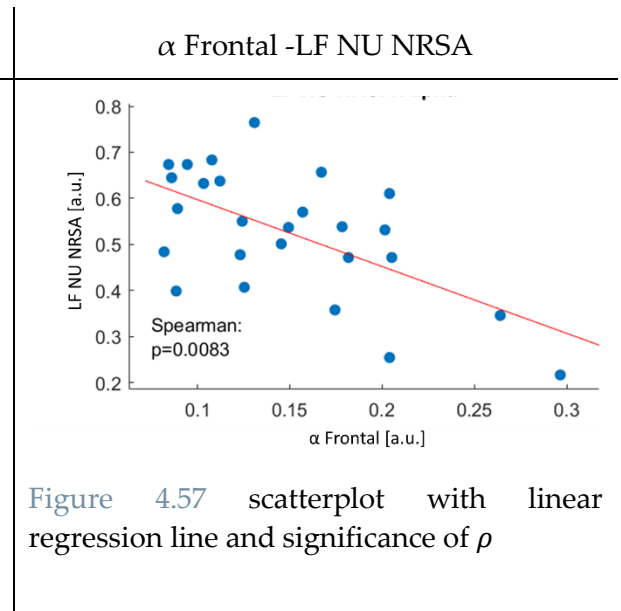


Figure 4.57 scatterplot with linear regression line and significance of ρ

The theta band is positively correlated with SDNN and RMMSD (Figure 4.58), both measures of variability of the HRV.

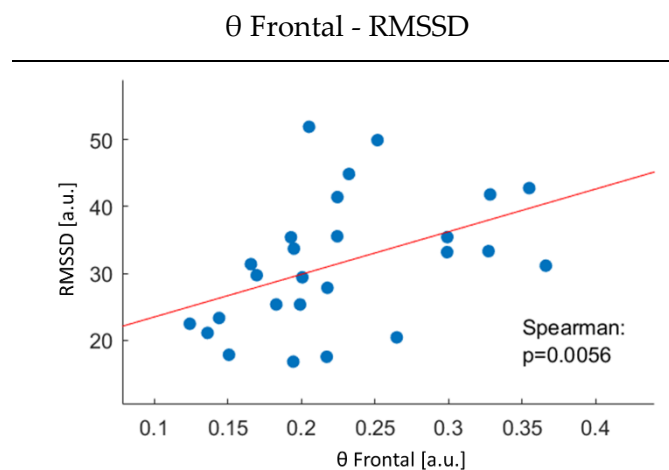


Figure 4.58 scatterplot with linear regression line and significance of ρ

4.7.1.3 Correlations with score and performance

The correlations between the HRV features computed during Code reading and the measures of performance were investigated. The score is the a-priori expected proficiency in C language, evaluated before the beginning of the experiment. The proficiency is a measure of the actual quality of the code produced during the Code writing phase. This analysis was inspired by some works in the literature that found higher levels of HRV during rest in subjects that subsequently demonstrated better performance [59]. Results are presented in Figure 4.59.

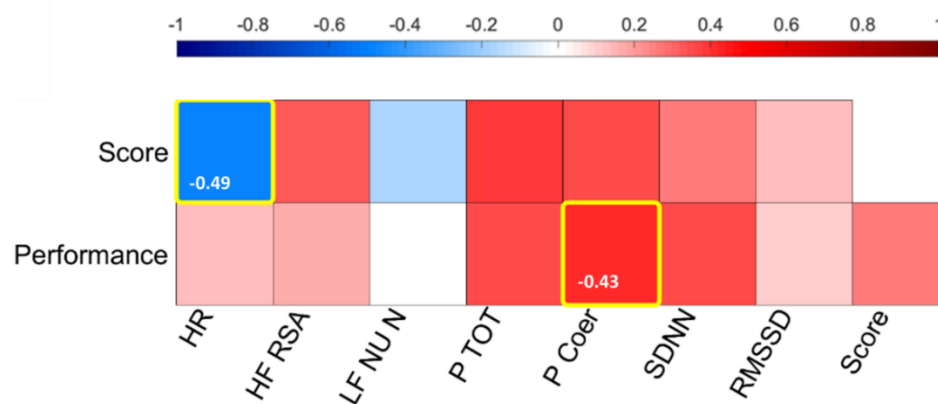


Figure 4.59: Correlation matrix. Score and performance – code reading

The positive correlation between the performance and the Coherent Power suggests that higher levels of parasympathetic activation during the Code reading phase, which is assumed to require low cognitive effort, are indicators of better performance in the more demanding task. The trends observed in the Total Power and SDNN (i.e., positive correlation with cognitive performance) are consistent with the literature but are not significant.

Figure 4.60 reports the correlations obtained between HRV and the performance measured in the Code writing phase. The only feature which correlates with the score and the performance is now “SDNN” a measure of the total power of the HRV signal. A possible interpretation of these results, confirmed also by the correlation with Completion and LF, is that a sympathetic activation during the execution of the Code writing task, but not Code during reading, is associated with better performance.

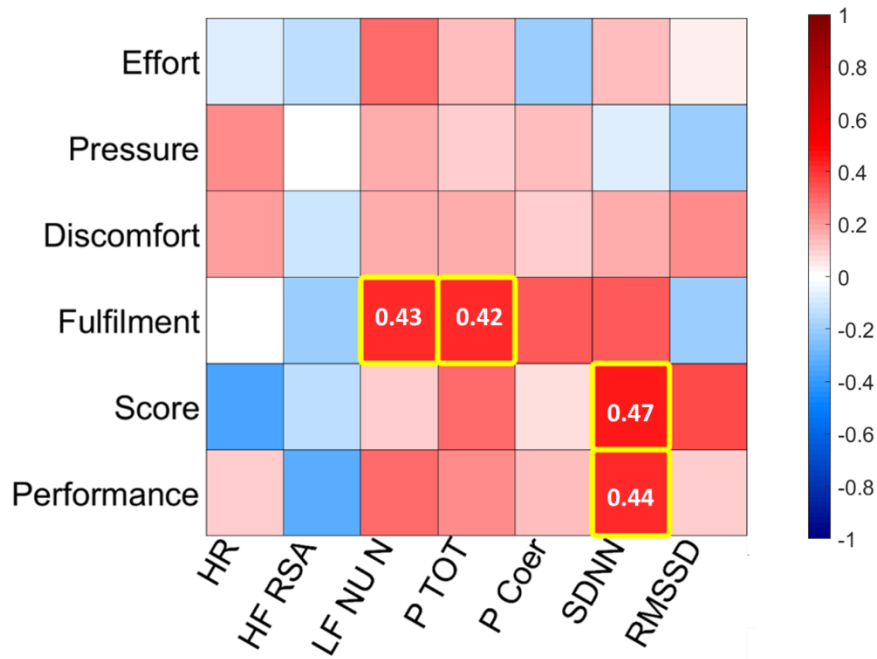


Figure 4.60 Correlation matrix. Categorical outcomes – code writing

4.7.2 N-Back protocol

This chapter reports the correlations obtained among EDA features, between EDA and HRV features and between the features and the outcome measures. For the correlation analysis features have not been normalized with the baseline.

4.7.2.1 Correlations among EDA features

The correlations presented in Figure 4.61 were obtained considering the features computed in all the tasks of the protocol (i.e., for each subject one point was obtained for every task).

The variables extracted are highly correlated with each other, which is expected since they all measure the activation of the sympathetic nervous system. Nevertheless, this result highlights a redundancy in the extracted descriptors which should not be all used simultaneously in a classification model.

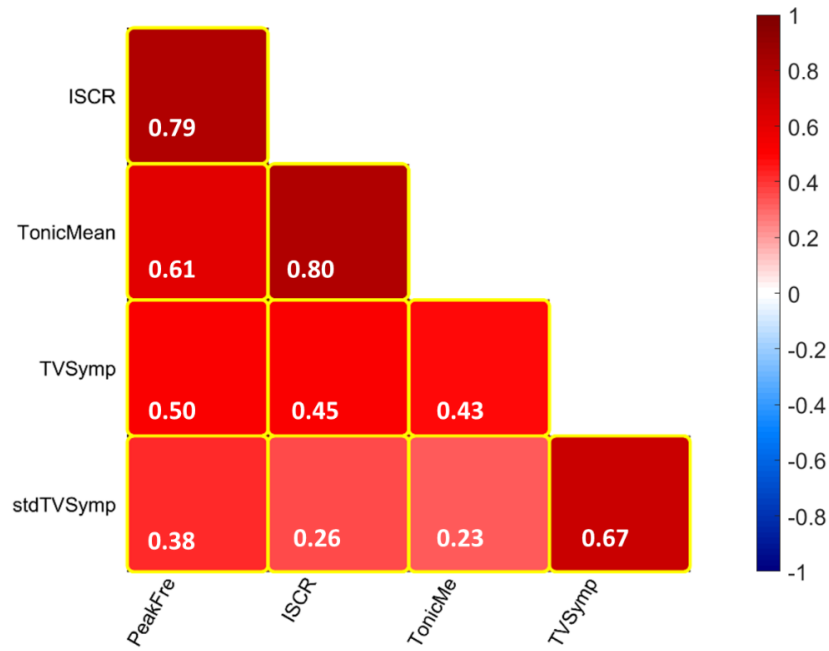


Figure 4.61: Correlation matrix. EDA features

Figure 4.62 shows the scatterplot of the two features that are more highly correlated.

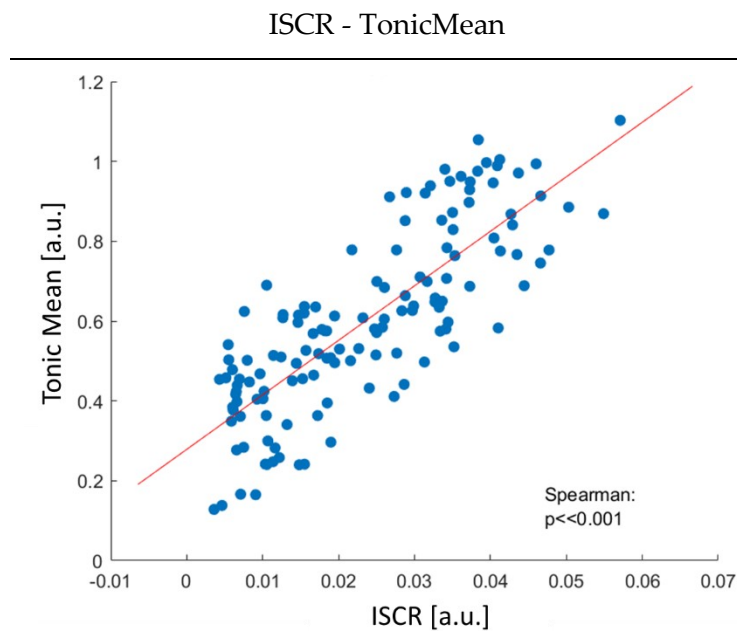


Figure 4.62: scatterplot with linear regression line and significance of ρ

4.7.2.2 Correlations among HRV and EDA features

Also in Figure 4.63, reporting the correlations among HRV and EDA features, all the tasks of the protocol were used.

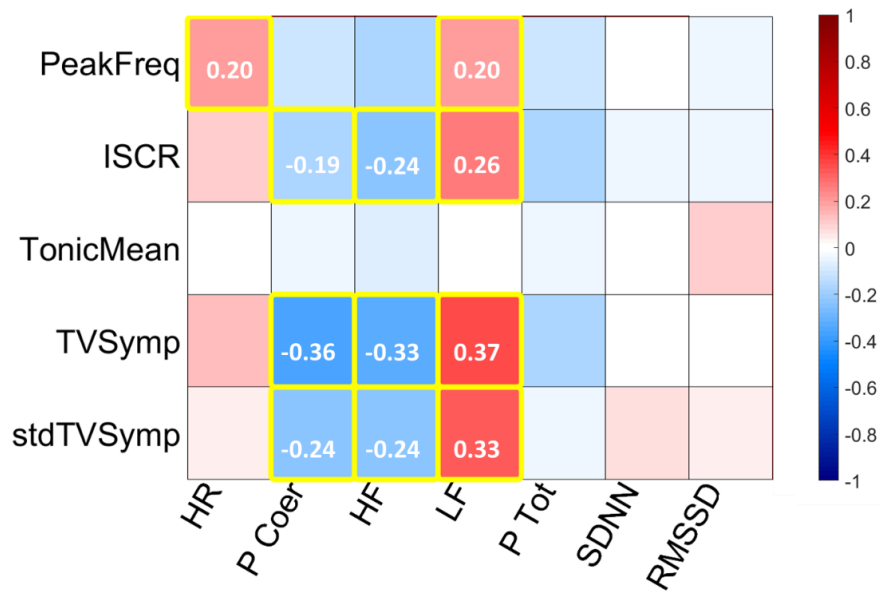


Figure 4.63: Correlation matrix. EDA-HRV features

Consistently with the sympathetic origin of the EDA signal, most features correlate positively with LF, as shown more in details in Figure 4.64.

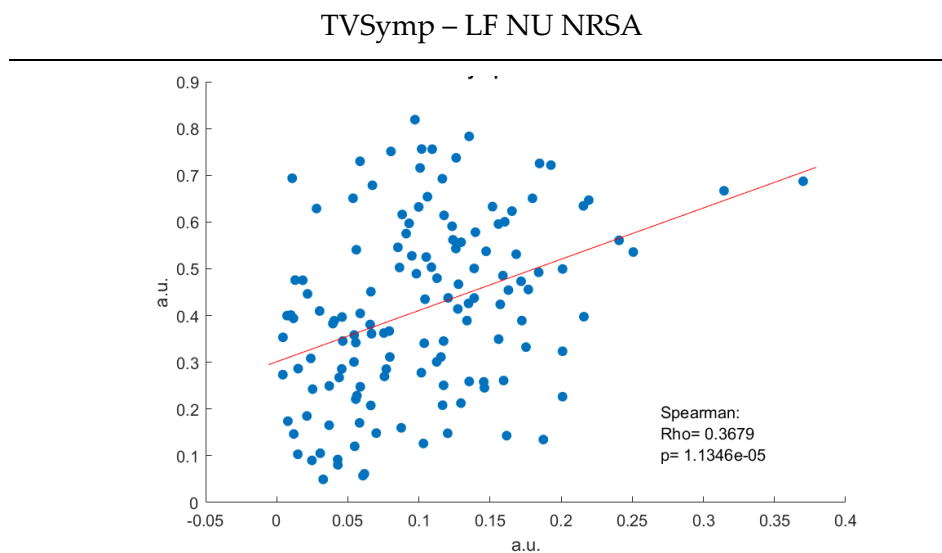


Figure 4.64: scatterplot with linear regression line and significance of ρ

Negative correlations were also found with measures of parasympathetic activity, namely power in HF and coherent power. Fewer correlations were found with the total power of the HRV, either measured in frequency and time domain.

In general, the ρ coefficient was relatively low also for significant results. This means that the features extracted from the two systems, even if they have some correlation, are not redundant and bring heterogeneous information.

4.7.2.3 *Correlations with the score*

Correlations between the score and the autonomic descriptors were analysed in order to assess if they can be used as predictors of performance. In addition to the correlations obtained considering the time window in which the cognitive task was performed, also the correlations obtained with the Sit phase were analysed, in order to assess possible correlations with performance and autonomic activity at rest.

No significant results were found. Some hypotheses can be made to explain this.

First, as mentioned in chapter 2.2.3, the number of subjects that could be used for this type of correlation is lower than the total number of subjects.

Secondly, it is possible that the protocol design influenced the results since some confounding factors may have influenced the score obtained by the participants. For example, subjects that already had some familiarity with the N-back test performed better than subjects that performed the test for the first time during the experiment.

The complete results are reported in Appendix (Table A-7, Table A-8, Table A-9, Table A-10)

5. Conclusion and future development

Despite the practical advantages of autonomic signals in real-world applications, most research studies that investigate the effect that cognitive functions have on biological signals focus on the monitoring of the Central Nervous System. We know however that autonomic signals such as HRV, EDA and respiratory activity are valid correlates of many psychophysiological and behavioural states thanks to the deep interrelations between the Central and Autonomic branches of the nervous system [3].

The focus of the present work was to address the open problems identified in the literature and listed in chapter 1.5: identify more robust and flexible methods for the computation of quantitative measures of cognitive load from autonomic signals, and further study the EDA signal and its relationship with the HRV during cognitive tasks.

The bivariate time-variant approach adopted for the analysis of the HRV and respiratory signals allowed to overcome the problems related to the non-stationarity and the variations of the respiratory frequency (and consequently the frequency range of the RSA) and proved to be adequate for this specific application.

The EDA signal was analysed both in the time and time-frequency domains and compared to the HRV signal to address the scarcity of works that apply the analysis of this signal to the monitoring of cognitive load.

In addition, the time-variant autoregressive algorithm was adapted and applied to the EDA signal, opening the possibility of a multivariate online analysis of the three signals.

The methods applied captured significant task-dependent variations in autonomic indices in both protocols.

In the study of the HRV and respiratory signals, the results obtained confirm that

during cognitive tasks the total power of the HRV is reduced, a result consistent with other works in the literature. Two mechanisms are linked to this effect: the increased heart rate and the decreased effect of the RSA. In the N-back protocol, it was also observed a significant reduction in the parasympathetic and an increase in the sympathetic tone during the cognitive task compared to low effort tasks.

Additionally, the descriptors obtained from the EDA signal proved to be very sensitive to the cognitive task and less sensitive to the stressors commonly used in the analysis of the HRV to elicit a sympathetic and parasympathetic activation: sit to stand and controlled respiration.

Indeed, EDA features did not vary significantly between the controlled respiration and the standing tasks while the HRV features did. On the contrary, the Stand and the N-back tasks induced similar effects in the HRV features which makes it more difficult to discriminate between them while the descriptors extracted from the EDA signal behaved differently under the two experimental conditions.

These results, confirmed by the low correlation coefficients identified among the features extracted from the two signals, suggest that the information provided by the two is not redundant but rather should be used in combination to discriminate conditions in which the sympathetic activation is induced by the cognitive load from the ones in which is induced by orthostatic stressors.

The most natural future development of this work would be to create a larger dataset obtained from a bigger and more heterogeneous population sample using different cognitive tasks to improve the external validity of the study.

Furthermore, such a dataset could be used to build a machine learning model able to discriminate among different levels of cognitive load using as input the features discussed in this thesis. A model able to recognize and quantify the cognitive effort from autonomic signals could find a practical application for example in smartphones connected to wearable devices, which are already widely used.

Anyway, before translating the results into practical applications it should be noted that measuring mental workload, mental effort, working memory load, mental stress, mental fatigue, and other relevant parameters related to cognitive functions poses some inevitable difficulties. These definitions are somehow fuzzy, deeply interrelated with each other and therefore difficult to isolate and measure independently. These metrics are also connected to affective aspects in complex and unpredictable ways. For these reasons, the interpretation of the results is not trivial.

Specifically, the two protocols discussed in this thesis were designed to induce cognitive load and not stress. This was achieved by informing the participants that they were not judged for their performance and no feedback for their results would be provided. Nevertheless, it is reasonable to hypothesise that some volunteers may

also have experienced stress which is a possible confounding factor. Indeed, cognitive load and stress have been shown to be different biobehavioural states: high cognitive workload can be achieved without stress and vice-versa [97].

This suggests that to better interpret the results obtained and design better experimental protocols biomedical engineers should work together with experts in psychology and psychophysiology.

Bibliography

- [1] E. Ratti, S. Waninger, C. Berka, G. Ruffini, and A. Verma, "Comparison of Medical and Consumer Wireless EEG Systems for Use in Clinical Trials," *Front. Hum. Neurosci.*, vol. 11, pp. 1–7, 2017.
- [2] E. Kandel, J. Schwartz, T. Jessel, S. Siegelbaum, and A. Hudspeth, *Principles of neural science*. 2013.
- [3] J. F. Thayer and R. D. Lane, "Claude Bernard and the heart – brain connection : Further elaboration of a model of neurovisceral integration," *Neurosci. Biobehav. Rev.*, vol. 33, pp. 81–88, 2009.
- [4] M. E. Dawson, A. M. Schell, and D. L. Fillion, "The electrodermal system," in *Handbook of Psychophysiology, Fourth Edition*, 2016, pp. 200–219.
- [5] W. B. Cannon, "The Wisdom of the Body," *Nature*, vol. 133, no. 3351, p. 82, 1934.
- [6] M. N. Levy, "Autonomic Interactions in Cardiac Control," *Ann. N. Y. Acad. Sci.*, vol. 601, no. 1, pp. 209–221, 1990.
- [7] F. Shaffer, R. McCraty, and C. L. Zerr, "A healthy heart is not a metronome: an integrative review of the heart's anatomy and heart rate variability," *Front. Psychol.*, vol. 5, no. September, pp. 1–19, 2014.
- [8] R. Barbieri, A. M. Bianchi, J. K. Triedman, L. Mainardi, S. Cerutti, and J. P. Saul, "Model Dependency of Multivariate Autoregressive spectral Analysis," *IEEE Eng. Med. Biol. Mag.*, vol. 16, no. 5, pp. 74–85, 1997.
- [9] F. Yasuma and J. Hayano, "Respiratory Sinus Arrhythmia * Why Does the Heartbeat Synchronize With," *Chest*, vol. 125, no. 2, pp. 683–690, 2004.
- [10] R. Edelberg, "Electrodermal Mechanisms: A critique of the two-effector hypothesis and a proposed replacement," in *Progress in Electrodermal Research*, Springer, Boston, MA, 1993, pp. 7–29.
- [11] H. Critchley, "Electrodermal Responses : What Happens in the Brain," *Neuroscientist*, vol. 8, no. 2, pp. 132–142, 2002.
- [12] Task Force of The European Society of Cardiology and North American Society of

- Pacing and Electrophysiology, "Heart rate variability," *Eur. Heart J.*, pp. 354–381, 1996.
- [13] J. Pan and W. J. Tompkins, "A Real-Time QRS Detection Algorithm," *IEEE Trans. Biomed. Eng.*, vol. BME-32, no. 3, pp. 230–236, 1985.
- [14] P. Kligfield *et al.*, "Recommendations for the Standardization and Interpretation of the Electrocardiogram. Part I: The Electrocardiogram and Its Technology A Scientific Statement From the American Heart Association Electrocardiography and Arrhythmias Committee, Council on Clin," *J. Am. Coll. Cardiol.*, vol. 49, no. 10, pp. 1109–1127, 2007.
- [15] H. Monkaresi, R. A. Calvo, and H. Yan, "A machine learning approach to improve contactless heart rate monitoring using a webcam," *IEEE J. Biomed. Heal. Informatics*, vol. 18, no. 4, pp. 1153–1160, 2014.
- [16] D. McDuff, S. Gontarek, and R. Picard, "Remote Measurement of Cognitive Stress via Heart Rate Variability," *Annu Int Conf IEEE Eng Med Biol Soc.*, pp. 3–6, 2014.
- [17] O. Carr, M. de Vos, and K. Saunders, "Heart rate variability in bipolar disorder and borderline personality: a clinical review," *Evid. based Ment. Heal.*, vol. 21, 2018.
- [18] S. Analyses and T. Musha, "1/f Fluctuation of Heartbeat Period," *IEEE Trans. Biomed. Eng.*, vol. BME-29, no. 6, pp. 456–457, 1982.
- [19] W. Roel, J. M. Karemaker, and J. A. N. Strackee, "Comparing Spectra of a Series of Point Events Particularly for Heart Rate Variability Data," *IEEE Trans. Biomed. Eng.*, no. 4, pp. 384–387, 1984.
- [20] F. Shaffer and J. P. Ginsberg, "An Overview of Heart Rate Variability Metrics and Norms," *Front. Public Heal.*, vol. 5, no. September, pp. 1–17, 2017.
- [21] C. Braun, P. Kowallik, A. Freking, D. Haderler, K.-D. Kniffki, and M. Meesmann, "Demonstration of nonlinear components in heart rate variability of healthy persons," *Am. J. Physiol.*, 1998.
- [22] A. L. Goldberger, D. R. Rigney, and B. J. West, "Chaos and Fractals in Human Physiology," *Sci. Am.*, 1990.
- [23] C. E. Shannon, "A Mathematical Theory of Communication," *Bell Syst. Tech. J.*, vol. 27, no. April 1924, pp. 379–423, 1948.
- [24] J. R. Moorman, "Physiological time-series analysis using approximate entropy and sample entropy," *Am. J. Physiol. Hear. Circ. Physiol.*, pp. 2039–2049, 2000.
- [25] E. Petrucci *et al.*, "Assessment of Heart Rate Variability Changes During Dipyridamole Infusion and Dipyridamole-Induced Myocardial Ischemia: A Time Variant Spectral Approach," *J. Am. Coll. Cardiol.*, vol. 28, no. 4, 1996.
- [26] G. A. Reyes, D. E. L. Paso, W. Langewitz, L. J. M. Mulder, A. V. A. N. Roon, and S.

- Duschek, "The utility of low frequency heart rate variability as an index of sympathetic cardiac tone: A review with emphasis on a reanalysis of previous studies," *Psychophysiology*, vol. 50, no. 5, pp. 477–487, 2013.
- [27] D. L. Eckberg, "Sympathovagal balance: A critical appraisal," *Circulation*, vol. 96, no. 9, pp. 3224–3232, 1997.
- [28] G. E. Billman, "The LF / HF ratio does not accurately measure cardiac sympatho-vagal balance," *Front. Physiol.*, vol. 4, no. February, pp. 1–5, 2013.
- [29] S. Ghiasi *et al.*, "A New Sympathovagal Balance Index from Electrodermal Activity and Instantaneous Vagal Dynamics: A Preliminary Cold Pressor Study," in *Annual International Conference of the IEEE Engineering in Medicine and Biology Society. IEEE Engineering in Medicine and Biology Society*, 2018.
- [30] A. Boardman, F. S. Schindwein, and A. P. Rocha, "A study on the optimum order of autoregressive models for heart rate variability," *Physiol. Meas.*, no. February 2014, 2002.
- [31] S. Cerutti and C. Marchesi, *ADVANCED METHODS OF BIOMEDICAL SIGNAL PROCESSING*. 2011.
- [32] A. M. Bianchi, L. Mainardi, E. Petrucci, M. G. Signorini, M. Mainardi, and S. Cerutti, "Time-Variant Power Spectrum Analysis for the Detection of Transient Episodes in HRV Signal," *IEEE Trans. Biomed. Eng.*, pp. 136–144, 1993.
- [33] R. Bailón, L. Mainardi, M. Orini, L. Sörnmo, and P. Laguna, "Biomedical Signal Processing and Control Analysis of heart rate variability during exercise stress testing using respiratory information," *Biomed. Signal Process. Control*, vol. 5, no. 4, pp. 299–310, 2010.
- [34] S. Silvestri and E. Schena, "Contact-Based Methods for Measuring Respiratory Rate," *Sensors*, vol. 19, no. 4, pp. 1–47, 2019.
- [35] M. Chu *et al.*, "Respiration rate and volume measurements using wearable strain sensors," *npj Digit. Med.*, no. September 2018, pp. 1–9, 2019.
- [36] A. Bonarini, M. Matteucci, and S. Tognetti, "CHEST EXPANSION RECONSTRUCTION FROM RESPIRATION SOUND BY USING ARTIFICIAL NEURAL NETWORKS," in *Advances in Medical, Signal and Information Processing*, 2008.
- [37] G. B. Moody, R. G. Mark, A. Zoccola, and S. Mantero, "Derivation of Respiratory Signals From Multi-Lead ECGs.," *Comput. Cardiol.*, no. November, pp. 113–116, 1985.
- [38] S. C. Müller, "Using Biometric Sensors to Increase Developers' Productivity," 2016.
- [39] E. Vanegas, R. Igual, and I. Plaza, "Sensing Systems for Respiration Monitoring: A Technical Systematic Review," *Sensors*, vol. 20, 2020.

- [40] A. Bianchi, B. Bontempi, S. Cerutti, P. Gianoglio, G. Comi, and M. G. N. Sora, "Spectral analysis of heart rate variability signal and respiration in diabetic subjects," *Med. Biol. Eng. Comput.*, vol. 28, no. 3, pp. 205–211, 1989.
- [41] A. Porta *et al.*, "Multimodal Signal Processing for the Analysis of Cardiovascular Variability," *Philos. Trans. R. Soc. A*, vol. 367, no. 1887, pp. 391–409, 2008.
- [42] G. Baselli, A. Porta, and S. Cerutti, "Spectral decomposition in multichannel recordings based on multivariate parametric identification," *IEEE Trans. Biomed. Eng.*, vol. 44, no. 11, pp. 1092–1101, 1997.
- [43] C. Granger, "Investigating Causal Relations by Econometric Models and Cross-spectral Methods," *Econom. Soc.*, vol. 37, no. 3, pp. 424–438, 1969.
- [44] Society For Psychophysiological Research Ad Hoc Committee On Electrodermal Measurements, "Publication recommendations for electrodermal measurements," *Psychophysiology*, vol. 49, pp. 1017–1034, 2012.
- [45] "What is EDA? And how does it work?" [Online]. Available: <https://imotions.com/blog/eda/>. [Accessed: 14-Oct-2021].
- [46] J. Shukla, M. B.- Angeles, J. Oliver, G. C. Nandi, and S. M. Ieee, "Feature Extraction and Selection for Emotion Recognition from Electrodermal Activity," *IEEE Trans. Affect. Comput.*, 2019.
- [47] M. Benedek and C. Kaernbach, "A continuous measure of phasic electrodermal activity," *J. Neurosci. Methods*, vol. 190, no. 1, pp. 80–91, 2010.
- [48] D. R. Bach, G. Flandin, K. J. Friston, and R. J. Dolan, "Time-series analysis for rapid event-related skin conductance responses," *J. Neurosci. Methods*, vol. 184, no. 2, pp. 224–234, 2009.
- [49] M. Benedek and C. Kaernbach, "Decomposition of skin conductance data by means of nonnegative deconvolution," *Psychophysiology*, vol. 47, pp. 647–658, 2010.
- [50] A. Greco, S. Member, G. Valenza, A. Lanata, E. P. Scilingo, and L. Citi, "cvxEDA: A Convex Optimization Approach to Electrodermal Activity Processing," *IEEE Trans. Biomed. Eng.*, vol. 63, no. 4, pp. 797–804, 2016.
- [51] H. P. Quintero, J. Lorian, and A. Orjuela-Canon, "Power Spectral Density Analysis of Electrodermal Activity for Sympathetic Function Assessment," *Ann. Biomed. Eng.*, vol. 44, no. 10, pp. 3124–3135, 2016.
- [52] G. Rocco *et al.*, "Exploration of the physiological response to an online gambling task by frequency domain analysis of the electrodermal activity *," in *Annual International Conference of the IEEE Engineering in Medicine and Biology Society.*, 2020, pp. 91–94.
- [53] H. F. Posada-quintero, J. P. Florian, Á. D. Orjuela-cañón, and K. H. Chon, "Highly sensitive index of sympathetic activity based on time-frequency spectral analysis of

- electrodermal activity," pp. 582–591, 2021.
- [54] T. Chaspari, A. Tsiartas, L. I. S. Duker, S. A. Cermak, and S. S. Narayanan, "EDA-gram: Designing electrodermal activity fingerprints for visualization and feature extraction," *Proc. Annu. Int. Conf. IEEE Eng. Med. Biol. Soc. EMBS*, vol. 2016-October, pp. 403–406, 2016.
- [55] J. R. Stroop, "Studies of interference in serial verbal reactions," *J. Exp. Psychol.*, vol. XVIII, no. 6, 1935.
- [56] W. K. Kirchner, "AGE DIFFERENCES IN SHORT-TERM RETENTION OF RAPIDLY CHANGING INFORMATION," *J. Exp. Psychol.*, vol. 55, no. 4, 1958.
- [57] A. L. Hansen and J. F. Thayer, "Vagal influence on working memory and attention," *Int. J. Psychophysiol.*, vol. 48, pp. 263–274, 2003.
- [58] H. E. Rosvold, A. F. Mirsky, I. Sarason, E. D. Bransome, and L. H. Beck, "A Continuous Performance Test of Brain Damage," *J. Consult. Psychol.*, vol. 20, no. 5, pp. 343–350, 1956.
- [59] G. Forte, F. Favieri, and M. Casagrande, "Heart Rate Variability and Cognitive Function : A Systematic Review," *Front. Neurosci.*, vol. 13, no. July, pp. 1–11, 2019.
- [60] G. Alba, J. Vila, P. Montoya, B. Rey, and M. Munoz, "The Relationship Between Heart Rate Variability and Electroencephalography Functional Connectivity Variability Is Associated With Cognitive Flexibility," *Front. Hum. Neurosci.*, vol. 13, no. February, pp. 1–12, 2019.
- [61] R. Backs and K. Seljos, "Metabolic and cardiorespiratory measures of mental effort : the effects of level of difficulty in a working memory task," *Int. J. Psychophysiol.*, vol. 16, pp. 57–68, 1994.
- [62] N. Hjortskov, D. Rissén, A. K. Blangsted, N. Fallentin, U. Lundberg, and K. Søgaard, "The effect of mental stress on heart rate variability and blood pressure during computer work," *Eur. J. Appl. Physiol.*, vol. 92, no. 1–2, pp. 84–89, 2004.
- [63] B. Helge, J. F. Thayer, J. C. Laberg, B. Wormnes, M. Raadal, and E. Skaret, "Attentional and physiological characteristics of patients with dental anxiety," *J. Anxiety Disord.*, vol. 17, pp. 75–87, 2003.
- [64] M. Grassmann, E. Vlemincx, A. Von Leupoldt, J. M. Mittelstadt, and O. Van den Bergy, "Respiratory Changes in Response to Cognitive Load: A Systematic Review," *Hindawi Publ. Corp.*, p. 16, 2016.
- [65] R. G. O. Connell, C. A. M. A. Bellgrove, P. M. Dockree, and I. H. Robertson, "Reduced electrodermal response to errors predicts poor sustained attention performance in attention deficit hyperactivity disorder," *Neuroreport*, vol. 15, no. 16, pp. 5–8, 2004.
- [66] L. Munro and M. Dawson, "Electrodermal lability and rapid performance decrement

- in a degraded stimulus continuous performance task," *J. Exp. Psychophysiol.*, 1987.
- [67] J. M. Hinson, T. L. Jameson, and P. Whitney, "Somatic markers , working memory , and decision making," *Cogn. Affect. Behav. Neurosci. Vol.*, vol. 2, no. 4, pp. 341–353, 2002.
- [68] H. F. Posada-quintero and K. H. Chon, "Phasic Component of Electrodermal Activity is more Correlated to Brain Activity than Tonic Component," *2019 IEEE EMBS Int. Conf. Biomed. Heal. Informatics*, pp. 1–4, 2019.
- [69] H. F. Posada-quintero and J. B. Bolkhovskiy, "Human Performance Deterioration Due to Prolonged Wakefulness Can Be Accurately Detected Using Time-Varying Spectral Analysis of Electrodermal Activity," *Hum. Factors J. Hum. Factors Ergon. Soc.*, 2018.
- [70] H. Posada-Quintero and J. B. Bolkhovskiy, "Sleep Deprivation in Young and Healthy Subjects Is More Sensitively Identified by Higher Frequencies of Electrodermal Activity than by Skin Conductance Level Evaluated in the Time Domain," *Front. Physiol.*, 2017.
- [71] Y. Goren, L. R. Davrath, I. Pinhas, E. Toledo, and S. Akselrod, "Individual time-dependent spectral boundaries for improved accuracy in time-frequency analysis of heart rate variability," *IEEE Trans. Biomed. Eng.*, vol. 53, no. 1, pp. 35–42, 2006.
- [72] R. Bailon, P. Laguna, L. Mainardi, and L. Sornmo, "Analysis of heart rate variability using time-varying frequency bands based on respiratory frequency.," *Conf. Proc. IEEE Eng. Med. Biol. Soc.*, pp. 6675–6678, 2007.
- [73] A. Hernando *et al.*, "Inclusion of Respiratory Frequency Information in Heart Rate Variability Analysis for Stress Assessment," *IEEE J. Biomed. Heal. informatics*, vol. 20, no. 4, pp. 1016–1025, 2016.
- [74] C. Varon *et al.*, "Unconstrained Estimation of HRV Indices After Removing Respiratory Influences From Heart Rate," *IEEE J. Biomed. Heal. informatics*, vol. 23, no. 6, pp. 2386–2397, 2019.
- [75] L. Goncales, K. Farias, B. Da Silva, and J. Fessler, "Measuring the cognitive load of software developers: A systematic mapping study," *IEEE Int. Conf. Progr. Compr.*, vol. 2019-May, pp. 42–52, 2019.
- [76] "Tricentis Software Fail Watch Finds 3.6 Billion People." [Online]. Available: <https://www.globenewswire.com/news-release/2018/01/24/1304535/0/en/Tricentis-Software-Fail-Watch-Finds-3-6-Billion-People-Affected-and-1-7-Trillion-Revenue-Lost-by-Software-Failures-Last-Year.html>. [Accessed: 03-Nov-2021].
- [77] A. F. Huang, B. Bin Liu, and C. B. Huang, "A taxonomy system to identify human error causes for software defects," *Proc. - 18th ISSAT Int. Conf. Reliab. Qual. Des.*, no. December 2014, pp. 44–49, 2012.

- [78] R. Couceiro *et al.*, “Biofeedback Augmented Software Engineering : Monitoring of Programmers ’ Mental Effort,” *Proc. - 41st Int. Conf. Softw. Eng. New Ideas Enrging Results*, pp. 37–40, 2019.
- [79] R. Couceiro *et al.*, “Pupillography as Indicator of Programmers’ Mental Effort and Cognitive Overload,” *Proc. - 49th Annu. IEEE/IFIP Int. Conf. Dependable Syst. Networks, DSN 2019*, pp. 638–644, 2019.
- [80] A. Calcagno *et al.*, “EEG monitoring during software development,” in *20th IEEE Mediterranean Electrotechnical Conference, MELECON 2020 - Proceedings*, 2020, pp. 325–329.
- [81] J. Castelhana, I. C. Duarte, C. Ferreira, J. Duraes, H. Madeira, and M. Castelo-Branco, “The role of the insula in intuitive expert bug detection in computer code: an fMRI study,” *Brain Imaging Behav.*, vol. 13, no. 3, pp. 623–637, 2019.
- [82] “ProComp Infiniti System w/ BioGraph Infiniti Software - T7500M.” [Online]. Available: <https://thoughttechnology.com/procomp-infiniti-system-w-biograph-infiniti-software-t7500m/>. [Accessed: 24-Oct-2021].
- [83] “b3lab.” [Online]. Available: <https://www.b3lab.deib.polimi.it/>. [Accessed: 04-Nov-2021].
- [84] “Biomarketing | Pheel - Physiology Emotion Experience Lab | Politecnico Milano.” [Online]. Available: <http://pheel.polimi.it/>. [Accessed: 04-Nov-2021].
- [85] “Kaiser Window - MATLAB & Simulink.” [Online]. Available: <https://www.mathworks.com/help/signal/ug/kaiser-window.html>. [Accessed: 04-Nov-2021].
- [86] V. Madisetti and D. Williams, *Digital Signal Processing Handbook*. 1999.
- [87] A. Delgado-Bonal and A. Marshak, “Approximate Entropy and Sample Entropy: A Comprehensive Tutorial,” *Entropy*, vol. 21, 2019.
- [88] M. J. Lewis and A. L. Short, “Sample entropy of electrocardiographic RR and QT time-series data during rest and exercise,” *Physiol. Meas.*, vol. 28, pp. 731–744, 2007.
- [89] M. H. Hayes, *Statistical Digital Signal Processing and Modeling*. 1996.
- [90] H. F. Posada-Quintero, J. P. Florian, Á. D. Orjuela-cañón, and K. H. Chon, “Highly sensitive index of sympathetic activity based on time-frequency spectral analysis of electrodermal activity,” *Am. J. Physiol. Regul. Integr. Comp. Physiol.*, vol. 311, no. 3, pp. 582–591, 2021.
- [91] T. R. Fortescue, L. S. Kershenbaum, and B. E. Ydstie, “Implementation of self-tuning regulators with variable forgetting factors,” *Automatica*, vol. 17, no. 6, pp. 831–835, 1981.

- [92] "Linear or rank correlation - MATLAB corr." [Online]. Available: <https://www.mathworks.com/help/stats/corr.html>. [Accessed: 22-Oct-2021].
- [93] D. J. Best and D. E. Roberts, "Algorithm AS 89: The Upper Tail Probabilities of Spearman's Rho," *J. R. Stat. Soc. Ser. C (Applied Stat.)*, vol. 24, no. 3, pp. 377–379, 1975.
- [94] R. Sjouwerman and T. B. Lonsdorf, "Latency of skin conductance responses across stimulus modalities," *Psychophysiology*, vol. 56, no. 4, 2019.
- [95] J. Rittweger, M. Lambertz, and P. Langhorst, "Influences of mandatory breathing on rhythmical components of electrodermal activity," *Clin. Physiol.*, vol. 17, pp. 609–618, 1997.
- [96] C. L. Lim, M. Seto-poon, P. D. Clouston, and J. G. L. Morris, "Sudomotor nerve conduction velocity and central processing time of the skin conductance response," *Clin. Neurophysiol.*, vol. 114, pp. 2172–2180, 2003.
- [97] A. W. K. Gaillard and C. J. E. Wientjes, "Mental load and work stress as two types of energy mobilization Mental load and work stress as two types of energy mobilization," *Work Stress An Int. J. Work , Heal. Organ.*, pp. 37–41, 1994.

A. Appendix

A.1 Statistical analysis - BASE

A.1.1 Differences across tasks

RLE

	FRIEDMAN	PAIRED COMPARISONS					
		RP-WR	RP-RC	RP-RT	WR-RC	WR-RT	RC-RT
HR	<0.01	0.4919↑	1	0.0684↓	0.0265↓	<0.01↓	0.9283↓
P TOT	<0.01	1	<0.01↑	0.0159↑	0.0159↑	0.0265↑	1
HF	0.0129	0.3466↓	1	1	0.0265↑	0.0265↑	1
HF RSA	0.7212	-	-	-	-	-	-
P COER	<0.01	1	0.0684↑	0.4919↑	0.0159↑	0.1611↑	1
P COER NU	0.8732	-	-	-	-	-	-
LF NU	0.1068	-	-	-	-	-	-
LF NRSA	0.9536	-	-	-	-	-	-
LF/HF	0.1218						

Table A-1 *p-values*. RP = Read Problem; WR = Writing; RC = Read Code; RT= Read Text

	SDNN	RMSSD	PNN50	SAMPEN	RESP RATE
WR-RC	<0.01 ↑	0.3396	0.0942	0.1465	0.0215 ↓

Table A-2: *p-values*. WR = Writing; RC = Read CodeSPLIT

FRIEDMAN		PAIRED COMPARISONS		
		WR-RC	WR-RT	RC-RT
HR	<0.01	0.5094↓	<0.01 ↓	0.1495↓
P TOT	0.0125	0.7179↑	<0.01 ↑	0.2326↑
HF	0.049	0.2327↑	0.0558↑	1
HF RSA	0.1160	-	-	-
P COER	0.1160	-	-	-
P COER NU	0.5836	-	-	-
LF NU	0.7351	-	-	-
LF NRSA	0.3973	-	-	-
LF/HF	0.9260	-	-	-

Table A-3 *p-values* WR = Writing; RC = Read Code; RT = Read Text

	SDNN	RMSSD	PNN50	SAMPEN	RESP RATE
WR-RC	0.1272↑	0.6848	0.3804↑	0.8926	0.2734↓

Table A-4: *p-values*. WR = Writing; RC = Read Code

A.2 Statistical analysis- N-Back

	FRIEDMAN	PAIRED COMPARISONS					
		Sit- Stand	Sit-Resp	Sit-NB	Stand- Resp	Stand- NB	Resp-NB
HR	<0.01	<0.01↑	0.0504↓	0.8401↑	<0.01↓	<0.01↓	1
P TOT	0.0159	0.2101↓	1	<0.01↓	0.2101↑	1	<0.01↓
HF	<0.01	0.0368↓	0.0504↑	0.4388↓	<0.01↑	1	<0.01↓
HF RSA	<0.01	0.0368↓	1	<0.01↓	<0.01↑	1	<0.01↓
LF NU	<0.01	<0.01↑	<0.01↑	1	<0.01↑	<0.01↑	<0.01↑
LF NU NRSA	<0.01	<0.01↑	1	<0.01↑	<0.01↓	1	<0.01↑
LF/HF	<0.01	<0.01↑	<0.01↓	0.5501	<0.01↓	0.6831↓	<0.01↑
P COER	<0.01	1	1	0.1611↓	0.6831↑	0.2712	<0.01↓
P COER NU	<0.01	<0.01↓	1	<0.01↓	<0.01↑	1	<0.01↓
RMSSD	<0.01	<0.01↓	1	0.5501↓	<0.01↑	<0.01↑	0.6831↓
SDNN	0.0293	0.0266↓	1	1	0.1611↑	0.8401↑	1
PNN50	<0.01	<0.01↓	1	0.8775↓	<0.01↑	0.3579↑	0.1074↓
SAMPEN	<0.01	<0.01↓	1	1	0.0368↑	<0.01↑	1
RESP. RATE	<0.01	0.9122		<0.01↑		<0.01↑	

Table A-5: *p-values of HRV and Respiratory features*

FRIEDMAN		PAIRED COMPARISONS					
PEAK FREQ.	<0.01	0.0154↑	0.4325↑	<0.01↑	1	<0.01↑	<0.01↑
PEAK AMP.	<0.01	0.1375↑	0.0490↑	<0.01↑	1	0.0667↑	0.1805↑
ISCR	<0.01	0.0190↑	0.2101↑	<0.01↑	1	<0.01↑	<0.01↑
RISE TIME	0.3442						
TONICMEAN	<0.01	0.2101↑	0.0504↑	<0.01↑	1	<0.01↑	<0.01↑
TVSYMP	<0.01	0.2061↑	<0.01↑	<0.01↑	0.8313	<0.01↑	0.0357↑
STDTVSYMP	<0.01	1	1	<0.01↑	1	0.1787↑	0.0483↑

Table A-6: *p-values of EDA features*

A.2.2 Correlations

For the sake of a more readable representation some indexes have been rescaled with logarithmic or square root transformations. For the study of correlations the Spearman's non parametric index was used, therefore the results are invariant to monotonic transformation and are not affected by the beforementioned transformations.

Correlations with time and score

Sit Phase

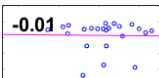
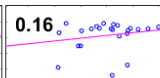
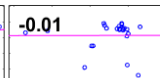
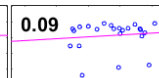
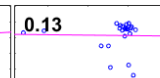
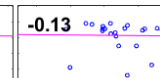
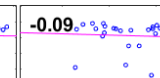
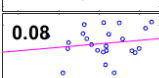
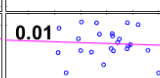
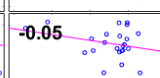
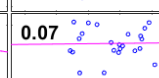
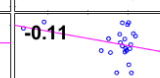
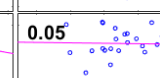
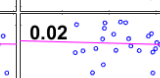
Score							
Time							
	HR	P Coer	HF	LF	P Tot	SDNN	RMSSD

Table A-7: *Correlations of score and HRV features. Sit phase*

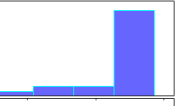
Score	0.30	0.16	0.16	-0.01	-0.22	
Time	-0.18	-0.11	-0.23	-0.17	0.08	-0.37
	Peak Freq	ISCR	TonicMean	TVSymp	stdTVSymp	Score

Table A-8: Correlations of score and EDA features. Sit phase

N-Back phase

Score	-0.34	0.13	0.17	-0.36	0.35	0.06	0.21
Time	0.26	-0.02	-0.27	0.11	-0.36	0.14	-0.17
	HR	P Coer	HF	LF	P Tot	SDNN	RMSSD

Table A-9: Correlations of score and HRV features. N-Back phase


Score	0.11	0.03	0.03	-0.28	-0.21	
Time	0.14	0.02	-0.26	-0.16	0.14	-0.35
	Peak Freq	ISCR	TonicMean	TVSymp	stdTVSymp	Score

Table A-10: Correlations of score and EDA features. N-Back phase

List of Figures

Figure 1.1: Main subdivisions of the nervous system.....	3
Figure 1.2: The Autonomous nervous system. Adapted from [2].....	4
Figure 1.3: Central control of the HRV. Adapted from [3].....	6
Figure 1.4: The eccrine sweat gland anatomy. From[4].	7
Figure 1.5: ECG signal and corresponding RR series. Adapted from [17].....	8
Figure 1.6: Typical HRV spectrum. Adapted from [25].....	10
Figure 1.7: Respiratory signal recorded with a girth sensor	12
Figure 1.8: ECG and respirogram and respective tachogram and respirogram [40]. .	13
Figure 1.9: Decomposed EDA signal, adapted from [45].	15
Figure 1.10: Adapted from [4].	16
Figure 2.1: Schematic representation of the BASE protocol.....	32
Figure 2.2: Schematic representation of the N-Back protocol.....	36
Figure 3.1: GUI Interface for manual correction of the peaks.....	38
Figure 3.2: Raw and filtered rspirogram.....	39
Figure 3.3: Block-scheme of the bivariate model.	40
Figure 3.4: Bivariate closed-loop model.....	42
Figure 3.5: Noise generated model.	43
Figure 3.6: Instantaneous respiratory frequency raw and smoothed.....	48
Figure 3.7 Block diagram. Sympathetic regulation over EDA and NRSA.....	59
Figure 4.1: Percentage of values outside the confidence interval.	64
Figure 4.2: Prediction error with spectrum and ACF.....	65

Figure 4.3: Histogram of the standard score of the error (blu) and normal distribution (orange).....	65
Figure 4.4: Input signals and $\Phi(1,1)$ before and after the control on the error.....	67
Figure 4.5: Dynamics of the gain matrix K.	68
Figure 4.6 <i>Tachogram and its spectrogram</i>	69
Figure 4.7 <i>Respirogram and its spectrogram</i>	70
Figure 4.8: <i>Spectrum of the coherence. Run 1 subject 4</i>	70
Figure 4.9: Partial spectrogram PSD12	71
Figure 4.10 Partial spectrogram PSD11	71
Figure 4.11: Spectrogram of the tachogram.....	72
Figure 4.12: Partial Spectrogram PSD11.....	73
Figure 4.13: Partial spectrogram PSD12	73
Figure 4.14: HRV time-frequency features with and without respiratory information. Writing in red and Read problem in green.	75
Figure 4.15: HRV features without and with respiratory information.....	76
Figure 4.16: LF and HF computed on total and partial spectra. Sit to Stand.....	77
Figure 4.17: Ledalab Decomposition of EDA	78
Figure 4.18: Identified peaks on phasic signal.	79
Figure 4.19: Error variance in AR batch analysis of EDA.....	80
Figure 4.20: Error variance in TVAR analysis of EDA.	80
Figure 4.21: The prediction error, its spectrum and ACF from EDA TVAR	81
Figure 4.22: Forgetting factor with Fortescue.....	81
Figure 4.23: EDA Spectrograms. a) non parametric b) parametric batch c) ARTVAR	82
Figure 4.24: Phasic signal and TVSymp computed with the 3 methods.	83
Figure 4.25 Cross-correlation EDA-RR.....	85
Figure 4.26 Estimated time delay EDA-RR.....	85
Figure 4.27 Magnitude squared coherence EDA Phasic-NRSA	86
Figure 4.28 Heart Rate across tasks of BASE	87
Figure 4.29 P Tot. BASE protocol	88

Figure 4.30 SDNN. BASE protocol.....	89
Figure 4.31 HF. BASE protocol.....	90
Figure 4.32 P Coer. BASE protocol.....	90
Figure 4.33 Respiratory Rate in Resp Per Minute.....	91
Figure 4.34 LF NU. BASE protocol.	92
Figure 4.35 LF NU NRSA. BASE protocol	92
Figure 4.36 P Tot. N-Back Protocol	94
Figure 4.37 SDNN. N-Back Protocol.....	94
Figure 4.38 HF. N-Back Protocol.....	95
Figure 4.39 P Coer. N-Back Protocol.....	95
Figure 4.40 HR. N-Back Protocol	95
Figure 4.41 Respiratory Rate.....	95
Figure 4.42 P Coer NU as percentage	96
Figure 4.43 LF NU NRSA	96
Figure 4.44 LF NU. N-Back protocol	96
Figure 4.45 RMSSD. N-Back protocol.....	97
Figure 4.46 SampEn. N-Back protocol.....	97
Figure 4.47: ISCR. N-Back Protocol.....	99
Figure 4.48: Peak Frequency. N-Back Protocol	99
Figure 4.49: Tonic Mean. N-Back Protocol.....	100
Figure 4.50 TVSymp. N-Back Protocol.....	100
Figure 4.51 StdTVSymp. N-Back Protocol	100
Figure 4.52: TVSymp. First subject of the N-Back Protocol.....	101
Figure 4.53: Correlation matrix. HRV features. Significant ρ are framed in yellow .	103
Figure 4.54 Correlation matrix. Theta band. Code writing	104
Figure 4.55 Correlation matrix. Alpha band. Code writing	104
Figure 4.56 scatterplot with linear regression line and significance of ρ	105
Figure 4.57 scatterplot with linear regression line and significance of ρ	105
Figure 4.58 scatterplot with linear regression line and significance of ρ	105

Figure 4.59: Correlation matrix. Score and performance – code reading.....	106
Figure 4.60 Correlation matrix. Categorical outcomes – code writing.....	107
Figure 4.61: Correlation matrix. EDA features.....	108
Figure 4.62: scatterplot with linear regression line and significance of ρ	108
Figure 4.63: Correlation matrix. EDA-HRV features	109
Figure 4.64: scatterplot with linear regression line and significance of ρ	109

List of Tables

Table 2-1 Instrumentation used in BASE	30
Table 2-2 Instrumentation used in N-Back	34
Table 3-1 Features extracted from $\Phi\mathbf{1}, \mathbf{1}$	49
Table 3-2 Features computed from the product of $\Phi\mathbf{1}, \mathbf{1}$ with \mathbf{C}	49
Table 3-3 Features computed from partial spectrograms.....	49
Table 3-4 Ledalab output signals	51
Table 3-5 Ledalab impulse characteristics	52
Table 3-6 EDA time-domain features	55
Table 3-7 EDA time-frequency domain features	56
Table 4-1 Significant p-values in RLE.....	93
Table 4-2 Significant p-values in RLE.....	93
Table 4-3 Significant p-values in SPLIT	93
Table 4-4 p-values N-Back, HRV features	98
Table 4-5: p-values N-Back, EDA features.....	102
Table A-1 <i>p-values. RP = Read Problem; WR = Writing; RC = Read Code; RT= Read Text</i>	123
Table A-2: <i>p-values. WR = Writing; RC = Read Code</i>	124
Table A-3 <i>p-values WR = Writing; RC = Read Code; RT = Read Text</i>	124
Table A-4: <i>p-values. WR = Writing; RC = Read Code</i>	124
Table A-5: <i>p-values of HRV and Respiratory features</i>	125
Table A-6: <i>p-values of EDA features</i>	126
Table A-7: <i>Correlations of score and HRV features. Sit phase</i>	126

Table A-8: <i>Correlations of score and EDA features. Sit phase</i>	127
Table A-9: <i>Correlations of score and HRV features. N-Back phase</i>	127
Table A-10: <i>Correlations of score and EDA features. N-Back phase</i>	127

